DOCTORAL DISSERTATION

Complex bifurcation structures in SIRWS and SIRWJS models of pertussis with asymmetric partition of immunity period

Author: Richmond Opoku-Sarkodie
Supervisors: Mónika Polner and Ferenc A. Bartha

Doctoral School of Mathematics,
Bolyai Institute, University of Szeged

2024

Acknowledgements

This endeavor would not have been possible without the help of God Almighty, who gave me the strength to embark on this research. My sincere gratitude also goes to my beloved wife, Nana Ama Opoku-Sarkodie, and my three lovely children, Maame Akosua, Kofi Konadu, and Afia Konadu for their love and patience throughout my Ph.D. studies. I would also like to thank my supervisors, Dr. M. Polner and Dr. F. A. Bartha for their exceptional academic supervision. Additionally, I would like to express my sincere gratitude to Professor Gergely Röst for his valuable input into this work. Finally, my colleague Bornali Das and the entire staff of Bolyai Institute deserve a special mention for their support.

Contents

Chapter 1

Introduction

Pertussis is a communicable disease caused by the bacterium Bordetella pertussis. The bacterium attacks the cilia which are located in the upper respiratory system. The disease is characterized by the release of toxins causing inflammation in the airways of the infected individual. Excessive coughing and breathing difficulties are the critical symptoms associated with pertussis [1]. The typical mode of transmission includes coughing, sneezing, or sharing indoor air [2]. The severity of the disease is considerably higher in children compared to adults, hence, vaccination is recommended at an early age. One in five babies receiving treatment in a hospital after contracting pertussis may get pneumonia, and one in a hundred may die [3]. Other severe outcomes include brain damage, breathing irregularities, and erratic and uncontrolled shaking [4]. As immunity wanes [5], adults and adolescents become at risk of infection, and upon contracting the disease, they may infect children they interact with. A WHO report in 2008 by [6] revealed that one hundred and ninety-five thousand (195000) children died from pertussis. Out of an estimated five million cases, reported by [1], eighty-five thousand nine hundred (85900) deaths occurred in infants younger than a year. In 2018, the European Centre for Disease Control and Prevention (ECDC) reported that kids below the age of one year had an incidence rate of approximately 44.4 per 100000

population [7]. Annual cases of pertussis reported by [8] in 2009 were forty-eight million, five hundred thousand (48.5 million), with two hundred and ninety-five thousand (295000) fatalities. From the above-mentioned facts about pertussis, it is apparent that the infection is a global health issue that deserves a great deal of attention.

We aim to mathematically model and study the transmission dynamics of pertussis with a special focus on the waning of immunity and we do so by leveraging compartmental modeling techniques for infectious diseases. The origins of such methods date back to the formulation of the Susceptible-Infectious-Recovered (SIR) model in 1927 by Kermack and McKendrick [9]. Ever since its conception it has been used, together with its variants, to investigate the dynamics of numerous infections *e.g.* measles [10], tuberculosis [11], HIV [12], ebola [13], influenza [14], and the recent coronavirus disease (COVID-19) [15]. Typically, the models confer life-long immunity upon recovery, so in order to investigate scenarios where immunity is temporary, some changes are needed. Common examples are the SIRS and SIS models that may be applied to study the dynamics of infections where immunity wanes over time or the individual gains no immunity at all upon recovery, respectively. From the vast family of compartmental models, we focus on those that account for both waning and boosting of immunity. Principal among these is the SIRWS model, an extension of the aforementioned SIRS model, that includes an intermediate state for individuals with waned immunity that may be boosted upon re-exposure. This model has been readily applied to investigate the dynamics of pertussis. Earlier investigations [16–20] assumed identical expected duration for the transitions from the state of full immunity to waned ($R \to W$) and thereon to none ($W \to S$). This is the so-called symmetric partitioning of the immune period. Introducing an extra compartment to the SIRWS model for individuals undergoing secondary infections resulted in the SIRWJS model and, again, the partitioning of the immunity period was assumed to be symmetric in [18]. As a summary, both of these models examine the dynamics of infections in which immunity upon recovery is temporal (*e.g.* pertussis) and immune boosting upon re-exposure may occur either directly ($W \to R$) or via secondary infections

$(W \to J \to R)$.

The novelty of the research presented in this thesis is proposing a new, potentially asymmetric partitioning of the total immune period and investigating its effect on the dynamics of the SIRWS and SIRWJS models. We will see that the disease dynamics can change considerably leading to scenarios with complex bifurcations. As these models are actively used in studying pertussis, we believe that our results will contribute to a better understanding of the transmission dynamics of the disease.

1.1 Structure of the dissertation

The dissertation comprises four chapters. In Chapter 2, we briefly introduce transmission models based on compartmental ordinary differential equations (ODE) followed by the basics of stability and bifurcation analysis of equilibria. The chapter is concluded with an overview of `MatCont` [21–23], a Matlab package for numerical bifurcation analysis based on continuation techniques. Chapter 3 describes the SIRWS system with our proposed asymmetric partitioning of the immunity period and presents in-depth analytical and numerical investigations of the model. Finally, Chapter 4 focuses on the analysis of an SIRWJS-type system, again, with our proposed asymmetric partitioning of the immunity period.

Chapter 2

Mathematical background

This chapter introduces compartmental ODE models of infectious diseases and discusses relevant mathematical theorems. First, the Susceptible-Infectious-Recovered (SIR), Susceptible-Infectious-Susceptible (SIS), and Susceptible-Infectious-Recovered-Susceptible (SIRS) compartmental models will be presented. Next, we demonstrate the analytical computation of equilibria, after which we perform their stability analysis. Furthermore, we discuss three bifurcations, namely, the transcritical, saddle-node, and Hopf bifurcations. Finally, we provide an overview of `MatCont`, a numerical continuation package used for bifurcation analysis.

2.1 Compartmental ODE models of infectious diseases

Compartmental ODE transmission models categorize the population into subgroups (compartments) defined by a selected set of properties/attributes relevant to disease transmission, progression, or outcome. Typically, as the property matching an individual changes, that person transitions to the appropriate compartment, or if no such category exists that individual may be removed from the system entirely (new individuals may appear as well *e.g.* due to migration or birth). In this dissertation, we model these transitions by ordinary differential equations (ODE), *i.e.* by flows, hence, a model description results in a system

of ODEs capturing the transmission dynamics of an infectious disease. In the following, we introduce the basic concepts of this technique by presenting the SIR, SIS, and SIRS models in detail.

2.1.1 Classical SIR model without vital dynamics

The long-established SIR model was developed by Kermack and McKendrick [9]. The model was first applied to study the transmission of measles and influenza in a population. Down the line, the SIR model has been used to study the spread of many infectious diseases, e.g. [24–27]. The description of the various compartments is as follows. The individuals in the S compartment are susceptible that is they are prone to the disease. Those who are infected and infectious reside in the I compartment. Disease transmission, *i.e.* a transition from S to I, is modeled by a fraction of the possible encounters between members of these two compartments characterized by the transmission rate β. An infected individual recovers at the rate γ and subsequently transitions into the R compartment representing individuals who have recovered, or more precisely, who has quit the infectious chain *i.e.* neither can they infect anyone nor can they get infected again. As members of R stay there for all time, the model confers lifelong immunity to the recovered individuals. A typical assumption, that we adapt as well, is considering the total population to be constant.

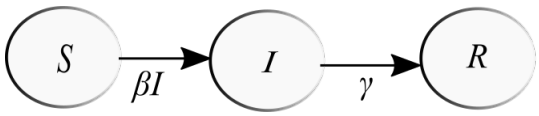

Figure 2.1: SIR: Susceptible (S), Infectious (I), and Recovered (R) without vital dynamics.

The transition diagram of the SIR model is depicted in Figure 2.1 and the aforementioned

dynamics are described by the following system of ordinary differential equations

$$\frac{dS}{dt} = -\beta IS, \tag{2.1a}$$
$$\frac{dI}{dt} = \beta IS - \gamma I, \tag{2.1b}$$
$$\frac{dR}{dt} = \gamma I, \tag{2.1c}$$

with initial conditions $S(0)$, $I(0)$ and $R(0)$. It is apparent from (2.1) that for all $t \geq 0$, the sum of (2.1a)-to-(2.1c) is zero *i.e.* $\frac{dS}{dt} + \frac{dI}{dt} + \frac{dR}{dt} = 0$, therefore, $S(t) + I(t) + R(t) = N$, where N is a constant. The population is considered to be normalized to 1 that is $N = 1$ and the compartments represent the respective fractions of it. This formulation does not consider vital dynamics comprising natural birth and death.

There is no closed-form solution of (2.1), various analytical and numerical techniques are applied to study the behavior of the solutions. Beginning from (2.1a), $\frac{dS}{dt} < 0$ means that $S(t)$ decreases and, likewise, $\frac{dR}{dt} > 0$ from (2.1c) means that $R(t) > 0$ for all time. Now concerning (2.1b), it is straightforward to observe that the monotonicity of $I(t)$ cannot be guaranteed. Assuming $\frac{dI}{dt} < 0$, leads to $\beta I(t)S(t) - \gamma I(t) < 0$ and, then $\frac{\beta S(t)}{\gamma} < 1$. Now, if $\frac{\beta S(0)}{\gamma} < 1$, then $I(t)$ decreases for all time and, on the other hand, if $\frac{\beta S(0)}{\gamma} > 1$, then $I(t)$ increases until it attains its maximum value at the time when $\frac{\beta S(t)}{\gamma} = 1$. The quantity $\frac{\beta S(0)}{\gamma}$, or specifically $\frac{\beta}{\gamma}$ with the standard assumption $S(0) \approx 1$, is the so-called basic reproduction number of (2.1), which will be discussed in detail in a later section. The solutions of (2.1a) and (2.1b) by integration are $S(t) = S(0)e^{-\beta \int_0^t I(s)ds}$ and $I(t) = I(0)e^{\int_0^t \beta S(s) - \gamma ds}$, respectively. Considering non-negative initial conditions, the solutions remain non-negative for all time.

Now, we discuss two key characteristics of the model, namely, the final size and the peak size. During an epidemic, some individuals may remain unaffected, giving rise to the notion of the so-called final epidemic size which describes what portion of the population got infected in

total. As every infected individual eventually transitions to R, the final size may be described by the limit $\lim_{t\to\infty} R(t)$ (if it exists). As $S(t)$ decreases for all time and remains non-negative, this indicates that $\lim_{t\to\infty} S(t) = S_\infty$ exists. On the other hand, $\lim_{t\to\infty} I(t) = 0$ has to hold, hence, we get the existence of the aforementioned limit and a formula for the final size as $1-S_\infty$. Now, dividing (2.1a) by (2.1b) gives $\frac{dI}{dS} = -1+\frac{\gamma}{\beta S}$. Then, by integration, we obtain $I(t) = -S(t) + \frac{\gamma}{\beta}\ln S(t) + C$, where $C = I(0) + S(0) - \frac{\gamma}{\beta}\ln S(0)$. Substituting C into the formula then yields

$$I(t) = -S(t) + \frac{\gamma}{\beta}\ln S(t) + I(0) + S(0) - \frac{\gamma}{\beta}\ln S(0). \tag{2.2}$$

Finding the limit of (2.2) as $t \to \infty$ gives $I_\infty = -S_\infty + \frac{\gamma}{\beta}\ln S_\infty + I(0) + S(0) - \frac{\gamma}{\beta}\ln S(0)$. Using that $\lim_{t\to\infty} I(t) = I_\infty = 0$ and assuming that $I(0)$ is very small, we obtain the so-called *final size relation* as

$$\ln\left(\frac{S_\infty}{S(0)}\right) \approx -\frac{\beta}{\gamma}(S(0) - S_\infty). \tag{2.3}$$

The other key characteristic, the peak size, is based on the fact that the number of infections $I(t)$ reaches its peak when $S(t) = \frac{\gamma}{\beta}$. Let us denote by I_{peak} the proportion of infected individuals at this time and replace $S(t)$ in (2.2) with $\frac{\gamma}{\beta}$ to obtain

$$I_{peak} = -\frac{\gamma}{\beta} + \frac{\gamma}{\beta}\ln\frac{\gamma}{\beta} + I(0) + S(0) - \frac{\gamma}{\beta}\ln S(0), \tag{2.4}$$

the so-called *peak size relation*.

So far, we have gained some analytical insight into the solutions of (2.1). Next, we consider numerical simulations using parameters from [16] (mimicking characteristics of pertussis). Figure 2.2 presents a plot demonstrating the monotonic behavior of $S(t)$ and $R(t)$ represented by the blue and green curves, respectively. The infectious population $I(t)$, plotted in red, behaves differently. We observe an increase in $I(t)$ until it reaches the peak that is where

$S(t) = \gamma/\beta$. Beyond this critical point, the infectious population becomes decreasing.

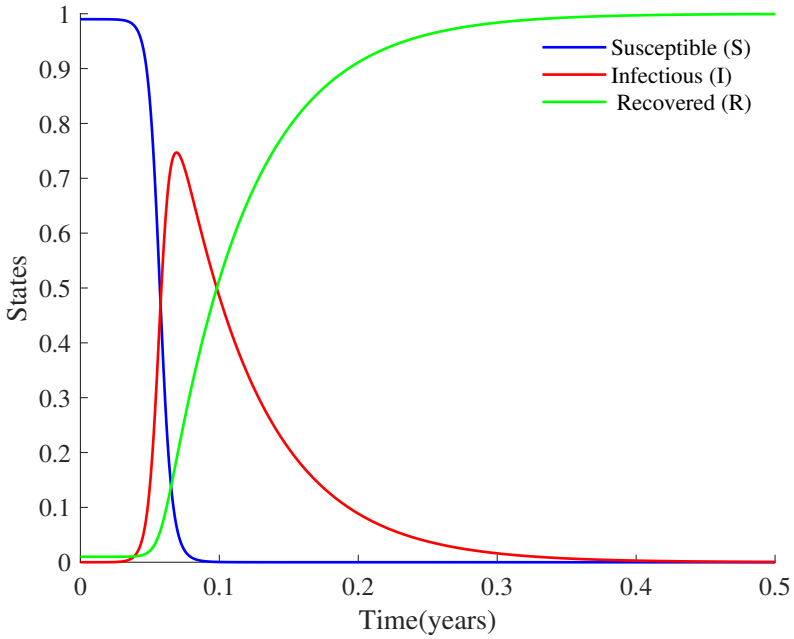

Figure 2.2: SIR (2.1): Simulation with $\beta = 260$ and $\gamma = 17$.

Finally, we mention here that an analogous model to (2.1) is used frequently in epidemiology where the total population is not normalized to 1. That approach results in the following system of ordinary equations

$$\frac{dS}{dt} = -\beta IS/N, \tag{2.5a}$$

$$\frac{dI}{dt} = \beta IS/N - \gamma I, \tag{2.5b}$$

$$\frac{dR}{dt} = \gamma I, \tag{2.5c}$$

with the total population being constant $S + I + R = N$.

2.1.2 SIR model with vital dynamics

This section presents the SIR model augmented with vital dynamics that is we account for birth and natural death whilst considering a constant population. The flow chart of the augmented model is depicted in Figure 2.3.

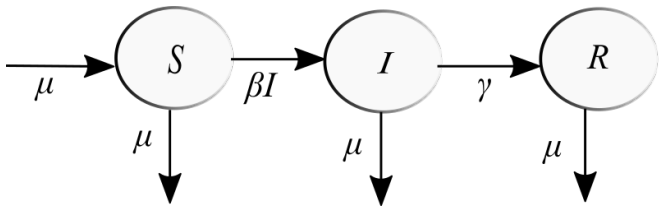

Figure 2.3: SIR: Susceptible (S), Infectious (I), and Recovered (R) with vital dynamics.

The system of ordinary differential equations describing the dynamics are

$$\frac{dS}{dt} = \mu(1 - S) - \beta IS, \tag{2.6a}$$

$$\frac{dI}{dt} = \beta IS - \gamma I - \mu I, \tag{2.6b}$$

$$\frac{dR}{dt} = \gamma I - \mu R, \tag{2.6c}$$

where μ represents the death rate. All other parameters have the same interpretation as in the previous section.

Now, let us look for equilibria of (2.6). In epidemiological scenarios, it is common to encounter two kinds of equilibria namely the disease-free (**DFE**) and the endemic equilibrium (**EE**) referring to the steady states when there are no infected and the point where the disease is prevalent in the population, respectively. An equilibrium of (2.6) is denoted by

(S^*, I^*, R^*) and solves the steady state equations

$$\mu(1 - S^*) - \beta I^* S^* = 0, \tag{2.7a}$$

$$\beta I^* S^* - \gamma I^* - \mu I^* = 0, \tag{2.7b}$$

$$\gamma I^* - \mu R^* = 0. \tag{2.7c}$$

From (2.7b), we get that either $I^* = 0$ or $\beta S^* - \gamma - \mu = 0$. Considering $I^* = 0$ readily yields $R^* = 0$ from (2.7c) and $S^* = 1$ from (2.7a). Thus, $\mathbf{DFE_{SIR}} = (1, 0, 0)$. Now, assuming $I^* \neq 0$ means $\beta S^* - \gamma - \mu = 0$ that, in turn, gives

$$S^* = \frac{\gamma + \mu}{\beta}. \tag{2.8}$$

Substituting S^* into (2.7a) and solving for I^* results in

$$I^* = \frac{\mu}{\beta}\left(\frac{\beta}{\gamma + \mu} - 1\right). \tag{2.9}$$

Finally, putting I^* into (2.7c) yields

$$R^* = \frac{\gamma}{\beta}\left(\frac{\beta}{\gamma + \mu} - 1\right). \tag{2.10}$$

By introducing the notation

$$\mathcal{R}_0 = \frac{\beta}{\gamma + \mu}, \tag{2.11}$$

the formulae (2.8), (2.9), and (2.10) transform into

$$\mathbf{EE_{SIR}} = (S^*, I^*, R^*) = \left(\frac{1}{\mathcal{R}_0}, \frac{\mu}{\beta}(\mathcal{R}_0 - 1), \frac{\gamma}{\beta}(\mathcal{R}_0 - 1)\right). \tag{2.12}$$

We note that $\mathcal{R}_0$ is referred to as the basic reproduction number of (2.6), a concept that we will discuss in a later part of this chapter.

We conclude our overview of the model by considering parameters, again, from [16] for the purposes of a numerical simulation. Figure 2.4 displays oscillatory convergence of solutions towards the endemic equilibrium.

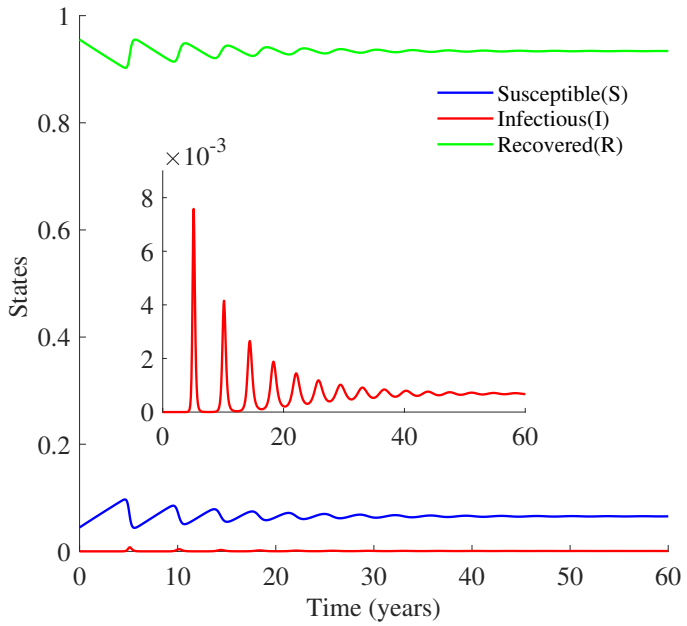

Figure 2.4: SIR (2.6): Simulation with $\beta = 260$, $\gamma = 17$, and $\mu = 0.0125$.

2.1.3 SIS model with vital dynamics

Another epidemiological model of interest is the SIS model which captures the transmission dynamics of a disease with no immunity upon recovery. That is the individuals may transition from the susceptible class to the infecteds and, then, back to being susceptible.

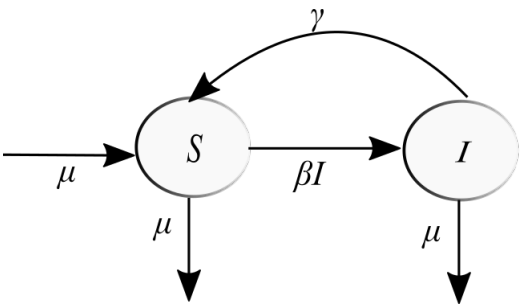

Figure 2.5: SIS: Susceptible (S) and Infectious (I).

Figure 2.5 depicts the transition diagram of the SIS model and the system of ordinary differential equations describing the dynamics are given as

$$\frac{dS}{dt} = \mu(1-S) - \beta IS + \gamma I, \tag{2.13a}$$

$$\frac{dI}{dt} = \beta IS - (\gamma + \mu)I, \tag{2.13b}$$

with the initial conditions $S(0) > 0$, $I(0) > 0$ such that $S(0) + I(0) = 1$.

We find the equilibria by solving the steady-state equations

$$\mu(1-S^*) - \beta I^* S^* + \gamma I^* = 0, \tag{2.14a}$$

$$\beta I^* S^* - (\gamma + \mu)I^* = 0. \tag{2.14b}$$

From (2.14b), $I^* = 0$ or $\beta S^* - (\gamma + \mu) = 0$. If $I^* = 0$, then $S^* = 1$ from (2.14a), thus $\mathbf{DFE_{SIS}} = (1, 0)$. On the other hand, if $I^* \neq 0$, then $\beta S^* - (\gamma + \mu) = 0$ that results in

$$S^* = \frac{\gamma + \mu}{\beta}. \tag{2.15}$$

Substituting S^* into (2.14a) and solving for I^* then gives

$$I^* = 1 - S^* = 1 - \frac{\gamma + \mu}{\beta} \tag{2.16}$$

leading to $\mathbf{EE_{SIS}} = \left(\frac{\gamma+\mu}{\beta}, 1 - \frac{\gamma+\mu}{\beta}\right)$. Finally, using the notation in (2.11), we obtain

$$\mathbf{EE_{SIS}} = (S^*, I^*) = \left(\frac{1}{\mathcal{R}_0}, 1 - \frac{1}{\mathcal{R}_0}\right). \tag{2.17}$$

Here we note that albeit we are considering a different model, the quantity denoted by $\mathcal{R}_0$ plays an identical role to that before.

Again, we utilized the parameters from [16] for the numerical simulation displayed in Figure 2.6 showing convergence to the endemic equilibrium.

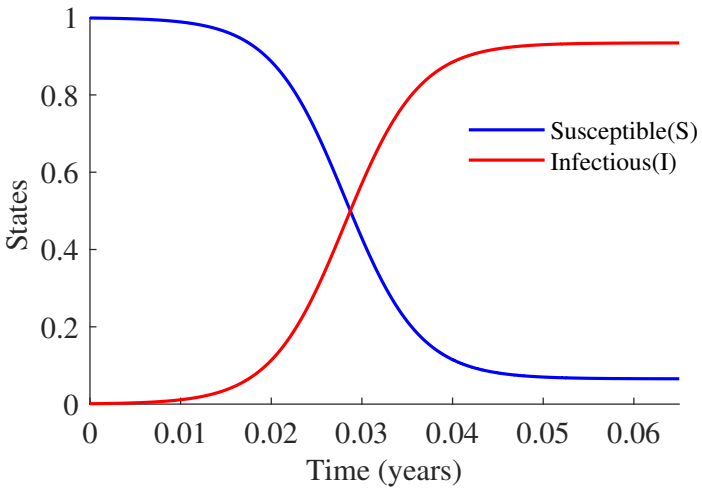

Figure 2.6: SIS (2.13): Simulation with $\beta = 260$, $\gamma = 17$, and $\mu = 0.0125$.

2.1.4 SIRS model with vital dynamics

Now, we alter the SIR model to include short-term resistance to re-infection upon recovery. This modification leads to the so-called SIRS model. Immunity is temporal and losing it results in an onward transition into the susceptible compartment.

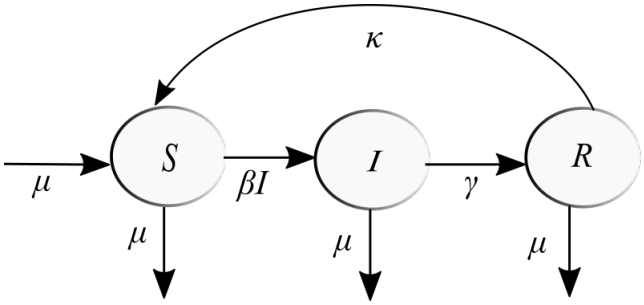

Figure 2.7: SIRS: Susceptible (S), Infectious (I) and Recovered (R).

Figure 2.7 depicts the transition diagram of the SIRS model. κ is the immune decay rate, all other parameters and compartments are as discussed earlier. The model dynamics are described by the following system of ordinary differential equations

$$\frac{dS}{dt} = \mu(1-S) - \beta IS + \kappa R, \tag{2.18a}$$

$$\frac{dI}{dt} = \beta IS - \gamma I - \mu I, \tag{2.18b}$$

$$\frac{dR}{dt} = \gamma I - \kappa R - \mu R. \tag{2.18c}$$

Again, let (S^*, I^*, R^*) represent an equilibrium solution of (2.18), which is obtained by solving the steady-state equations

$$\mu(1-S^*) - \beta I^* S^* + \kappa R^* = 0, \tag{2.19a}$$

$$\beta I^* S^* - \gamma I^* - \mu I^* = 0, \tag{2.19b}$$

$$\gamma I^* - \kappa R^* - \mu R^* = 0. \tag{2.19c}$$

From (2.19b), either $I^* = 0$ or $\beta S^* - (\gamma + \mu) = 0$. If $I^* = 0$, then $R^* = 0$ from (2.19c) and $S^* = 1$ from (2.19b), thus, $\mathbf{DFE_{SIRS}} = (1, 0, 0)$. Otherwise, if $I^* \neq 0$, then $\beta S^* - (\gamma + \mu) = 0$ yielding

$$S^* = \frac{\gamma + \mu}{\beta} = \frac{1}{\mathcal{R}_0}. \tag{2.20}$$

From (2.19c), $I^* = R^*(\kappa+\mu)/\gamma$ follows. Then, substituting into (2.19a) gives

$$R^* = \frac{\gamma(\beta-(\gamma+\mu))}{\beta(\gamma+\mu+\kappa)} = \frac{\gamma(\mathcal{R}_0-1)}{\mathcal{R}_0(\gamma+\mu+\kappa)}. \tag{2.21}$$

Finally, from (2.19c) we get

$$I^* = \frac{(\kappa+\mu)(\beta-(\gamma+\mu))}{\beta(\gamma+\mu+\kappa)} = \frac{(\kappa+\mu)(\mathcal{R}_0-1))}{\mathcal{R}_0(\gamma+\mu+\kappa)} \tag{2.22}$$

leading to the endemic equilibrium

$$\mathbf{EE_{SIRS}} = (S^*, I^*, R^*) = \left(\frac{1}{\mathcal{R}_0}, \frac{(\kappa+\mu)(\mathcal{R}_0-1))}{\mathcal{R}_0(\gamma+\mu+\kappa)}, \frac{\gamma(\mathcal{R}_0-1)}{\mathcal{R}_0(\gamma+\mu+\kappa)}\right). \tag{2.23}$$

Once again, we use the parameters from [16] in our numerical simulation showing convergence to the endemic equilibrium, see Figure 2.8.

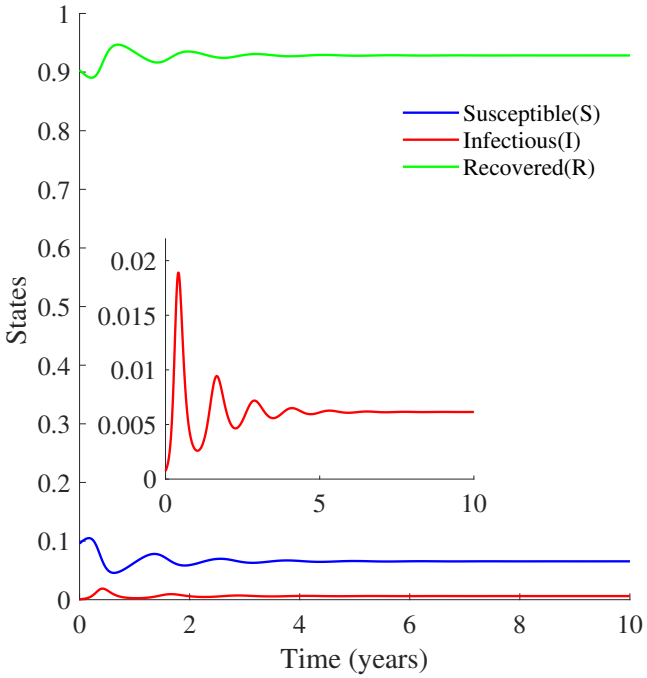

Figure 2.8: SIRS (2.5): Simulation with $\beta = 260$, $\gamma = 17$, $\kappa = 0.1$, and $\mu = 0.0125$.

2.1.5 Models with additional compartments

A plethora of compartmental ODE models have been investigated in epidemiological studies featuring many compartments and transitions. As a current example, COVID-19 was extensively studied via larger models considering compartments *e.g.* for individuals that are hospitalized, quarantined, waned immunity, vaccinated, furthermore, they are often inflated to account for age- and location specific features and rates [28–30]. Here, we just briefly present two additional systems that introduce solely the exposed compartment (E) in comparison to the first part of this section for modeling the latency period of an infection. The inclusion of the exposed class makes it possible to capture the dynamics of diseases where an infected individual does not become infectious immediately *e.g.* as in [31, 32] investigating COVID-19.

The most basic of such formulation is the SEIR model that, without vital dynamics, is given by

$$\frac{dS}{dt} = -\beta IS, \tag{2.24a}$$
$$\frac{dE}{dt} = \beta IS - \sigma E, \tag{2.24b}$$
$$\frac{dI}{dt} = \sigma E - \gamma I, \tag{2.24c}$$
$$\frac{dR}{dt} = \gamma I, \tag{2.24d}$$

with $S(0), E(0), I(0), R(0) \geq 0$, and $S(0) + E(0) + I(0) + R(0) = 1$. The exposed class contains individuals who are infected but are not yet able to transmit the infection further. As time progresses, the exposed individuals eventually become infectious and consequently transition into the I compartment at the rate σ. The time interval between becoming infected and developing symptoms is the so-called latent period [33]. Adding vital dynamics to the

model alters the system of equations as expected, namely,

$$\frac{dS}{dt} = \mu(1-S) - \beta IS, \tag{2.25a}$$
$$\frac{dE}{dt} = \beta IS - (\mu+\sigma)E, \tag{2.25b}$$
$$\frac{dI}{dt} = \sigma E - (\gamma+\mu)I, \tag{2.25c}$$
$$\frac{dR}{dt} = \gamma I - \mu R. \tag{2.25d}$$

Finally, we present the SE_1E_2IR system featuring two kinds of latent periods with possibly different lengths

$$\frac{dS}{dt} = \mu(1-S) - \beta IS, \tag{2.26a}$$
$$\frac{dE_1}{dt} = p\beta IS - (\sigma_1+\mu)E_1, \tag{2.26b}$$
$$\frac{dE_2}{dt} = (1-p)\beta SI - (\sigma_2+\mu)E_2, \tag{2.26c}$$
$$\frac{dI}{dt} = \sigma_1 E_1 + \sigma_2 E_2 - (\gamma+\mu)I, \tag{2.26d}$$
$$\frac{dR}{dt} = \gamma I - \mu R. \tag{2.26e}$$

The model was considered in [34] and consists of two latent states E_1 and E_2, with transition rates σ_1 and σ_2 to I, respectively. It is capturing the scenario where an infection results in the latent period of the first type with probability p and of the second type with $1-p$.

2.2 Basic reproduction number

One of the concerns of epidemiology is developing intervention strategies to eradicate or prevent disease spread in a population. The so-called *basic reproduction number*, denoted by $\mathcal{R}_0$, is defined as the expected number of secondary infections that one infected person would produce in an entirely susceptible population [35]. This is a critical numeric indicator

as its magnitude determines whether the outbreak of the epidemics is possible. If $\mathcal{R}_0 < 1$, the infections get eradicated, and if $\mathcal{R}_0 > 1$, the outbreak is expected when the infectious disease appears in the population. Recall the important role of the quantity $\frac{\beta S(t)}{\gamma}\Big|_{t=0}$ for the SIR model without vital dynamics in Section 2.1.1 and the notation (2.11) repeatedly appearing in the models discussed thereafter. As we will shortly see, these are actually the basic reproduction numbers for the respective systems. $\mathcal{R}_0$ may depend on numerous parameters characterizing the infectious chain *e.g.* transmission rate (denoted by β), rate of natural death (denoted by μ), and recovery rate (denoted by γ) in our examples. Furthermore, the basic reproduction number is proportional to the susceptible ratio of the population that is to $S(0)$ which is often absent from the formula due to the common assumption $S(0) \approx 1$. The value of $\mathcal{R}_0$ is specific not just to the disease but also to the target population. For example, it was estimated to be around $\mathcal{R}_0 = 2.2$ in Western Europe for COVID-19 and $\mathcal{R}_0 = 3.32$ in China [36]. After the start of an epidemic the *effective reproduction number* $\mathcal{R}_t$, an analogous quantity, serves as an indicator of its progresses. Roughly speaking it may be computed using the same way as $\mathcal{R}_0$ by considering the possible time-dependence of parameters and the changing ratio of susceptibles $S(t)$. A possible intervention goal is to drive $\mathcal{R}_t$ below 1 or at least decrease it as much as possible for example by decreasing β with reducing contacts within the society and mandating protective measures like face masks or by decreasing $S(t)$ *i.e.* via vaccination or controlled spread to achieve herd immunity.

We now turn to overview the steps involved in computing $\mathcal{R}_0$ (with the ratio of susceptibles factored out) following the generic method presented in [34]. First, we identify the infected subsystem or the disease states from the system of ODEs that are the sub-equations responsible for the creation of new infections. Second, we linearize the subsystem by computing the Jacobian at the disease-free equilibrium. Then, we decompose the Jacobian into $\mathbf{T} + \mathbf{\Sigma}$, where $\mathbf{T}$ is the transmission part, describing the creation of new infections, and $\mathbf{\Sigma}$ is the transition part showing changes in state. Finally, the next-generation matrix is obtained as $\mathbf{G} = -\mathbf{T}\mathbf{\Sigma}^{-1}$ the spectral radius of which is $\mathcal{R}_0$.

To demonstrate the computation, we start with (2.26). The infected subsystem is

$$\frac{dE_1}{dt} = p\beta IS - (\sigma_1 + \mu)E_1, \tag{2.27a}$$
$$\frac{dE_2}{dt} = (1-p)\beta SI - (\sigma_2 + \mu)E_2, \tag{2.27b}$$
$$\frac{dI}{dt} = \sigma_1 E_1 + \sigma_2 E_2 - (\gamma + \mu)I \tag{2.27c}$$

and the corresponding Jacobian evaluated at the **DFE** is then

$$\mathbf{J_{DFE}} = \begin{bmatrix} -(\sigma_1+\mu) & 0 & p\beta \\ 0 & -(\sigma_2+\mu) & (1-p)\beta \\ \sigma_1 & \sigma_2 & -(\gamma+\mu) \end{bmatrix}. \tag{2.28}$$

The decomposition into $\mathbf{T}$ and $\mathbf{\Sigma}$ yields

$$\mathbf{T} = \begin{bmatrix} 0 & 0 & p\beta \\ 0 & 0 & (1-p)\beta \\ 0 & 0 & 0 \end{bmatrix}$$

and

$$\mathbf{\Sigma} = \begin{bmatrix} -(\sigma_1+\mu) & 0 & 0 \\ 0 & -(\sigma_2+\mu) & 0 \\ \sigma_1 & \sigma_2 & -(\gamma+\mu) \end{bmatrix}.$$

Thus, the next-generation matrix is obtained as

$$\mathbf{G} = -\mathbf{T}\mathbf{\Sigma}^{-1} = \begin{bmatrix} 0 & 0 & p\beta \\ 0 & 0 & (1-p)\beta \\ 0 & 0 & 0 \end{bmatrix} \times \begin{bmatrix} \frac{1}{(\sigma_1+\mu)} & 0 & 0 \\ 0 & \frac{1}{(\sigma_2+\mu)} & 0 \\ \frac{\sigma_1}{(\gamma+\mu)(\sigma_1+\mu)} & \frac{\sigma_2}{(\gamma+\mu)(\sigma_2+\mu)} & \frac{1}{\gamma+\mu} \end{bmatrix}$$

$$= \begin{bmatrix} \frac{p\beta\sigma_1}{(\sigma_1+\mu)(\gamma+\mu)} & \frac{p\beta\sigma_2}{(\sigma_2+\mu)(\gamma+\mu)} & \frac{p\beta}{\gamma+\mu} \\ \frac{(1-p)\beta\sigma_1}{(\sigma_1+\mu)(\gamma+\mu)} & \frac{(1-p)\beta\sigma_2}{(\sigma_2+\mu)(\gamma+\mu)} & \frac{(1-p)\beta}{\gamma+\mu} \\ 0 & 0 & 0 \end{bmatrix}$$

the spectral radius of which is

$$\mathcal{R}_0 = \left(\frac{p\sigma_1}{\sigma_1+\mu} + \frac{(1-p)\sigma_2}{\sigma_2+\mu} \right) \frac{\beta}{\gamma+\mu}. \tag{2.29}$$

For the basic systems we discussed early in the chapter the above computation is much more straightforward as the infected subsystem is one dimensional in each of those settings. The SIR (2.18), SIS (2.6), and SIRS (2.13) models with vital dynamics share the infected subsystem $I^{'} = \beta I - I(\gamma+\mu)$, the Jacobian (simply the derivative) $\mathbf{J} = \beta - (\gamma+\mu)$, the decomposition $\mathbf{T} = \beta$ and $\mathbf{\Sigma} = -(\gamma+\mu)$, the next-generation "matrix" $\mathbf{G} = -\mathbf{T}\mathbf{\Sigma}^{-}1 = \beta \times \frac{1}{\gamma+\mu} = \frac{\beta}{\gamma+\mu}$, and the basic reproduction number $\mathcal{R}_0 = \frac{\beta}{\gamma+\mu}$. For the SIR without vital dynamics (2.1), we get $I' = \beta SI - \gamma I$ and, consequently, $\mathcal{R}_0 = \frac{\beta}{\gamma}$.

2.3 Local asymptotic stability (LAS) of equilibria

After determining an equilibrium of the transmission model, the next step is to perform local stability analysis by studying the linearized system at the steady-state following the Hartman-Grobman theorem [37, 38]. In practice, we analyze the eigenvalues of the Jacobian. An equilibrium is *hyperbolic* if none of the eigenvalues have a real part equal to zero. Considering the hyperbolic case, if the real part of every eigenvalue is negative, then locally all

solutions converge to said equilibrium, and hence it is locally asymptotically stable (LAS). On the other hand, if there is at least one eigenvalue with a positive real part, then the equilibrium is unstable.

2.3.1 Stability analysis of equilibria

We now perform the aforementioned analysis for both the disease-free and endemic equilibria of the SIR (2.6), SIS (2.13), and SIRS (2.18) models with vital dynamics. We recall that the basic reproduction number for all these systems is $\mathcal{R}_0 = \frac{\beta}{\gamma+\mu}$.

Stability of equilibria of the SIR model The Jacobian matrix of (2.6) is

$$\mathbf{J} = \begin{bmatrix} -(\mu+\beta I) & -\beta S & 0 \\ \beta I & -(\gamma+\mu-\beta S) & 0 \\ 0 & \gamma & -\mu \end{bmatrix}. \tag{2.30}$$

Evaluating at the $\mathbf{DFE_{SIR}}$ yields

$$\mathbf{J_{DFE}} = \begin{bmatrix} -\mu & -\beta & 0 \\ 0 & -(\gamma+\mu-\beta) & 0 \\ 0 & \gamma & -\mu \end{bmatrix}.$$

Then, the corresponding eigenvalues are

$$\lambda_1 = \beta - (\gamma+\mu), \quad \lambda_2 = \lambda_3 = -\mu,$$

two of which ($\lambda_2 = \lambda_3$) are always negative, whilst $\lambda_1 < 0$ iff $\beta < \gamma + \mu \Leftrightarrow \mathcal{R}_0 < 1$. Hence, the $\mathbf{DFE_{SIR}}$ is LAS when $\mathcal{R}_0 < 1$ and unstable for $\mathcal{R}_0 > 1$.

For the endemic equilibrium, we evaluate (2.30) at $\mathbf{EE_{SIR}}$ (2.12) leading to

$$\mathbf{J_{EE}} = \begin{bmatrix} -\mu - \beta \cdot \frac{\mu}{\beta} \cdot (\mathcal{R}_0 - 1) & -\beta \cdot \frac{1}{\mathcal{R}_0} & 0 \\ \beta \cdot \frac{\mu}{\beta} \cdot (\mathcal{R}_0 - 1) & -(\gamma + \mu - \beta \cdot \frac{1}{\mathcal{R}_0}) & 0 \\ 0 & \gamma & -\mu \end{bmatrix}. \tag{2.31}$$

Then, consider the characteristic polynomial $\det(\mathbf{J_{EE}} - \lambda I) =$

$$\det \begin{bmatrix} -\mu\mathcal{R}_0 - \lambda & -\frac{\beta}{\mathcal{R}_0} & 0 \\ \mu(\mathcal{R}_0 - 1) & -\lambda & 0 \\ 0 & \gamma & -\mu - \lambda \end{bmatrix} = \det \begin{bmatrix} -\mu\mathcal{R}_0 - \lambda & -\gamma - \mu & 0 \\ \mu(\mathcal{R}_0 - 1) & -\lambda & 0 \\ 0 & \gamma & -\mu - \lambda \end{bmatrix} =$$

$$\det \begin{bmatrix} -\mu - \lambda & -\gamma - \mu - \lambda & 0 \\ \mu(\mathcal{R}_0 - 1) & -\lambda & 0 \\ 0 & \gamma & -\mu - \lambda \end{bmatrix} = \det \begin{bmatrix} -\mu - \lambda & -\mu - \lambda & -\mu - \lambda \\ \mu(\mathcal{R}_0 - 1) & -\lambda & 0 \\ 0 & \gamma & -\mu - \lambda \end{bmatrix}$$

yielding the characteristic equation

$$(\lambda + \mu)\left(a_0\lambda^2 + a_1\lambda + a_2\right) = 0, \tag{2.32}$$

with

$$\begin{aligned} a_0 &= 1, \\ a_1 &= \mu\mathcal{R}_0, \\ a_2 &= \mu(\gamma + \mu)(\mathcal{R}_0 - 1). \end{aligned} \tag{2.33}$$

Clearly, $\lambda_1 = -\mu$ is an eigenvalue and the other two are given by

$$\lambda_2, \lambda_3 = \frac{-\mu\mathcal{R}_0 \pm \sqrt{(\mu\mathcal{R}_0)^2 - 4\mu(\gamma + \mu)(\mathcal{R}_0 - 1)}}{2}$$

implying that all three eigenvalues have negative real parts when $\mathcal{R}_0 > 1$ and, hence, the $\mathbf{EE_{SIR}}$ is LAS.

Stability of equilibria of the SIS model Next, the Jacobian matrix of (2.13) is

$$\mathbf{J} = \begin{bmatrix} -(\mu + \beta I^*) & \gamma - \beta S^* \\ \beta I^* & -(\gamma + \mu - \beta S^*) \end{bmatrix}. \tag{2.34}$$

Evaluate the Jacobian at $\mathbf{DFE_{SIS}}$ to get

$$\mathbf{J_{DFE}} = \begin{bmatrix} -\mu & \gamma - \beta \\ 0 & -(\gamma + \mu - \beta) \end{bmatrix}$$

which has the eigenvalues

$$\lambda_1 = \beta - (\gamma + \mu), \quad \lambda_2 = -\mu.$$

λ_2 is negative always and $\lambda_1 < 0$ iff $\beta < \gamma + \mu \Leftrightarrow \mathcal{R}_0 < 1$. Hence, the $\mathbf{DFE_{SIS}}$ is LAS when $\mathcal{R}_0 < 1$ and unstable for $\mathcal{R}_0 > 1$.

Turning to the other equilibrium, we evaluate the Jacobian (2.34) at $\mathbf{EE_{SIS}}$ and get (2.17)

$$\mathbf{J_{EE}} = \begin{bmatrix} -(\mu + \beta(\mathcal{R}_0 - 1)/\mathcal{R}_0) & \gamma - \beta/\mathcal{R}_0 \\ \beta(\mathcal{R}_0 - 1)/\mathcal{R}_0 & 0 \end{bmatrix}. \tag{2.35}$$

Thus,

$$\det(\mathbf{J_{EE}} - \lambda I) = \det \begin{bmatrix} -(\mu + \beta(\mathcal{R}_0 - 1)/\mathcal{R}_0) - \lambda & \gamma - \beta/\mathcal{R}_0 \\ \beta(\mathcal{R}_0 - 1)/\mathcal{R}_0 & -\lambda \end{bmatrix} =$$

$$\det \begin{bmatrix} -\beta(\mathcal{R}_0 - 1)/\mathcal{R}_0 - \mu - \lambda & -\mu \\ \beta(\mathcal{R}_0 - 1)/\mathcal{R}_0 & -\lambda \end{bmatrix} = \det \begin{bmatrix} -\mu - \lambda & -\mu - \lambda \\ \beta(\mathcal{R}_0 - 1)/\mathcal{R}_0 & -\lambda \end{bmatrix}.$$

Then, the characteristic equation is

$$(\lambda + \mu)\,(a_0\lambda + a_1) = 0, \tag{2.36}$$

with

$$\begin{aligned} a_0 &= 1, \\ a_1 &= \beta(\mathcal{R}_0 - 1)/\mathcal{R}_0. \end{aligned} \tag{2.37}$$

The eigenvalues of (2.36) are $\lambda_1 = -\mu$ and $\lambda_2 = -\beta(\mathcal{R}_0 - 1)$, therefore, $\mathbf{EE_{SIS}}$ is LAS for $\mathcal{R}_0 > 1$.

Stability of equilibria of the SIRS model Lastly, consider the Jacobian of (2.18)

$$\mathbf{J} = \begin{bmatrix} -(\mu + \beta I^*) & -\beta S^* & \kappa \\ \beta I^* & -(\gamma + \mu - \beta S^*) & 0 \\ 0 & \gamma & -(\kappa + \mu) \end{bmatrix} \tag{2.38}$$

and evaluate at $\mathbf{DFE_{SIRS}}$ as

$$\mathbf{J_{DFE}} = \begin{bmatrix} -\mu & -\beta & \kappa \\ 0 & -(\gamma+\mu-\beta) & 0 \\ 0 & \gamma & -(\kappa+\mu) \end{bmatrix}$$

that has the eigenvalues

$$\lambda_1 = \beta - (\gamma+\mu), \quad \lambda_2 = -\mu, \quad \text{and} \quad \lambda_3 = -(\mu+\kappa).$$

Again, all but λ_1 are always negative and $\lambda_1 < 0$ iff $\beta < \gamma + \mu \Leftrightarrow \mathcal{R}_0 < 1$. Thus, the $\mathbf{DFE_{SIRS}}$ is LAS when $\mathcal{R}_0 < 1$ and unstable for $\mathcal{R}_0 > 1$.

The Jacobian (2.38) evaluated at the $\mathbf{EE_{SIRS}}$ is (2.23)

$$\mathbf{J_{EE}} = \begin{bmatrix} -\mu - \frac{(\gamma+\mu)(\kappa+\mu)(\mathcal{R}_0-1)}{\gamma+\mu+\kappa} & -\beta/\mathcal{R}_0 & \kappa \\ \frac{(\gamma+\mu)(\kappa+\mu)(\mathcal{R}_0-1)}{\gamma+\mu+\kappa} & 0 & 0 \\ 0 & \gamma & -(\kappa+\mu) \end{bmatrix}. \tag{2.39}$$

Then,

$$\det(\mathbf{J_{EE}} - \lambda I) = \det \begin{bmatrix} -\mu - \frac{(\gamma+\mu)(\kappa+\mu)(\mathcal{R}_0-1)}{\gamma+\mu+\kappa} - \lambda & -\beta/\mathcal{R}_0 & \kappa \\ \frac{(\gamma+\mu)(\kappa+\mu)(\mathcal{R}_0-1)}{\gamma+\mu+\kappa} & -\lambda & 0 \\ 0 & \gamma & -\kappa-\mu-\lambda \end{bmatrix}$$

that we simplify by adding the second and subtracting the third row from the first and get

$$\det \begin{bmatrix} -\mu-\lambda & -\mu-\lambda & -\mu-\lambda \\ \frac{(\gamma+\mu)(\kappa+\mu)(\mathcal{R}_0-1))}{\gamma+\mu+\kappa} & -\lambda & 0 \\ 0 & \gamma & -\kappa-\mu-\lambda \end{bmatrix}.$$

Hence, the characteristic equation is

$$(\lambda+\mu)\left(a_0\lambda^2+a_1\lambda+a_2\right)=0, \tag{2.40}$$

with

$$\begin{aligned} a_0 &= 1, \\ a_1 &= \kappa+\mu+\frac{(\gamma+\mu)(\kappa+\mu)(\mathcal{R}_0-1)}{(\gamma+\mu+\kappa)}, \\ a_2 &= (\gamma+\mu)(\kappa+\mu)(\mathcal{R}_0-1). \end{aligned} \tag{2.41}$$

One eigenvalue is negative $\lambda_1=-\mu$ and the two others are given by

$$\lambda_2,\lambda_3=\frac{-\left(\kappa+\mu+\frac{(\gamma+\mu)(\kappa+\mu)(\mathcal{R}_0-1)}{(\gamma+\mu+\kappa)}\right)}{2}\pm \frac{\sqrt{\left(\kappa+\mu+\frac{(\gamma+\mu)(\kappa+\mu)(\mathcal{R}_0-1)}{(\gamma+\mu+\kappa)}\right)^2-4(\gamma+\mu)(\kappa+\mu)(\mathcal{R}_0-1)}}{2},$$

thus, all three have negative real parts when $\mathcal{R}_0>1$ and, hence, $\mathbf{EE_{SIRS}}$ is LAS.

Stability of equilibria of models with many compartments Performing the stability analysis for these "simple" models is rather straightforward due to the low degree of the characteristic polynomial. For models with more compartments we typically encounter polynomials of higher degree, hence, no explicit formulae for their roots may be derived. To tackle this challenge, we turn to an alternative technique and, instead of trying to solve the

characteristic equation, the next section presents how tractable conditions for stability may be derived from the coefficients of the characteristic polynomial.

2.3.2 Routh-Hurtwitz stability criterion

Historically, the need to establish a stability criterion for high degree polynomials comes from the middle of the nineteenth century [39, 40]. E.J. Routh was the first to solve the problem [41], then, independently, similar results were obtained by A. Hurwitz [42], where he found that, in order for all the roots to have negative real parts i.e lie in the left-half plane, some conditions must be imposed on the coefficients. Their results are referred to as the so-called Routh-Hurtwitz stability criterion that is, given a polynomial, derived from the Routh array built as follows.

Let us consider the n^{th} order characteristic polynomial

$$P(\lambda) = a_0\lambda^n + a_1\lambda^{n-1} + a_2\lambda^{n-2} + \cdots + a_{n-1}\lambda^1 + a_n\lambda^0, \tag{2.42}$$

where

$$a_i > 0, \quad \text{for } i = 0, 1, 2, 3, \ldots, n.$$

Then, the corresponding Routh array depicted in Table 2.1 with elements $b_{k,j}$, where $b_{k,j}$ is the element in the k^{th} row and j^{th} column, is obtained by performing the operations

1. The first row of the Routh-array is filled with the coefficients of (2.42) with even indices and the second row is filled with coefficients with odd indices padded with zeroes.

2. The remaining rows are filled using the formula

$$b_{k,j} = \frac{-\det(M_{k,j})}{b_{k-1,1}}, \quad M_{k,j} = \begin{bmatrix} b_{k-1,1} & b_{k-1,j+1} \\ b_{k-2,1} & b_{k-2,j+1} \end{bmatrix}$$

Table 2.1: Routh array

λ^n	$b_{1,1} = a_0$	$b_{1,2} = a_2$	$b_{1,3} = a_4$	$b_{1,4} = a_6$	$\dots$
λ^{n-1}	$b_{2,1} = a_1$	$b_{2,2} = a_3$	$b_{2,3} = a_5$	$b_{2,4} = a_7$	$\dots$
λ^{n-2}	$b_{3,1} = \frac{a_1 a_2 - a_0 a_3}{a_1}$	$b_{3,2} = \frac{a_1 a_4 - a_5 a_0}{a_1}$	$b_{3,3} = \frac{a_1 a_6 - a_7 a_0}{a_1}$	$\dots$	$\dots$
λ^{n-3}	$b_{4,1} = \frac{b_{3,1} a_3 - b_{3,2} a_1}{b_{3,1}}$	$b_{4,2} = \frac{b_{3,1} a_5 - b_{3,3} a_1}{b_{3,1}}$	$b_{4,3}$	$\dots$	$\dots$
$\vdots$	$\vdots$	$\vdots$	$\vdots$	$\vdots$	$\vdots$
λ^1	$b_{k-1,1}$	$b_{k-1,2}$	$b_{k-1,3}$	$\dots$	$\dots$
λ^0	$b_{k,1} = a_n$	0	0	0	0

Consequently, in the first two rows at most the first $\lfloor \frac{n}{2} \rfloor + 1$ entries are non-zero. Then, at most the first $\lfloor \frac{n}{2} \rfloor$ entries are non-zero in rows three and four and every two rows one may establish that the number of non-zero elements is decreasing by one. Thus, in the final row, at most one element is non-zero i.e. a_n. After the Routh array is completed, the stability criterion is derived from its first column as stated in the following Lemma.

Lemma 2.1. *Consider the n^{th} order characteristic polynomial*

$$P(\lambda) = a_0\lambda^n + a_1\lambda^{n-1} + a_2\lambda^{n-2} + \cdots + a_{n-1}\lambda^1 + a_n\lambda^0,$$

where all the coefficients are positive. Then all roots of $P(\lambda)$ have negative real parts iff all elements in the first column of Table 2.1 are positive.

We remark that the number of sign changes in the first column of Table 2.1 corresponds to the number of roots with positive real parts.

We illustrate these conditions by starting with a simple polynomial of degree one

$$P(\lambda) = a_0\lambda^1 + \lambda^0 a_1. \tag{2.43}$$

The corresponding Routh array is

$$\begin{array}{c|cc|} \lambda^1 & a_0 & 0 \\ \lambda^0 & a_1 & 0 \end{array}.$$

We can infer that the root of (2.43) has negative real part provided the conditions

$$a_i > 0 \quad \text{for } i = 0, 1 \tag{2.44}$$

are satisfied by Lemma 2.1.

For a polynomial of degree two

$$P(\lambda) = a_0\lambda^2 + a_1\lambda^1 + \lambda^0 a_2, \tag{2.45}$$

we obtain the Routh array

$$\begin{array}{c|ccc|} \lambda^2 & a_0 & a_2 & 0 \\ \lambda^1 & a_1 & 0 & 0 \\ \lambda^0 & a_2 & 0 & 0 \end{array}.$$

By applying Lemma 2.1, we find that both roots of (2.45) have negative real parts iff

$$a_i > 0 \quad \text{for } i = 0, 1. \tag{2.46}$$

For a polynomial of degree three

$$P(\lambda) = a_0\lambda^3 + a_1\lambda^2 + a_2\lambda^1 + \lambda^0 a_3, \tag{2.47}$$

we get the Routh array

$$\begin{array}{c|ccc} \lambda^3 & a_0 & a_2 & 0 \\ \lambda^2 & a_1 & a_3 & 0 \\ \lambda^1 & \frac{a_1a_2-a_0a_3}{a_1} & 0 & 0 \\ \lambda^0 & a_3 & 0 & 0 \end{array}.$$

Then, Lemma 2.1 leads to the following set of inequalities

$$\begin{aligned} a_i > 0, \quad \text{for } i = 0, 1, 2, 3, \text{ and} \\ a_1a_2 > a_0a_3. \end{aligned} \tag{2.48}$$

Lastly, for polynomial of degree four

$$P(\lambda) = a_0\lambda^4 + a_1\lambda^3 + a_2\lambda^2 + a_3\lambda^1 + \lambda^0 a_4, \tag{2.49}$$

we have the Routh array

$$\begin{array}{c|ccc} \lambda^4 & a_0 & a_2 & a_4 \\ \lambda^3 & a_1 & a_3 & 0 \\ \lambda^2 & \frac{a_1a_2-a_0a_3}{a_1} & a_4 & 0 \\ \lambda^1 & \frac{a_1a_2a_3-a_0a_3^2-a_1^2a_4}{a_1a_2-a_0a_3} & 0 & 0 \\ \lambda^0 & a_4 & 0 & 0 \end{array}$$

yielding the following inequalities by Lemma 2.1

$$\begin{aligned} a_i > 0, \quad \text{for } i = 0, 1, 2, 3, 4, \\ a_1a_2 > a_0a_3, \quad \text{and} \quad a_1a_2a_3 > a_0a_3^2 + a_1^2a_4. \end{aligned} \tag{2.50}$$

Recall the characteristic polynomials (2.36), (2.32), and (2.40) computed earlier in this chapter for the **EE** of various compartmental models. For each of these polynomials, $(\lambda+\mu)$ has been factorized separating the eigenvalue $-\mu$, hence, for stability analysis it is sufficient to apply the Routh-Hurwitz criterion to the remaining term that is of at most degree two.

Thus, we only need to investigate the positivity of the coefficients that is clearly equivalent with $\mathcal{R}_0 > 1$, just as we have concluded before.

The Routh-Hurwitz stability criterion will be used in Chapters 3 and 4 to investigate a third and fourth-order characteristic polynomial where direct computation of roots is not feasible.

2.4 Bifurcations of equilibria

In our discussions in Section 2.3 on the stability of equilibria for various models, we concluded that the **DFE** exists for all parameters and it is LAS when $\mathcal{R}_0 < 1$ and unstable when $\mathcal{R}_0 > 1$. It is apparent that the dynamics changes significantly when $\mathcal{R}_0 = 1$, resulting in a bifurcation of this equilibrium. Moreover, we also found that when $\mathcal{R}_0 > 1$ there exists a LAS positive **EE**. Later, we will see that this phenomenon corresponds to a transcritical bifurcation. In this section, we give a brief overview of all bifurcations that we observed in our models, namely, the transcritical, saddle-node, and Hopf bifurcations. For a detailed analysis we refer to [43, 44].

2.4.1 Transcritical bifurcation

In a transcritical bifurcation two curves of equilibria intersect at a critical bifurcation parameter value. Both curves existed on either side of the bifurcation value, however, the stability of the fixed point along each curve change on passing through the critical point.

The general conditions for the transcritical bifurcation to occur lead to the normal form equation

$$\frac{dy}{dt} = g_{\mp}(y, p) = py \mp y^2, \quad y \in \mathbb{R}^1, \tag{2.51}$$

where $p \in \mathbb{R}$ is the bifurcation parameter.

A sketch of the function g_- and g_+ for representative p values, and the corresponding phase diagrams for equation (2.51) are plotted in Figures 2.9, 2.10, respectively. On the phase

diagram the stationary points are marked as circles (empty when unstable and filled when stable) and the arrows indicate whether the solution is increasing or decreasing.

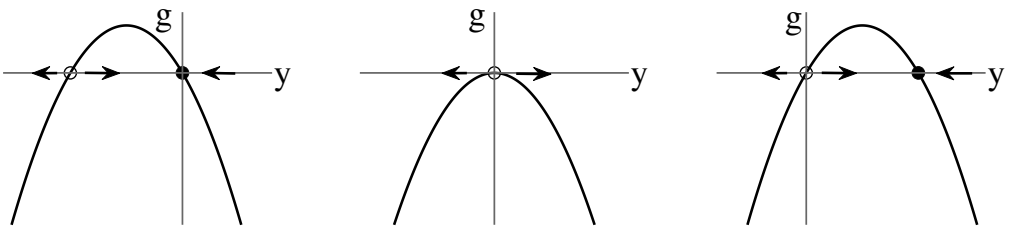

(a) $p < 0$ (b) $p = 0$ (c) $p > 0$

Figure 2.9: Graph of g_- and phase diagrams for representative values of the parameter p.

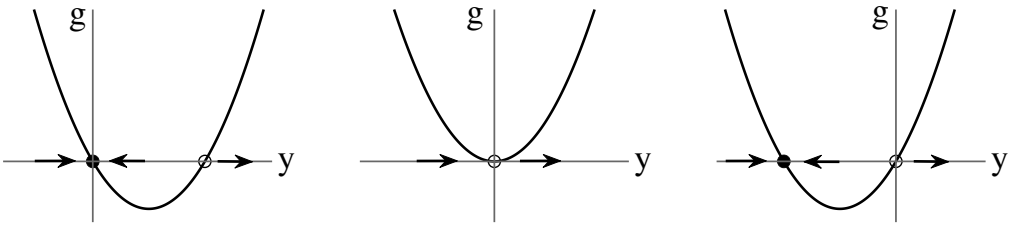

(a) $p > 0$ (b) $p = 0$ (c) $p < 0$

Figure 2.10: Graph of g_+ and phase diagrams for representative values of the parameter p.

The bifurcation diagrams for these two cases are shown in Figure 2.11, where we also indicate stabilities of the different branches of fixed points.

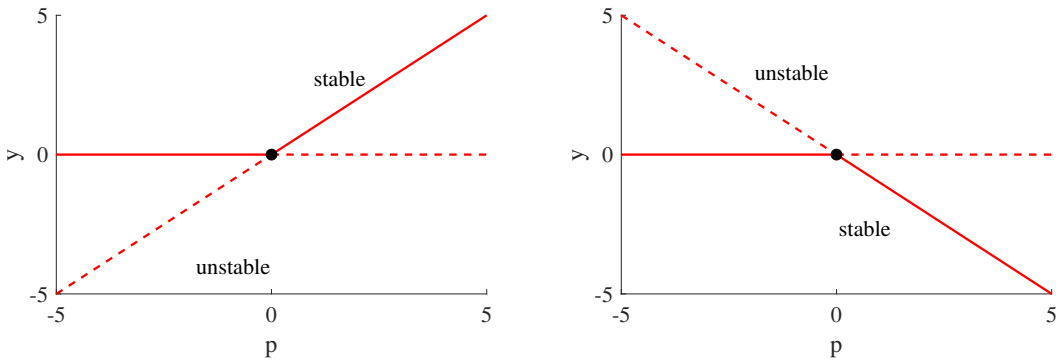

(a) Forward transcritical bifurcation (b) Backward transcritical bifurcation

Figure 2.11: Transcritical bifurcation at $p = 0$. Continuous lines denote stable, whilst dashed lines unstable equilibrium.

Thus, an exchange of stability has occurred at $p = 0$. This type of bifurcation is called a transcritical bifurcation and they can be of forward or backward type corresponding to g_- or g_+, respectively.

In our later sections, we will be able to establish transcritical bifurcations of both types in higher dimensional nonlinear systems. The analysis used here is based on the general center manifold theory and for detailed analysis we refer to [45–47].

2.4.2 Saddle-node bifurcation

The bifurcation of an equilibrium point where one goes from zero to two fixed points as a parameter is varied is called saddle-node. This bifurcation is also referred to as a tangent or fold bifurcation.

Consider again the normal forms for this bifurcation

$$\frac{dy}{dt} = g_{\pm}(y, p) = p \pm y^2, \; y \in \mathbb{R}^{\mathbb{1}}, \tag{2.52}$$

where $p \in \mathbb{R}$ is the bifurcation parameter. In Figures 2.12, 2.13 we plotted the graphs of g_+ and g_-, respectively, and the corresponding phase diagrams for three representative

parameter values.

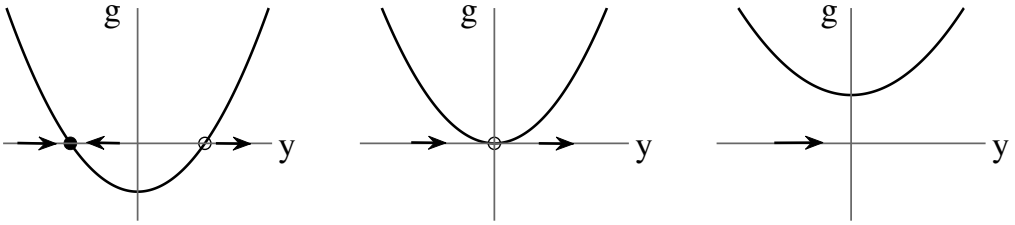

(a) $p < 0$ (b) $p = 0$ (c) $p > 0$

Figure 2.12: Graph of g_+ and phase diagram for various values of bifurcation parameter p.

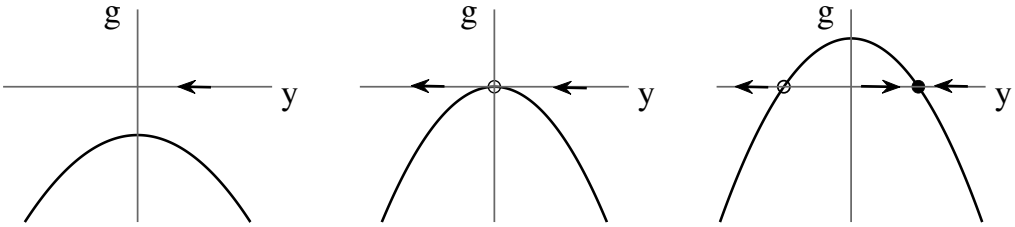

(a) $p < 0$ (b) $p = 0$ (c) $p > 0$

Figure 2.13: Graph of g_- and phase diagram for various values of the parameter p.

The bifurcation diagrams for these two cases are shown in Figure 2.14, where we also indicate stabilities of the different branches of fixed points.

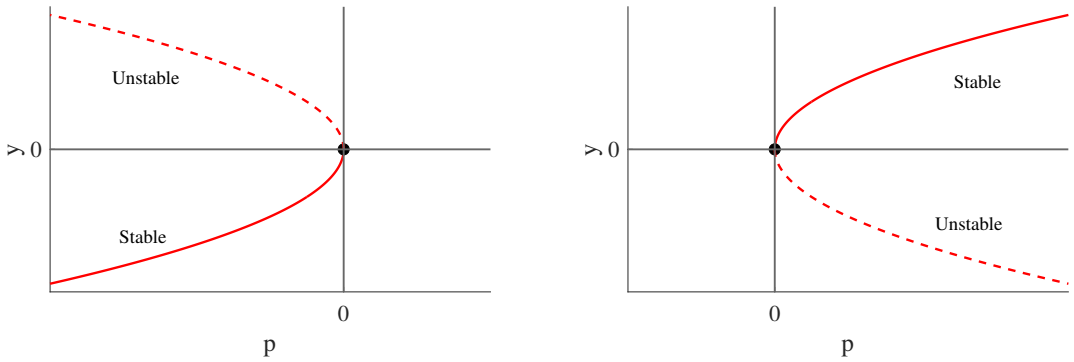

Figure 2.14: Saddle-node bifurcation at $p = 0$. Continuous curves denote stable, whilst dashed curves unstable equilibrium.

It is important to note here that in the investigation of our nonlinear model, apart from the bifurcations of equilibria, we found saddle-node (or fold) bifurcations on limit cycles, which are important in the study of oscillatory behavior in dynamical systems. In a saddle-node bifurcation of cycles, there are two limit cycles in the system, one stable and one unstable, that collide at a critical value of a parameter. At the bifurcation point, the two limit cycles coalesce and disappear, [43]. The presence of such bifurcations was investigated only in our numerical study of the pertussis model in Sections 3.4, 4.4.3.

2.4.3 Hopf bifurcation

Hopf bifurcation of a fixed point of a vector field is where the linearization has a pair of (nonzero) purely imaginary eigenvalues. Provided a nondegeneracy condition (involving the quadratic and cubic nonlinear terms) holds, this bifurcation gives rise to a unique periodic orbit.

Consider the following normal forms

$$\frac{dx}{dt} = px - y + ax(x^2 + y^2), \tag{2.53a}$$
$$\frac{dy}{dt} = x + py + ay(x^2 + y^2), \tag{2.53b}$$

with $a = \pm 1$, where $p \in \mathbb{R}$ is the bifurcation parameter. The number a tells us whether the bifurcating periodic orbit is stable ($a < 0$) or unstable ($a > 0$). The case $a < 0$ is referred to as a supercritical bifurcation, and the case $a > 0$ is referred to as a subcritical bifurcation. The bifurcation diagrams are plotted in Figure 2.15.

The equilibrium of this system is $(0, 0)$ and the Jacobian evaluated at this equilibrium is

$$\mathbf{J} = \begin{bmatrix} p & -1 \\ 1 & p \end{bmatrix}$$

with corresponding eigenvalues $\lambda_{1,2} = p \pm i$, thus the equilibrium is stable when $p < 0$ and unstable when $p > 0$. At the bifurcation point $p = 0$, there is a pair of purely imaginary eigenvalues and the system undergoes a Hopf bifurcation.

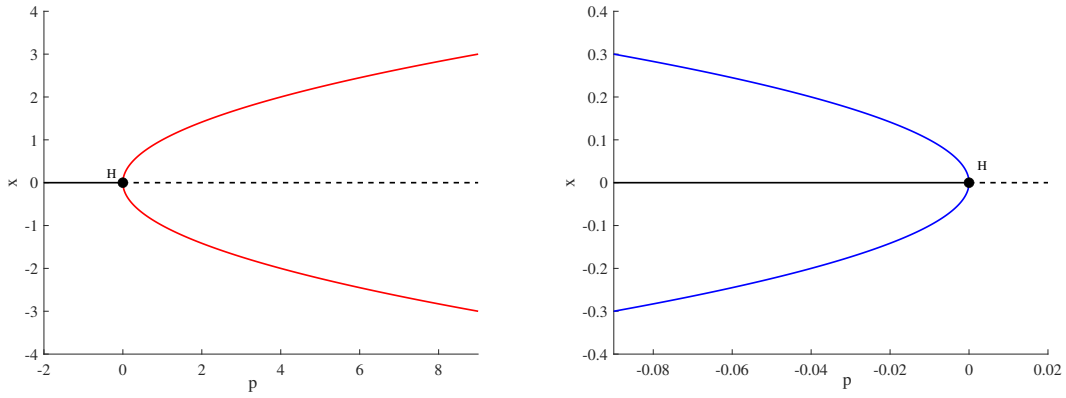

Figure 2.15: Supercritical (left) and subcritical (right) Hopf bifurcation diagram. Stable and unstable equilibrium are shown by the black continuous and dashed lines, respectively. The red and blue curves represent the maximum and minimum values of the periodic solutions, respectively.

2.5 MatCont

`MatCont` is a Matlab numerical continuation package for bifurcation analysis [48] and was used to construct all bifurcation diagrams throughout this dissertation.

The software package is accompanied by a Graphical User Interface (GUI) for the hands-on numerical study of parametrized nonlinear ODEs and computes curves of equilibria, Hopf points, limit cycles, limits points, branch points of equilibria, bifurcation points of limit cycles, and homoclinic orbits [21, 23, 48]. It implements a prediction-correction method based on the Moore-Penrose matrix pseudoinverse (also known as the generalized inverse) to construct the curves. In addition to this, time integration makes use of standard Matlab ODE solvers. Despite the fact that this program is primarily designed for parametrized dynamical systems, the numerical continuation techniques can be applied to analyze discretized

solutions of partial differential equations [23].

We now discuss some features of the GUI and how they function. One of these features is the system window, see Figure 2.16, where we input the system of differential equations (2.53) with $a = -1$ as an illustration.

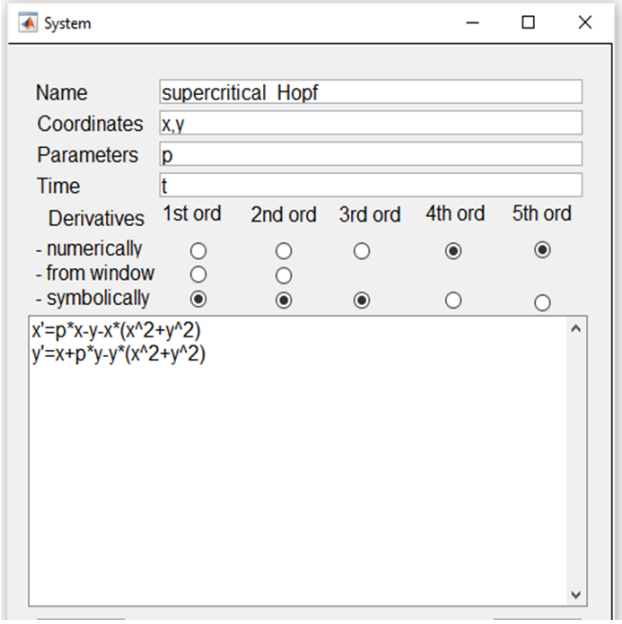

Figure 2.16: `MatCont` system window displaying the system of ODEs in (2.53).

The origin is an equilibrium of the system for all $p \in \mathbb{R}$. Continuation w.r.t. parameter p leads to the bifurcation diagram in Figure 2.17. Throughout this thesis we will construct such bifurcation diagrams but showing the branching of only one component of the variables in the system, such as in Figure 2.15. There is a Hopf bifurcation at $p = 0$ along the equilibrium branch, labeled by H and the bifurcation is supercritical because the computed first Lyapunov coefficient is -2. Thus stable periodic oscillations emerge. The computation process can be paused, continued, or terminated when a bifurcation point is detected and the coordinates of such points are computed.

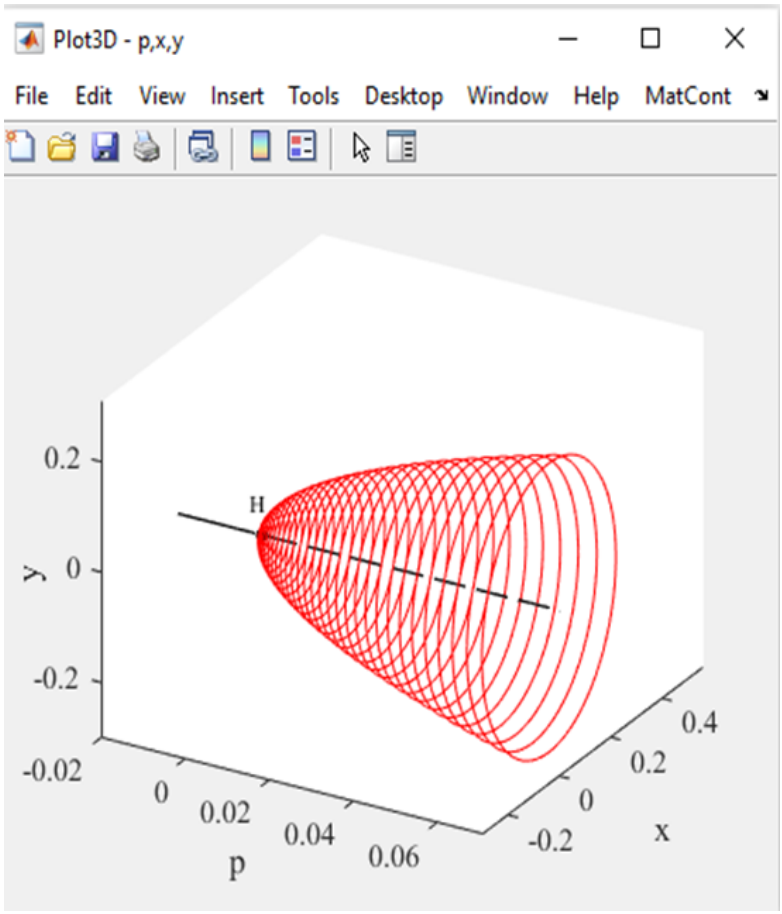

Figure 2.17: Graphic window of `MatCont` displaying the supercritical Hopf bifurcation.

Parametrization of the system under investigation is done in the starter window and the adjustment of these parameters is done in the integrator window. There is also the main window from which all other windows are launched.

2.6 Summary

The compartmental ODE models of infectious diseases were introduced in this chapter. Then, stability analysis of the SIR, SIS, and SIRS models as well as the computation of the disease-free and endemic equilibria was discussed. The chapter also gave an overview of the well-known Routh-Hurwitz stability criteria and their application. Finally, the transcritical,

saddle-node, and Hopf bifurcations were discussed together with `MatCont`, a software designed for numerical bifurcation analysis. In the next chapter, these methods will be applied to investigate the dynamics of the SIRWS system.

Chapter 3

Dynamics of an SIRWS model with waning of immunity and varying immune boosting period

Published in the Journal of Biological Dynamics
Authors: Richmond Opoku-Sarkodie, Ferenc A. Bartha, Mónika Polner, Gergely Röst [61].

3.1 Introduction

The susceptible-infectious-recovered (SIR) approach has been widely applied in diverse forms to understand the transmission dynamics of communicable diseases. For many infections, immunity is not lifelong, and after some time, recovered individuals may become susceptible again. Prior to that, repeated exposure to the pathogen might boost the immune system, thus prolonging the length of immune period. A very general framework of waning-boosting dynamics has been introduced in [49]. Special cases of that are the SIRWS compartmental models, where W is the collection of individuals whose immunity is waning but can be boosted upon repeated exposure without experiencing the disease again.

SIRWS models formulated as systems of ordinary differential equations were studied in [16,

19, 50–52]. In these models, the immunity period is divided into two parts: upon recovery, previously infected individuals move to R, and from there they may transit to W as time elapses. If they are exposed again while being in W, their immunity can be boosted and they move back R. Otherwise, they eventually lose their immunity, become susceptible again, and move back to S. The aforementioned studies model these two phases of the immune period by a symmetric partitioning, by assuming identical rates of transition from R to W and from W to S.

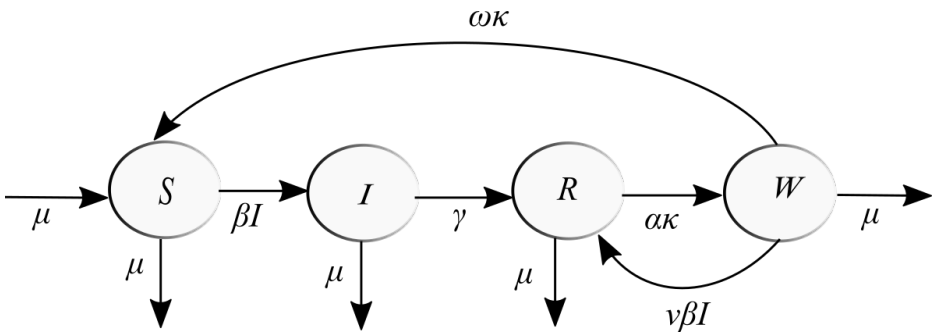

Figure 3.1: Flow diagram of the SIRWS system (3.1).

In contrast, our work removes this symmetry constraint, and we analyze how the different partitioning of the immune period into R and W, and varying boosting rates affect the dynamics of the model. First, the existence of equilibria and analytic conditions for their local stability are established. Then, using numerical tools and methods, we observe the emergence of complex phenomena through various bifurcations, such as endemic double bubbles, and multiple regions of bistability.

3.2 Modified SIRWS model

This section describes the SIRWS compartmental model in which the population is divided as follows. The individuals susceptible to infection are placed in S, those currently infectious in I, and those recovered from infection are divided into two compartments based on their immunity level. The fully immune are found in R and those with waned immunity are in

W. Figure 3.1 shows the model's flow diagram, which is governed by the system of ordinary differential equations

$$\frac{dS}{dt} = -\beta IS + \omega\kappa W + \mu(1 - S), \tag{3.1a}$$
$$\frac{dI}{dt} = \beta IS - \gamma I - \mu I, \tag{3.1b}$$
$$\frac{dR}{dt} = \gamma I - \alpha\kappa R + \nu\beta IW - \mu R, \tag{3.1c}$$
$$\frac{dW}{dt} = \alpha\kappa R - \omega\kappa W - \nu\beta IW - \mu W, \tag{3.1d}$$

where β, γ, and μ are referred to as the infection rate, recovery rate, and birth and death rate, respectively. Recovered individuals may lose immunity by the chain of transitions $R \to W \to S$. The average duration of immune protection, that is the average time required to complete both of these transitions is $\kappa^{-}1$ and, hence, κ is the immunity waning rate. Members of W are still immune to infection and are subject to immune boosting upon re-exposure. The frequency of that re-exposure is modulated by the boosting force ν. In our analysis, hosts going through boosting are not infectious, such as in [16, 19, 49, 52], as opposed to [18].

The population is normalized to 1 that is $N(t) = S(t) + I(t) + R(t) + W(t) = 1$ for all $t \geq 0$. Vital dynamics is modeled with the rate μ for birth and death, and disease-induced fatality is not considered. In earlier SIRWS model studies, e.g. [16, 19, 50, 52], the immune waning rates are the same for individuals who move from the recovered compartment to the waning compartment and for those who transition onward to the susceptible compartment. In contrast, we consider an asymmetric partition of the immunity period by introducing the parameters $\alpha > 1$ and $\omega > 1$ setting the average time spent in R and W to $(\alpha\kappa)^{-1}$ and $(\omega\kappa)^{-1}$, respectively. Hence,

$$\frac{1}{\alpha\kappa} + \frac{1}{\omega\kappa} = \frac{1}{\kappa} \qquad \text{that is} \qquad \omega = \frac{\alpha}{\alpha - 1}. \tag{3.2}$$

Note that the special case $\alpha = \omega = 2$, representing the symmetric partition of the immunity period is what was considered in the aforementioned studies.

By considering various limiting scenarios of boosting for (3.1), it is apparent that the system exhibits SIRS-like dynamics as $\nu \to 0+$ and SIR-like dynamics as $\nu \to \infty$. In addition, we observe SIR-like dynamics as SIR-like dynamics as $\alpha \to 1+$ ($\omega \to \infty$) and SIS-like dynamics as $\alpha \to \infty$ ($\alpha \to \infty$).

3.3 Equilibria and stability

This section first investigates system (3.1) in order to establish the formulae for the equilibria of our SIRWS model. Then, we analyze the transcritical bifurcation where these equilibria exchange stability in Section 3.3.1. Finally, we derive the Routh-Hurwitz stability criterion in Section 3.3.2.

We begin by utilizing the relation

$$W(t) = 1 - S(t) - I(t) - R(t),$$

to obtain the reduced system

$$\frac{dS}{dt} = -\beta IS + \omega\kappa(1 - S - I - R) + \mu(1 - S), \tag{3.3a}$$

$$\frac{dI}{dt} = \beta IS - \gamma I - \mu I, \tag{3.3b}$$

$$\frac{dR}{dt} = \gamma I - \alpha\kappa R + \nu\beta I(1 - S - I - R) - \mu R. \tag{3.3c}$$

Note that the region relevant to our epidemiological setting

$$(S(t), I(t), R(t)) \in \mathcal{D} := \left\{(s, i, r) \in \mathbb{R}^3_{\geq 0} \mid 0 \leq s + i + r \leq 1\right\}$$

is forward invariant.

Now, let us turn our attention to equilibria of (3.3) and seek solutions to the steady-state equations

$$-\beta I^* S^* + \omega\kappa(1 - S^* - I^* - R^*) + \mu(1 - S^*) = 0, \tag{3.4a}$$

$$\beta I^* S^* - \gamma I^* - \mu I^* = 0, \tag{3.4b}$$

$$\gamma I^* - \alpha\kappa R^* + \nu\beta I^*(1 - S^* - I^* - R^*) - \mu R^* = 0. \tag{3.4c}$$

From (3.4b), we obtain that either $I^* = 0$ or $S^* = \frac{\gamma+\mu}{\beta}$. In the first case, $R^* = 0$ follows from (3.4c) and, finally, $S^* = 1$ from (3.4a). Hence we obtain $(1, 0, 0)$ the *disease free equilibrium* (DFE) of (3.3). In the latter case when

$$S^* = \tfrac{\gamma+\mu}{\beta}, \tag{3.5}$$

equation (3.4a) yields

$$I^* = \frac{(\mu + \omega\kappa)(1 - S^*) - \omega\kappa R^*}{\beta S^* + \omega\kappa} = \frac{c_0 c_1}{\beta} - \frac{\omega\kappa}{\gamma + \mu + \omega\kappa} R^*,$$

with

$$c_0 = \frac{1}{\gamma + \mu + \omega\kappa} \cdot \left(1 + \frac{\omega\kappa}{\mu}\right) \qquad \text{and}$$
$$c_1 = \mu(\beta - (\gamma + \mu)).$$

Then, using the formulae for S^* and I^*, (3.4c) results in a quadratic equation for R^*. It is straightforward to verify that the leading term coefficient is positive, hence, the graph of it

is an open-up parabola with the y-intercept

$$\frac{\gamma c_0 c_1}{\beta}\left(1+\frac{\nu c_0 c_1}{\mu+\omega\kappa}\right).$$

Moreover, the solutions are obtained as follows. Substituting the formulae for S^* and I^* into (3.4c), we obtain the quadratic equation

$$A(R^*)^2 + BR^* + C = 0,$$

with coefficients

$$\begin{aligned}
A &= \frac{\omega\kappa\nu\beta(\gamma+\mu)}{(\gamma+\mu+\omega\kappa)^2},\\
B &= \frac{\omega\kappa\nu(\gamma+\mu+c_0c_1)-[(\gamma+\mu)(\mu+\alpha\kappa+\omega\kappa+\nu c_0c_1)+\omega\kappa(\alpha\kappa+\beta\nu)]}{\gamma+\mu+\omega\kappa},\\
C &= \frac{c_0c_1}{\beta}[\beta\nu+\gamma-\gamma\nu-\mu\nu-c_0c_1\nu].
\end{aligned}$$

The y-intercept C may be simplified as

$$\begin{aligned}
C &= \frac{c_0c_1}{\beta}\left(\beta\nu+\gamma-\gamma\nu-\mu\nu-c_0c_1\nu\right),\\
&= c_0c_1\nu+\frac{c_0c_1\gamma}{\beta}-\frac{c_0c_1\nu}{\beta}\left(\gamma+\mu+c_0c_1\right),\\
&= c_0c_1\nu+\frac{c_0c_1\gamma}{\beta}-\frac{c_0c_1\nu}{\beta}(\beta-\frac{c_0c_1\gamma}{\omega\kappa+\mu}-c_0c_1+c_0c_1),\\
&= \frac{c_0c_1\gamma}{\beta}+\frac{c_0^2c_1^2\gamma\nu}{\beta(\omega\kappa+\mu)},\\
&= \frac{c_0c_1\gamma}{\beta}\left(1+\frac{c_0c_1\nu}{\omega\kappa+\mu}\right).
\end{aligned}$$

Then, the solution formula gives

$$R^*_{\pm} = \frac{-B}{2A} \mp \frac{\sqrt{B^2-4AC}}{2A}. \tag{3.6}$$

We split (3.6) into two parts and evaluate them separately.

$$
\begin{aligned}
\frac{-B}{2A} &= \frac{\gamma+\mu+\omega\kappa}{2\omega\kappa\nu\beta(\gamma+\mu)}\left((\gamma+\mu)(\mu+\alpha\kappa+\omega\kappa+\nu c_0c_1)+\omega\kappa(\alpha\kappa+\beta\nu)-\omega\kappa\nu(\gamma+\mu+c_0c_1)\right)\\
&= \frac{\gamma+\mu+\omega\kappa}{2\omega\kappa\nu\beta(\gamma+\mu)}\left((\gamma+\mu)(\alpha\kappa+\omega\kappa+\mu)+(\gamma+\mu)\nu c_0c_1+\omega\alpha\kappa^2+\omega\kappa\beta\nu-\omega\kappa\nu\left(\beta-\frac{\gamma c_0c_1}{\omega\kappa+\mu}\right)\right)\\
&= \frac{\gamma+\mu+\omega\kappa}{2\omega\kappa\beta}\left(\frac{(\gamma+\mu)(\alpha\kappa+\omega\kappa+\mu)+\omega\alpha\kappa^2}{\nu(\gamma+\mu)}+\frac{(\gamma+\mu)\nu c_0c_1}{\nu(\gamma+\mu)}+\frac{\omega\kappa\nu\gamma c_0c_1}{\nu(\gamma+\mu)(\omega\kappa+\mu)}\right)\\
&= \frac{\gamma+\mu+\omega\kappa}{2\omega\kappa\beta}\left(\frac{c_2}{\nu(\gamma+\mu)}+c_0c_1+\frac{\omega\kappa\gamma c_0c_1}{(\omega\kappa+\mu)(\gamma+\mu)}\right)\\
&= \frac{\gamma+\mu+\omega\kappa}{2\omega\kappa\beta}\left(\frac{c_2}{\nu(\gamma+\mu)}+c_0c_1+\frac{\omega\kappa\gamma(\beta-\gamma-\mu)}{(\omega\kappa+\mu+\gamma)(\gamma+\mu)}\right)\\
&= \frac{\gamma+\mu+\omega\kappa}{2\omega\kappa\beta}\left(\frac{c_2}{\nu(\gamma+\mu)}+c_0c_1+c_0c_1-\frac{c_1}{\gamma+\mu}\right)\\
&= \frac{\gamma+\mu+\omega\kappa}{2\omega\kappa\beta}\left(\frac{c_2}{\nu(\gamma+\mu)}+2c_0c_1-\frac{c_1}{\gamma+\mu}\right).
\end{aligned}
$$

where

$$c_2 = (\gamma+\mu)(\alpha\kappa+\omega\kappa)+\mu(\gamma+\mu)+\alpha\omega\kappa^2$$

Then, the other term in (3.6) is

$$
\begin{aligned}
&\mp\frac{\sqrt{B^2-4AC}}{2A} =\\
&\quad= \mp\frac{(\gamma+\mu+\omega\kappa)^2}{2\omega\kappa\nu\beta(\gamma+\mu)}\sqrt{\frac{(\mu(\beta-\gamma-\mu))^2}{(\gamma+\mu+\omega\kappa)^2}\nu^2+\frac{T_0}{(\gamma+\mu+\omega\kappa)^2}\nu+\frac{((\gamma+\mu)(\alpha\kappa+\omega\kappa+\mu)+\alpha\omega\kappa^2)^2}{(\gamma+\mu+\omega\kappa)^2}},
\end{aligned}
$$

with

$$
\begin{aligned}
T_0 &= 2(\beta-(\gamma+\mu))(\gamma\mu^2+\mu^3+\omega\kappa\mu^2+\alpha\kappa\mu^2+\alpha\gamma\kappa\mu+\omega\gamma\kappa\mu+2\alpha\omega\gamma\kappa^2+\alpha\omega\mu\kappa^2)\\
&= 4\gamma\alpha\omega\kappa^2(\beta-(\gamma+\mu))+2\mu(\beta-(\gamma+\mu))[(\gamma+\mu)(\omega\kappa+\alpha\kappa+\mu)+\alpha\omega\kappa^2]\\
&= c_3+2c_1c_2.
\end{aligned}
$$

where

$$c_3 = 4\gamma(\beta - (\gamma + \mu))\alpha\omega\kappa^2$$

Hence,

$$\begin{aligned}
&\mp\frac{\sqrt{B^2 - 4AC}}{2A} = \\
&= \mp\frac{(\gamma + \mu + \omega\kappa)^2}{2\omega\kappa\nu\beta(\gamma + \mu)}\sqrt{\frac{c_1^2}{(\gamma + \mu + \omega\kappa)^2}\nu^2 + \frac{(2c_1c_2 + c_3)}{(\gamma + \mu + \omega\kappa)^2}\nu + \frac{c_2^2}{(\gamma + \mu + \omega\kappa)^2}} \\
&= \mp\frac{\gamma + \mu + \omega\kappa}{2\omega\kappa\nu\beta(\gamma + \mu)}\sqrt{c_1^2\nu^2 + c_2^2 + 2\nu c_1c_2 + c_3\nu} \\
&= \mp\frac{\gamma + \mu + \omega\kappa}{2\omega\kappa\nu\beta(\gamma + \mu)}\sqrt{(c_1\nu + c_2)^2 + c_3\nu}.
\end{aligned}$$

Recombining the two terms yields the formula

$$R_{\pm}^* = \frac{\gamma + \mu + \omega\kappa}{2\beta\omega\kappa}\left[\left(2c_0 - \frac{1}{\gamma + \mu}\right)c_1 + \frac{1}{\nu(\gamma + \mu)}\left(c_2 \mp \sqrt{(c_1\nu + c_2)^2 + c_3\nu}\right)\right]. \tag{3.7}$$

Finally, substituting (3.7) into the formula for I^* results in

$$I_{\pm}^* = \frac{\pm\sqrt{(c_1\nu + c_2)^2 + c_3\nu} + (c_1\nu - c_2)}{2\beta\nu(\gamma + \mu)}. \tag{3.8}$$

Hence, we obtained the two remaining equilibria of (3.3), namely the *endemic equilibrium*

$$\mathbf{EE}_+ = (S^*, I_+^*, R_+^*),$$

and

$$\mathbf{EE}_- = (S^*, I_-^*, R_-^*).$$

Clearly, $I_-^* \leq 0$ whenever the square root is real as the inequality is readily satisfied for

$\beta < \gamma + \mu$ (then $c_1, c_3 < 0$) and directly follows from

$$\sqrt{(c_1\nu + c_2)^2 + c_3\nu} \geq |c_1\nu - c_2| \quad \Leftrightarrow \quad 4c_1c_2 + c_3 \geq 0, \tag{3.9}$$

when $\beta \geq \gamma + \mu$ (then $c_1, c_3 \geq 0$). Moreover, the condition $\beta \geq \gamma + \mu$ is sufficient (but not necessary) for $I^*_\pm \in \mathbb{R}$. Obviously, in the epidemiological setting of this chapter, solely $\mathbf{EE}_+$ may be admissible.

Another important implication of (3.9) is that

$$I^*_+ > 0 \Leftrightarrow \beta > \gamma + \mu \quad \text{and} \quad I^*_+ = 0 \text{ for } \beta = \gamma + \mu.$$

Observe that, in the case of equality, $(1, 0, 0) = \mathbf{EE}_+$ holds. Furthermore, again for $\beta \geq \gamma+\mu$, the parabola for R^* has a positive y-intercept, thus, both solutions are either positive or negative. Moreover, we have $R^*_- > 0$ as $2c_0 - \frac{1}{\gamma+\mu} > 0$ is satisfied and $c_1 \geq 0$. These imply the positivity of the other root which is $R^*_+ > 0$.

Now, summing (3.4a), (3.4b), and (3.4c) results in

$$(\omega\kappa + \mu + \nu\beta I^*)(1 - S^* - I^* - R^*) - \alpha\kappa R^* = 0,$$

hence, $S^* + I^* + R^* \leq 1$ must hold for non-negative S^*, I^*, R^* implying $\xi_+ \in \mathcal{D} \Leftrightarrow \beta \geq \gamma + \mu$.

Finally, note that the *basic reproduction number*, see *e.g.* [49], of the system (3.3) – and of (3.1) – is

$$\mathcal{R}_0 = \frac{\beta}{\gamma + \mu},$$

thus, we may rewrite the condition $\beta \geq \gamma + \mu$ as $\mathcal{R}_0 \geq 1$.

Before continuing the analysis, let us summarize our findings so far.

- There is a unique DFE $(1, 0, 0) \in \mathcal{D}$, which exists for all parameter values in the system.
- If $R_0 \leq 1$, then there is no other equilibrium in $\mathcal{D}$.
- If $R_0 > 1$, then there is a unique, positive $\mathbf{EE}_+ \in \mathcal{D}$.

3.3.1 Transcritical bifurcation at $\mathcal{R}_0 = 1$

For the stability analysis of the disease-free equilibrium $(1, 0, 0)$, consider the Jacobian matrix for our SIRWS system (3.3)

$$J = \begin{bmatrix} -(\omega\kappa + \mu + \beta I) & -\beta S - \omega\kappa & -\omega\kappa \\ \beta I & -(\gamma + \mu - \beta S) & 0 \\ -\nu\beta I & \gamma - 2\nu\beta I + \nu\beta(1 - S - R) & -(\alpha\kappa + \mu + \nu\beta I) \end{bmatrix} \tag{3.10}$$

and evaluate at the DFE $(1, 0, 0)$

$$J|_{(1,0,0)} = \begin{bmatrix} -(\omega\kappa + \mu) & -\beta - \omega\kappa & -\omega\kappa \\ 0 & -(\gamma + \mu - \beta) & 0 \\ 0 & \gamma & -(\alpha\kappa + \mu) \end{bmatrix}.$$

Then, the corresponding eigenvalues are

$$\lambda_1 = \beta - (\gamma + \mu), \quad \lambda_2 = -(\mu + \alpha\kappa), \quad \text{and} \quad \lambda_3 = -(\mu + \omega\kappa).$$

The two eigenvalues λ_2, λ_3 are negative and $\lambda_1 < 0$ iff $\beta < \gamma + \mu$. Hence, the DFE is locally asymptotically stable when $\mathcal{R}_0 < 1$ and unstable for $\mathcal{R}_0 > 1$.

The following Theorem describes the bifurcation associated with this stability change at $\mathcal{R}_0 = 1$ that is also demonstrated in Figure 3.2.

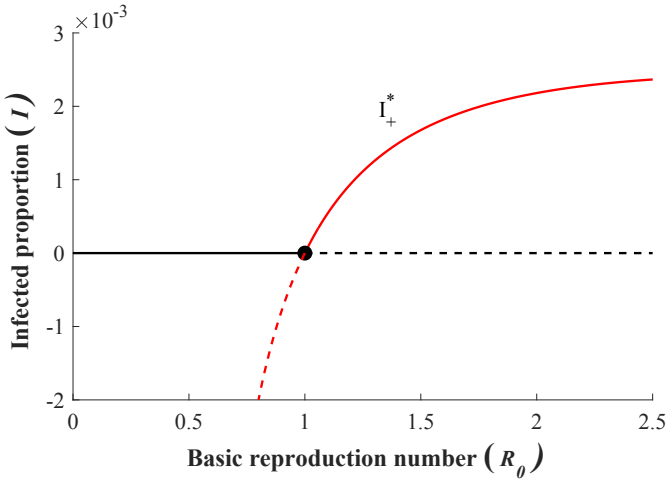

Figure 3.2: Transcritical bifurcation of forward type and the appearance of the LAS endemic equilibrium $\mathbf{EE}_+$ at $\mathcal{R}_0 = 1$.

The proof relies on Theorem 4.1 of [45] based on center manifold theory [46, 47]. For the sake of completeness, we present the relevant version of the original theorem.

Theorem 3.1. *Let $f \in C^2(\mathbb{R}^n \times \mathbb{R}, \mathbb{R}^n)$ and consider the system of ordinary differential equations*

$$\frac{dx}{dt} = f(\mathbf{x}, b),$$

with b as a parameter. Assume that $\mathbf{0}$ is an equilibrium point, i.e., $f(\mathbf{0}, b) = 0$ for all $b \in \mathbb{R}$. In addition, assume the following:

(i) The linearization of the system at $(\mathbf{0}, 0)$

$$A := D_{\mathbf{x}} f(\mathbf{0}, 0) = \left(\frac{\partial f_i}{\partial \mathbf{x}_j}(\mathbf{0}, 0) \right)_{i,j=1}^{n}$$

has zero as a simple eigenvalue and all other eigenvalues of A have negative real parts.

(ii) The matrix A has a non-negative right eigenvector w and a left eigenvector v corresponding to the zero eigenvalue.

Let f_k be the k-th component of f and define

$$Z_1 = \sum_{k,i,j=1}^{n} v_k w_i w_j \frac{\partial^2 f_k}{\partial \mathbf{x}_i \partial \mathbf{x}_j}(\mathbf{0}, 0) \qquad \textit{and}$$
$$Z_2 = \sum_{k,i=1}^{n} v_k w_i \frac{\partial^2 f_k}{\partial \mathbf{x}_i \partial b}(\mathbf{0}, 0).$$

If $Z_1 < 0$ and $Z_2 > 0$, then as b changes from negative to positive, the equilibrium $\mathbf{0}$ changes its stability from stable to unstable. At the same time, a negative unstable equilibrium becomes positive and locally asymptotically stable. Hence, a forward bifurcation occurs at $b = 0$.

Theorem 3.2. *A transcritical bifurcation of forward-type occurs at $\mathcal{R}_0 = 1$.*

Proof. Fix all parameters but β that will serve as the bifurcation parameter with $\beta^* = \gamma + \mu$ corresponding to the critical case $\mathcal{R}_0 = 1$.

We show that the conditions of Theorem 3.1 proposed by [45] are satisfied for the system $\dot{\mathbf{x}} = f(\mathbf{x}, b)$, where

$$f = (f_1, f_2, f_3) \equiv (f_S, f_I, f_R)$$

is obtained by applying the substitutions $\beta \to b + \beta^*$ and $(S, I, R) \to (x_S, x_I, x_R) + \xi_0$ to equations (3.3a), (3.3b), and (3.3c), with

$$\mathbf{x} = (x_1, x_2, x_3) \equiv (x_S, x_I, x_R).$$

The matrix $A = D_{\mathbf{x}} f(\mathbf{0}, 0)$ $(= J|(1, 0, 0)$ with $\beta = \beta^*)$ has one simple zero eigenvalue and two eigenvalues with negative real part

$$\lambda_1 = 0, \quad \lambda_2 = -(\mu + \alpha\kappa), \quad \lambda_3 = -(\mu + \omega\kappa).$$

Now, let us calculate

$$Z_1 = \sum_{k,i,j=1}^{3} v_k w_i w_j \frac{\partial^2 f_k}{\partial x_i \partial x_j}(\mathbf{0}, 0) \qquad \text{and}$$
$$Z_2 = \sum_{k,i=1}^{3} v_k w_i \frac{\partial^2 f_k}{\partial x_i \partial b}(\mathbf{0}, 0),$$

where w, v are the right and left eigenvectors of A corresponding to the zero eigenvalues.

Note that we may fix $w_2 = 1$ as $Aw = 0$ is underdetermined. Then,

$$w_1 = -\left[1 + \frac{\alpha\kappa\gamma}{(\omega\kappa + \mu)(\alpha\kappa + \mu)} + \frac{\gamma}{\alpha\kappa + \mu}\right] \qquad \text{and}$$
$$w_3 = \frac{\gamma}{\alpha\kappa + \mu}$$

follow. Analogously, we find a left eigenvector $v = (0, 1, 0)$.

As $v_1 = v_3 = 0$, the sums get reduced to the terms containing

$$f_2 \equiv f_I = (b + \beta^*)x_I(x_S + 1) - (\gamma + \mu)x_I.$$

Clearly, the nonzero second-order partial derivatives of f_I at $(\mathbf{0}, 0)$ are

$$\frac{\partial^2 f_I}{\partial x_I \partial b}(\mathbf{0}, 0) = 1 \quad \text{and} \quad \frac{\partial^2 f_I}{\partial x_I \partial x_S}(\mathbf{0}, 0) = \beta^* = \gamma + \mu.$$

Hence,

$$\begin{aligned} Z_1 &= 2v_2 w_1 w_2 \frac{\partial^2 f_I}{\partial x_I \partial x_S}(\mathbf{0}, 0) \\ &= -2\left[1 + \frac{\alpha\kappa\gamma}{(\omega\kappa + \mu)(\alpha\kappa + \mu)} + \frac{\gamma}{\alpha\kappa + \mu}\right](\gamma + \mu) \quad \text{and} \\ Z_2 &= v_2 w_2 \frac{\partial^2 f_I}{\partial x_I \partial b}(\mathbf{0}, 0) = 1. \end{aligned}$$

As $Z_1 < 0$ and $Z_2 > 0$ for all parameters, we can apply Theorem 3.1 noting that even though $w_1 < 0$, as the first component of $(1, 0, 0)$ is positive, $w_1 \geq 0$ is not required actually.

Translating the statement of the aforementioned Theorem to our original system (3.3), we obtain that when $\mathcal{R}_0$ increases through 1, a transcritical bifurcation of forward type occurs with the disease-free equilibrium losing and $\mathbf{EE}_+$ gaining local asymptotic stability (LAS), respectively. □

3.3.2 The Routh-Hurwitz criterion for $\mathbf{EE}_+$

This section analyzes the stability of the endemic equilibrium $\mathbf{EE}_+$ for fixed β, γ, κ, and μ, given that $\mathcal{R}_0 > 1$ holds.

Local asymptotic stability (LAS) is characterized by all eigenvalues of the Jacobian (3.10) at $\mathbf{EE}_+$ having negative real part. Therefore, we consider the matrix

$$J|_{\mathbf{EE}_+} = \begin{bmatrix} -(\omega\kappa + \mu + \beta I_+^*) & -(\gamma + \mu + \omega\kappa) & -\omega\kappa \\ \beta I_+^* & 0 & 0 \\ -\nu\beta I_+^* & \gamma - 2\nu\beta I_+^* + \nu\beta(1 - S^* - R_+^*) & -(\alpha\kappa + \mu + \nu\beta I_+^*) \end{bmatrix}$$

and, in turn, its characteristic polynomial

$$a_0\lambda^3 + a_1\lambda^2 + a_2\lambda + a_3 = 0,$$

with

$$
\begin{aligned}
a_0 &= 1, \\
a_1 &= \beta I_+^*(1+\nu) + (\alpha\kappa + \omega\kappa + 2\mu), \\
a_2 &= \beta I_+^*[(\alpha\kappa + \omega\kappa + 2\mu) + \gamma + \beta\nu I_+^* + \mu\nu] + (\omega\kappa + \mu)(\alpha\kappa + \mu), \\
a_3 &= \beta I_+^*[(\omega\kappa + \mu)(\alpha\kappa + \mu) + (\gamma + \mu)\beta\nu I_+^* + \gamma(\alpha\kappa + \omega\kappa + \mu) + \\
&\qquad \omega\kappa\beta\nu(1 - S^* - I_+^* - R_+^*)],
\end{aligned}
\tag{3.11}
$$

and S^*, I_+^*, R_+^* as given in (3.5), (3.7), and (3.8).

Utilizing the Routh-Hurwitz (RH) criterion [41, 53], which is discussed in Section 2.3.2, yields that $\mathbf{EE}_+$ is LAS iff the following inequalities are satisfied

$$
\begin{aligned}
a_i > 0, \quad \text{for } i = 0, 1, 2, 3, \text{ and} \\
a_1 a_2 > a_3.
\end{aligned}
$$

As the positivity of $a_0, \ldots, a_3$ is trivial, we are led to analyze the sign changes in the function

$$
y_\nu(\alpha) = a_1 a_2 - a_3, \tag{3.12}
$$

for $\alpha > 1$ and $\nu > 0$.

Transformation of $y_\nu(\alpha)$

The formulae in (3.8) and (3.11) appear to be (mostly) symmetric with respect to α and ω. Recall that these two parameters are closely related as

$$
\alpha + \omega = \alpha\omega = \frac{\alpha^2}{\alpha - 1}
$$

directly follows from (3.2). These considerations suggest to introduce the substitution

$$\eta = \kappa(\alpha + \omega) = \kappa(\alpha\omega) = \kappa\frac{\alpha^2}{\alpha - 1}, \tag{3.13}$$

with $\eta \in [4\kappa, \infty)$ and the $\alpha = \omega = 2$ case corresponding to $\eta = 4\kappa$. Nevertheless, in order to apply (3.13), we need to establish that a_3 in (3.11) may be considered as a function of η. This holds due to the equality

$$\begin{aligned}
&\omega\kappa\beta\nu(1 - S^* - I_+^* - R_+^*) = \\
&\quad \omega\kappa\beta\nu\left(1 - \frac{\gamma+\mu}{\beta}\right) - \omega\kappa\beta\nu\frac{\sqrt{(c_1\nu + c_2)^2 + c_3\nu} + (c_1\nu - c_2)}{2\beta\nu(\gamma+\mu)} \\
&\quad - \omega\kappa\beta\nu\frac{\gamma+\mu+\omega\kappa}{2\beta\omega\kappa}\left[\left(2c_0 - \frac{1}{\gamma+\mu}\right)c_1 + \frac{1}{\nu(\gamma+\mu)}\left(c_2 - \sqrt{(c_1\nu + c_2)^2 + c_3\nu}\right)\right] \\
&= \omega\kappa\nu\frac{c_1}{\mu} + \frac{\omega\kappa}{2}\frac{c_2 - \sqrt{(c_1\nu + c_2)^2 + c_3\nu}}{\gamma+\mu} - \frac{\omega\kappa}{2}\frac{c_1\nu}{\gamma+\mu} - \frac{\nu}{2}(\gamma+\mu+\omega\kappa)2c_0c1 \\
&\quad - \frac{\nu(\gamma+\mu)}{2}\left[-\frac{1}{\gamma+\mu}c_1 + \frac{1}{\nu(\gamma+\mu)}\left(c_2 - \sqrt{(c_1\nu + c_2)^2 + c_3\nu}\right)\right] \\
&\quad + \frac{\nu\cdot\omega\kappa}{2}\frac{c_1}{\gamma+\mu} - \frac{\omega\kappa}{2}\frac{c_2 - \sqrt{(c_1\nu + c_2)^2 + c_3\nu}}{\gamma+\mu} \\
&= \omega\kappa\nu\frac{c_1}{\mu} - \frac{\nu}{2}(\gamma+\mu+\omega\kappa)2c_0c1 + \frac{\nu}{2}c_1 - \frac{1}{2}\left(c_2 - \sqrt{(c_1\nu + c_2)^2 + c_3\nu}\right) \\
&= \omega\kappa\nu\frac{c_1}{\mu} - \nu\left(1 + \frac{\omega\kappa}{\mu}\right)c1 + \frac{\nu}{2}c_1 - \frac{1}{2}\left(c_2 - \sqrt{(c_1\nu + c_2)^2 + c_3\nu}\right) \\
&= \frac{\sqrt{(c_1\nu + c_2)^2 + c_3\nu} - (c_1\nu + c_2)}{2} = \beta\nu(\gamma+\mu)I_+^* - c_1\nu.
\end{aligned}$$

Then, one obtains that

$$y_\nu(\alpha) \equiv y_\nu(\eta) = \hat{a}_1\hat{a}_2 - \hat{a}_3,$$

with

$$\begin{aligned}
\hat{a}_1 &= \hat{I}(1+\nu) + (\eta + 2\mu), \\
\hat{a}_2 &= \hat{I}[(\eta+\mu) + (\gamma+\mu) + \mu\nu + \nu\hat{I}] + \mu(\eta+\mu) + \kappa\eta, \\
\hat{a}_3 &= \hat{I}[2\nu\hat{I}(\gamma+\mu) - \nu\mu(\beta - (\gamma+\mu)) + (\gamma+\mu)(\mu+\eta) + \kappa\eta],
\end{aligned}$$

where $\hat{I} = \beta I_+^*$.

Substitution (3.13) reveals an important feature of $y_\nu(\alpha)$, namely, there is a bijection $(1,2) \ni \alpha \mapsto \alpha' \in (2,\infty)$ such that $y_\nu(\alpha) = y_\nu(\alpha')$. In particular, local extrema at $\alpha \neq 2$ appear in pairs.

Furthermore, using the chain rule, we obtain that

$$\frac{\partial y_\nu}{\partial \alpha} = \frac{\partial y_\nu}{\partial \eta} \cdot \frac{\mathrm{d}\eta}{\mathrm{d}\alpha} = \frac{\partial y_\nu}{\partial \eta} \cdot \frac{\kappa\alpha(\alpha-2)}{(\alpha-1)^2}.$$

Clearly, $\alpha = 2$ (that is $\eta = 4\kappa$) is a critical point of y_ν for all immune boosting parameters ν.

We now present two Lemmas on derivatives of function compositions. The first is a version of the classical result by Faà di Bruno generalizing the chain rule.

Lemma 3.1 (Faà di Bruno)**.** *Let $f\colon I \to U$ and $g\colon U \to V$ be analytic functions, where $I, U, V \subseteq R$ are connected subsets. Consider the Taylor expansions $f(t) = \sum_{k=0}^{\infty} (f)_k (t-t_0)^k$ centered at $t_0 \in I$ with $t \in I$ and $g(x) = \sum_{k=0}^{\infty} (g)_k (x-x_0)^k$ centered at $x_0 = f(t_0)$ for $x \in U$. Then, the composite function $(g \circ f)$ attains the Taylor expansion $(g\circ f)(t) = \sum_{k=0}^{\infty} (g\circ f)_k (t-t_0)^k$ centered at t_0 with the coefficients*

$$(g \circ f)_0 = (g)_0 \qquad \textit{and}$$

$$(g \circ f)_k = \sum_{\substack{b_1+2b_2+\ldots+kb_k=k \\ m:=b_1+b_2+\ldots+b_k}} \frac{m!}{b_1!b_2!\ldots b_k!} (g)_m \prod_{i=1}^{k} \Big((f)_i \Big)^{b_i},$$

where $k \geq 1$ *and* $b_1, \ldots, b_k$ *are nonnegative integers.*

Using the results of Lemma 3.1 and assuming that the inner function has a vanishing first derivative and the outer function has a cascade of vanishing derivatives, the following Lemma establishes a similar property for the composite function.

Lemma 3.2. *Assume that* f *and* g *are as in Lemma 3.1 and that* $(f)_1 = 0$*. Then,*

(a) $(g \circ f)_2 = 0 \iff (g)_1 = 0$*,*

(b) if $(g)_i = 0$ *for* $i = 1, \ldots, k-1$*, then* $(g \circ f)_{2k} = 0 \iff (g)_k = 0$*,*

(c) if $(g)_i = 0$ *for* $i = 1, \ldots, k$*, then* $(g \circ f)_{2k+1} = 0$*.*

Proof. The claims directly follow from Lemma 3.1 by noting that in the formula of $(g \circ f)_k$, for terms with $m > k/2$, the inequality $b_1 > 0$ must hold, hence, any such term must evaluate to zero. □

By Lemma 3.2, either all derivatives of y_ν are zero at $\alpha = 2$ or the first non-vanishing derivative is of even order. As y_ν is analytic and not identically zero for any $\mathcal{R}_0 > 1$, the former is not possible, hence, $\alpha = 2$ is a local extremum for all boosting rates ν.

3.4 Numerical analysis

This section summarizes the results of our numerical stability and bifurcation analysis of system (3.3) with respect to varying waning and boosting dynamics. In the remaining

part of the chapter, all other parameters are considered to be fixed following [16] to model pertussis as

$$\begin{aligned} \gamma &= 17, \\ \kappa &= 1/10, \\ \mu &= 1/80, \\ \beta &= 260, \end{aligned} \tag{3.14}$$

corresponding to an average infectious period of 21 days, an average life expectancy of 80 years and a basic reproduction number $\mathcal{R}_0 = 15.28$.

First, Section 3.4.1 discusses how the local stability of $\mathbf{EE}_+$ changes given (3.14) with varying α and ν. Then, Section 3.4.2 analyzes these stability changes and the corresponding bifurcations. In addition, using numerical continuation methods, we observe the bistable regions in the (α, ν)-plane.

3.4.1 Analysis of the Routh-Hurwitz criterion for $\mathbf{EE}_+$

Before carrying out any numerical computations, let us analyze the asymptotic behaviour of (3.12) as $\nu \to 0^+$, $\nu \to \infty$, $\alpha \to 1^+$, and $\alpha \to \infty$. First, we find the limits of I_+^* and R_+^* as $\nu \to 0^+$, and $\nu \to \infty$

$$\lim_{\nu \to 0^+} I_+^* = \frac{(\alpha\kappa + \mu)(\gamma + \mu + \omega\kappa)c_1 c_0}{\beta c_2}, \quad \lim_{\nu \to \infty} I_+^* = \frac{|c_1| + c_1}{2\beta(\gamma + \mu)},$$

and that of R_+^* as $\nu \to 0^+$, and $\nu \to \infty$ are

$$\lim_{\nu \to 0} R_+^* = \frac{\gamma + \mu + \omega\kappa}{2\beta\omega\kappa} \left[\left(2c_0 - \frac{1}{\gamma + \mu} \right) c_1 - \frac{2c_1 c_2 + c_3}{2c_2(\gamma + \mu)} \right],$$

$$\lim_{\nu\to\infty} R_+^* = \frac{\gamma+\mu+\omega\kappa}{2\beta\omega\kappa}\left[\left(2c_0 - \frac{1}{\gamma+\mu}\right)c_1 - \frac{|c_1|}{(\gamma+\mu)}\right].$$

The limit of I_+^* as $\alpha \to \infty$

$$\lim_{\alpha\to\infty} I_+^* = \frac{1}{\beta(\gamma+\mu)}\left[c_1 + \frac{\gamma\kappa(\beta-(\gamma+\mu))}{\gamma+\mu+\kappa}\right],$$

and the limit of R_+^* as $\alpha \to 1^+$

$$\lim_{\alpha\to 1^+} R_+^* = \frac{1}{\beta(\gamma+\mu)}\left[\frac{c_1\gamma}{\mu} + \frac{\gamma\kappa(\beta-(\gamma+\mu))}{\gamma+\mu+\kappa}\right].$$

As a remark, the limit as $\alpha \to \infty$ and as $\alpha \to 1^+$ are the same.

$$\lim_{\alpha\to\infty} R_+^* = 0,$$

The results are summarized in Table 3.1. They are valid for all parametrizations of (3.3) and do not rely on (3.14).

lim	I_+^*	R_+^*	$y_\nu(\alpha)$
$\nu \to 0^+$	$\frac{4c_1c_2+c_3}{4\beta c_2(\gamma+\mu)}$	$\frac{\gamma(\beta-(\gamma+\mu))(\mu+\omega\kappa)}{\beta c_2}$	> 0
$\nu \to \infty$	$\frac{c_1}{\beta(\gamma+\mu)}$	$\frac{c_1\gamma}{\beta\mu(\gamma+\mu)}$	> 0
$\alpha \to 1^+$	$\frac{(\kappa+\mu)(\beta-(\gamma+\mu))}{\beta(\gamma+\mu+\kappa)}$	$\frac{\gamma(\beta-(\gamma+\mu))}{\beta(\gamma+\mu+\kappa)}$	> 0
$\alpha \to \infty$	$\frac{(\kappa+\mu)(\beta-(\gamma+\mu))}{\beta(\gamma+\mu+\kappa)}$	0	> 0

Table 3.1: Limits of I_+^*, R_+^*, and the sign of $y_\nu(\alpha)$

As a consequence of these limits, there exists a compact region K in the (α, ν)-plane such that the endemic equilibrium $\mathbf{EE}_+$ is LAS for $(\alpha, \nu) \in (1, \infty) \times (0, \infty) \setminus K$.

Double bubbles of instability

Section 3.4.1 has readily established that it is sufficient to consider a compact subset in the (α, ν)-plane for the stability analysis of $\mathbf{EE}_+$. Based on our experiments, we have restricted our attention to $(\alpha, \nu) \in [1.01, 18] \times [0.01, 18]$ and obtained the heatmap in Figure 3.3 when studying the positivity of $y_\nu(\alpha)$.

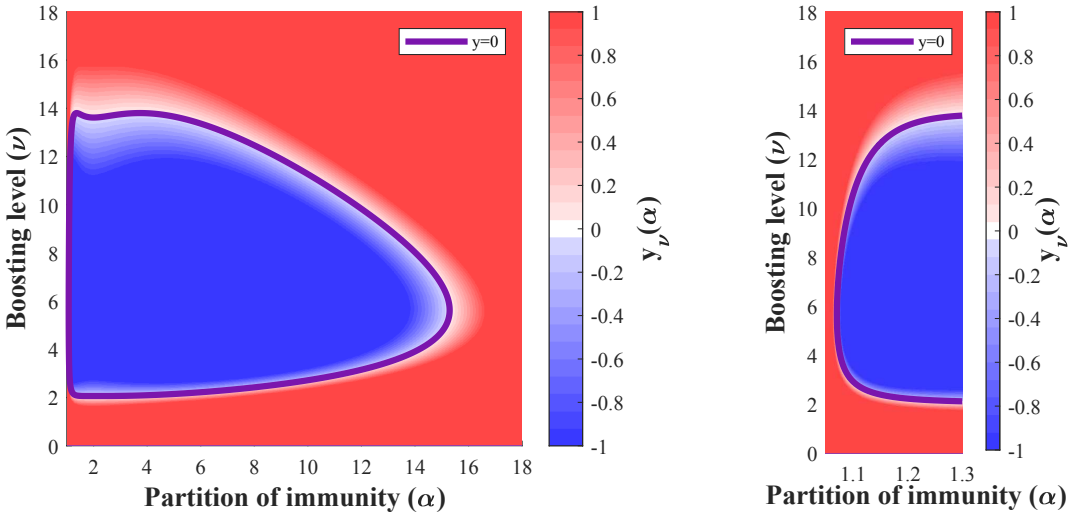

Figure 3.3: Heatmap of the Routh-Hurwitz criterion $y_\nu(\alpha)$ capped at $[-1, 1]$ with highlighted zero contour. Figure 3.3b zooms in on the region close to $\alpha = 1$.

It is apparent that, for an interval of α values, $y_\nu(\alpha)$ is initially positive for small ν, then, as the boosting rate increases the RH criterion becomes negative for an interval of ν values, after which, it turns positive again. Now, let us look at the heatmap from the other direction. Note that for most interesting boosting rates ν, a similar stability switch may be observed over an α-interval.

However, the dynamics are clearly more involved close to boosting rates around 14 as Figure 3.3 suggests the presence of multiple stability switches.

It is straightforward to localize such phenomena by finding local extrema of $y_\nu(\alpha)$ (as a

function of α) whose value is zero. Hence, we looked for intersections of the curves

$$y_\nu(\alpha) = 0 \qquad \text{and} \qquad \frac{\partial}{\partial \alpha} y_\nu(\alpha) \equiv y'_\nu(\alpha) = 0$$

as shown in Figure 3.4 together with the positivity analysis of the derivative. Our findings confirm the presence of multiple switches close to $\nu \approx 13.7$, moreover, they highlight the existence of similar dynamics close to $\nu \approx 2.06362$ as well. Note that Figure 3.3 gives no hint of the latter.

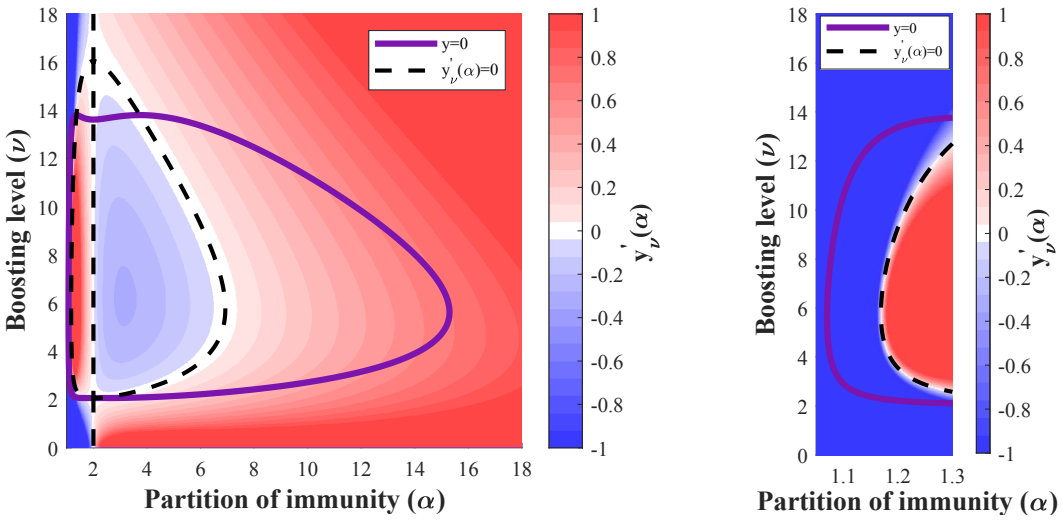

Figure 3.4: Heatmap of $y'_\nu(\alpha)$ capped at $[-1, 1]$ with highlighted zero contours of $y_\nu(\alpha)$ and $y'_\nu(\alpha)$. Figure 3.4b zooms in on the region close to $\alpha = 1$.

Recall from Section 3.3.2 that local extrema of $y_\nu(\alpha)$ – other than $\alpha = 2$ – appear in pairs. Hence, zooming in on these two regions, shown in Figure 3.5, reveals double bubbles of instability for certain boosting rates.

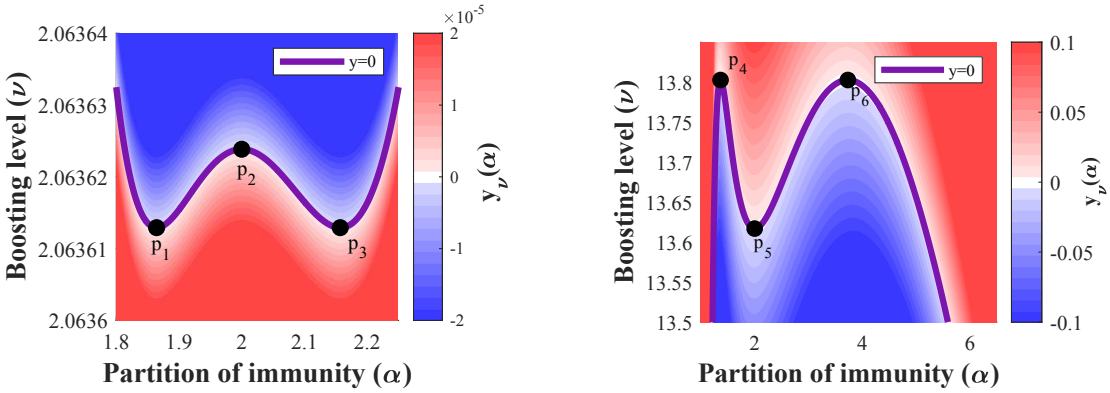

(a) $\nu \approx 2.06362$. (b) $\nu \approx 13.7$.

Figure 3.5: Zoomed-in heatmaps of the Routh-Hurwitz criterion $y_\nu(\alpha)$ with highlighted zero contour over regions of interest in the (α, ν)-plane. Critical points $p_i = (\alpha_i^*, \nu_i^*)$ on the contour are marked.

Note that the width of the ν-range where this phenomenon occurs in Figure 3.5a is less than $2 \cdot 10^{-5}$, thus, it should come as no surprise that it was not observable based on the original heatmap in Figure 3.3. The coordinates of the highlighted critical points are given in Table 3.2.

	α	ν
$p_1 = (\alpha_1^*, \nu_1^*)$	1.864273655292	2.063612920385
$p_2 = (\alpha_2^*, \nu_2^*)$	2.0	2.063623848262
$p_3 = (\alpha_3^*, \nu_3^*)$	2.157040937065	ν_1^*
$p_4 = (\alpha_4^*, \nu_4^*)$	1.366092512212	13.80272643151
$p_5 = (\alpha_5^*, \nu_5^*)$	2.0	13.61692960743
$p_6 = (\alpha_6^*, \nu_6^*)$	3.731549995264	ν_4^*

Table 3.2: Critical points on the contour $y_\nu(\alpha) = 0$ as marked in Figure 3.5.

3.4.2 Numerical bifurcation analysis

In the following, we present a numerical analysis of one parameter (α) and two parameter (α, ν) bifurcations of the endemic equilibria branch carried out using `MatCont` [22]. Here, we

also refer to Section 2.5 for an overview of the `MatCont` package. For theoretical background on bifurcation analysis, we refer to [43, 44].

Motivated by the results of Section 3.4.1, in particular the region depicted in Figure 3.3a, we computed the two-parameter (α, ν) bifurcation diagram of system (3.3), see Figure 3.6. To fully understand the bifurcation diagram, let us denote by K the open domain enclosed by the purple-colored Hopf curve, which is continuous when supercritical (called H_-) and dashed when subcritical (called H_+). A stable limit cycle bifurcates from the equilibrium if we cross H_- from outside to inside K, while an unstable cycle appears if we cross H_+ in the opposite direction. In other words, points on the dashed purple curve are Hopf points and the bifurcation is subcritical, thus generating unstable cycles, whereas the bifurcation of equilibria on the continuous purple curve is supercritical, thus generating stable cycles. We refer to Section 2.4.3 for an overview of this phenomenon.

It is apparent that for larger boosting rates (ν between $12 - 15$), the local stability analysis of $\mathbf{EE}_+$ is not sufficient to capture all interesting dynamics.

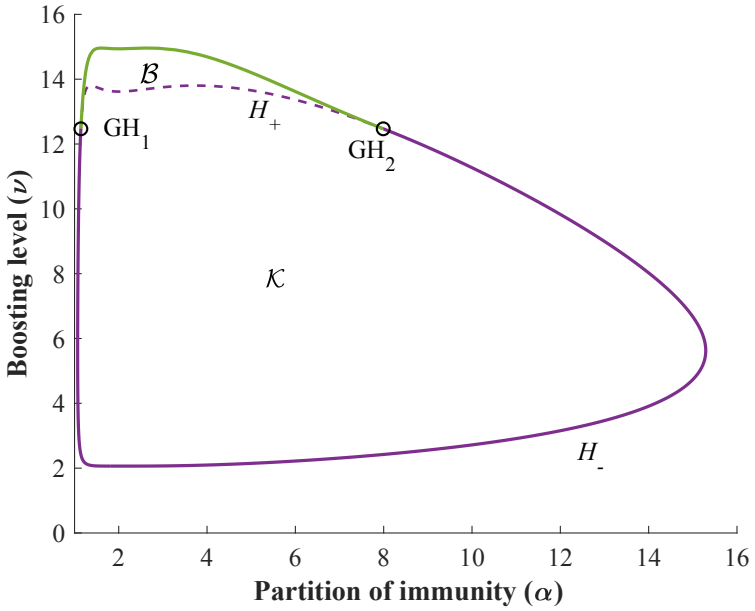

Figure 3.6: Two-parameter (α, ν) bifurcation diagram.

The two new critical points identified are $\mathrm{GH}_1 = (\alpha^*_{\mathrm{GH}_1}, \nu^*_{\mathrm{GH}_1})$ and $\mathrm{GH}_2 = (\alpha^*_{\mathrm{GH}_2}, \nu^*_{\mathrm{GH}_2} \equiv \nu^*_{\mathrm{GH}_1})$. The approximate coordinates of these *generalized Hopf points* are captured in Table 3.3 and they mark the parameter values where the Hopf bifurcation changes from supercritical to subcritical.

	α	ν
$\mathrm{GH}_1 = (\alpha^*_{\mathrm{GH}_1}, \nu^*_{\mathrm{GH}_1})$	1.1430260422	12.469198884
$\mathrm{GH}_2 = (\alpha^*_{\mathrm{GH}_2}, \nu^*_{\mathrm{GH}_2})$	7.9917337529	12.469198884

Table 3.3: Critical GH points as marked in Figure 3.6.

The branch of the limit points of periodic cycles appears in green, which together with the dashed purple curve H_+ enclose a bistability region $\mathcal{B}$, where there exists a stable periodic solution alongside the LAS endemic equilibrium.

Let us now examine the bifurcation diagram in more detail over regions, characterized by various levels of boosting rate ν, where the dynamics are similar.

In all bifurcation plots that follow, the endemic equilibria branch (particularly the I component) is marked with a black curve, solid when LAS and dashed when unstable. Red and blue curves represent branches of stable and unstable limit cycles, respectively, and Hopf bifurcation points are marked with purple dots.

Region: $0 \leq \nu < \nu^*_1 \equiv \nu^*_3$**.** The system has a stable point attractor for all $\alpha > 1$.

Region: $\nu^*_1 \equiv \nu^*_3 < \nu < \nu^*_2$**.** There are four supercritical Hopf bifurcation points on the endemic equilibria branch, see Figure 3.7 for a typical setting. Continuation of (the I-component of) limit cycles with respect to α starting from two Hopf bifurcation points, H_1 and H_2, forms an *endemic bubble* (the two branches of stable limit cycles coincide), see [54] for the origin of this concept. The same happens for the $\mathrm{H}_3, \mathrm{H}_4$ pair.

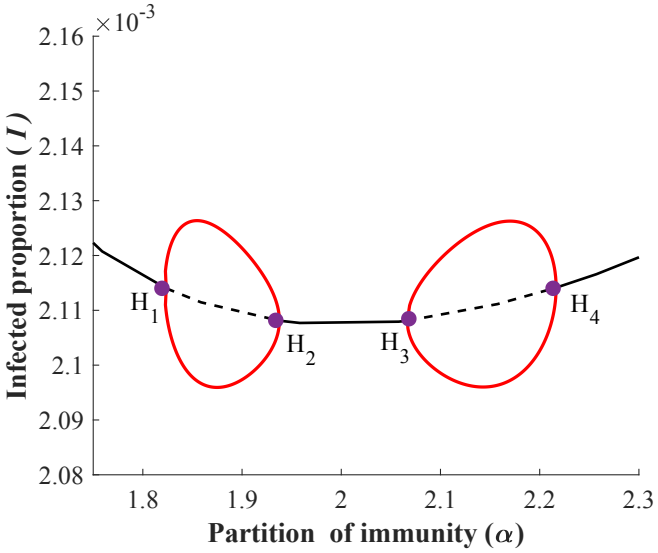

Figure 3.7: Bifurcation diagram w.r.t. α, when $\nu = 2.06362$.

Recall that these double bubbles of instability (endemic bubbles) were readily observed in Figure 3.5a. Such double bubbles have been conjectured in a delay differential model for waning and boosting [55]. For an overview of similar phenomena, the reader is referred to [56–58].

Region: $\nu_2^* < \nu < \nu^*_{\mathrm{GH}_1} \equiv \nu^*_{\mathrm{GH}_2}$**.** As the boosting rate increases, the middle supercritical Hopf points H_2 and H_3 (observed in the previous region) get closer to each other, and finally collide and we obtain a single endemic bubble, Figure 3.8.

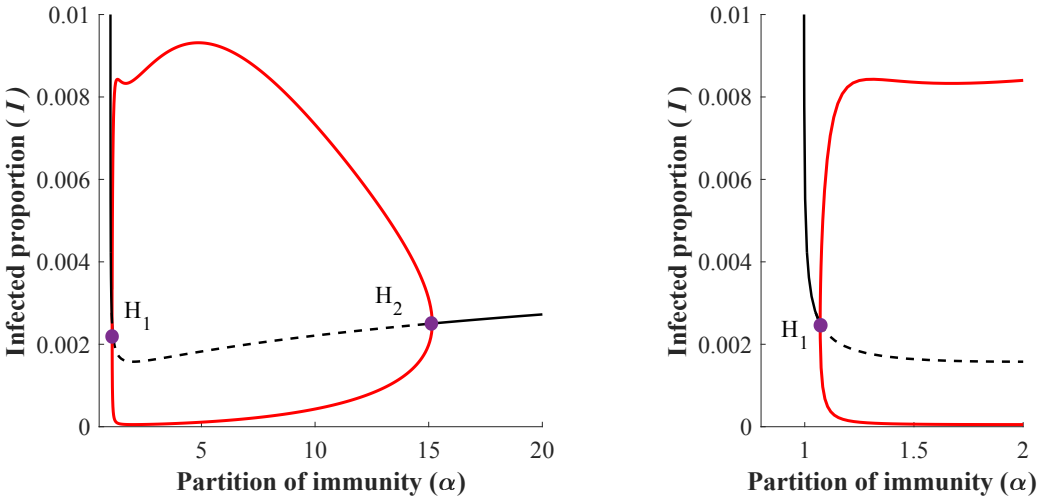

Figure 3.8: (a) Bifurcation diagram w.r.t. α, when $\nu = 5.8$; (b) Zoom of (a) close to the vertical line $\alpha = 1$.

Region: $\nu^*_{\mathrm{GH}_1} \equiv \nu^*_{\mathrm{GH}_2} < \nu < \nu^*_5$**.** As ν continues to grow in the two-parameter plane in Figure 3.6, two generalized Hopf points, GH_1 and GH_2, appear. They separate branches of sub- and supercritical Hopf bifurcations in the parameter plane. The stable limit cycles survive when we enter region $\mathcal{B}$. Crossing the subcritical Hopf boundary H_+ creates an extra unstable cycle inside the first one, while the equilibrium regains its stability. Two cycles of opposite stability exist inside the bistable region $\mathcal{B}$ and disappear at the green curve.

When we pass the generalized Hopf points and fix a ν in this region, then Figure 3.9 shows a typical bifurcation w.r.t. α. Observe here the two small α-parameter ranges of bistability where the $\mathbf{EE}_+$ and the larger amplitude periodic solution are both stable. The points marked with a green circle are limit points of periodic orbits. The stable and unstable cycles collide and disappear on the green curve in Figure 3.6, corresponding to a fold bifurcation of cycles.

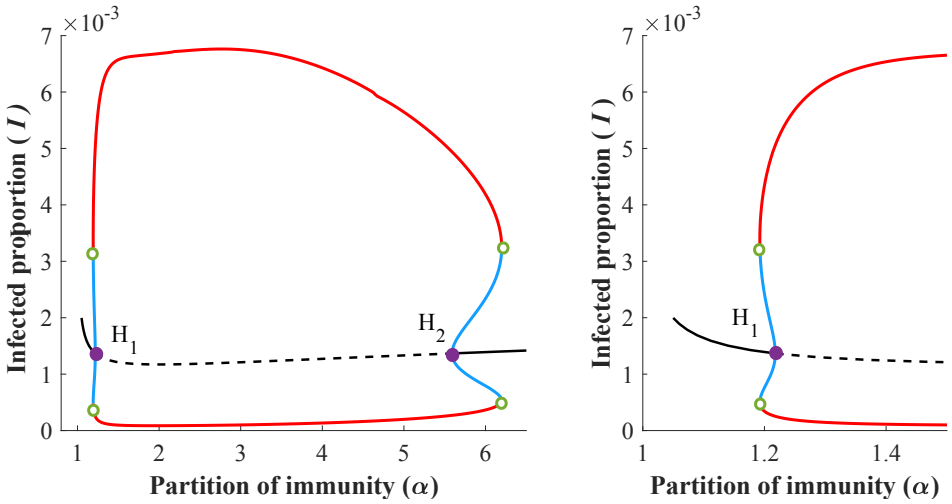

Figure 3.9: Bifurcation diagram w.r.t α, with $\nu = 13.5$ (left) and zoom into the bistable region around H_1 (right).

Region: $\nu_5^* < \nu < \nu_4^* \equiv \nu_6^*$**.** As we increase the boosting value, the dynamics are changing, as observed in the shape of the subcritical Hopf curve H_+ in Figure 3.10 and the heat map in Figure 3.5b.

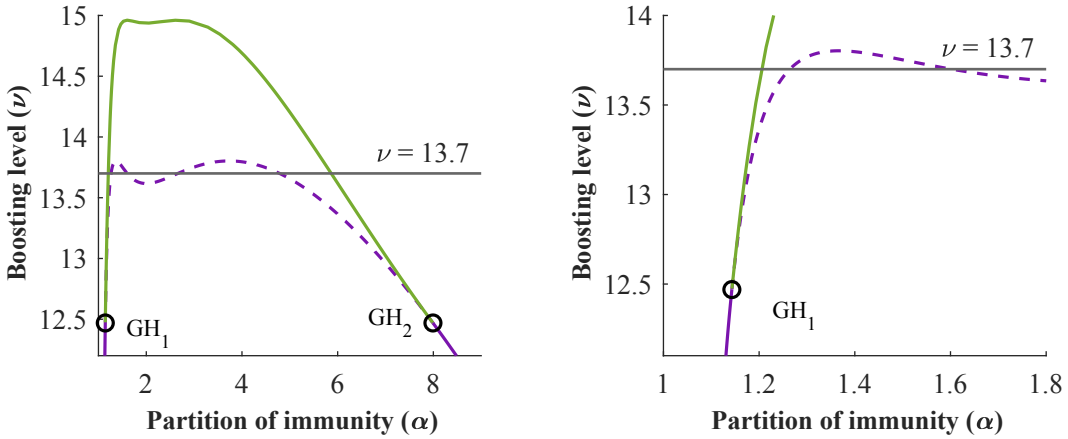

Figure 3.10: Two-parameter (α, ν) bifurcation diagram, bistability region.

In Figure 3.11, the bifurcation diagram confirms the existence of four subcritical Hopf bifurcation points. Here a small bubble appears inside the region of stable oscillations, which

leads to an additional bistable region compared to the previous case.

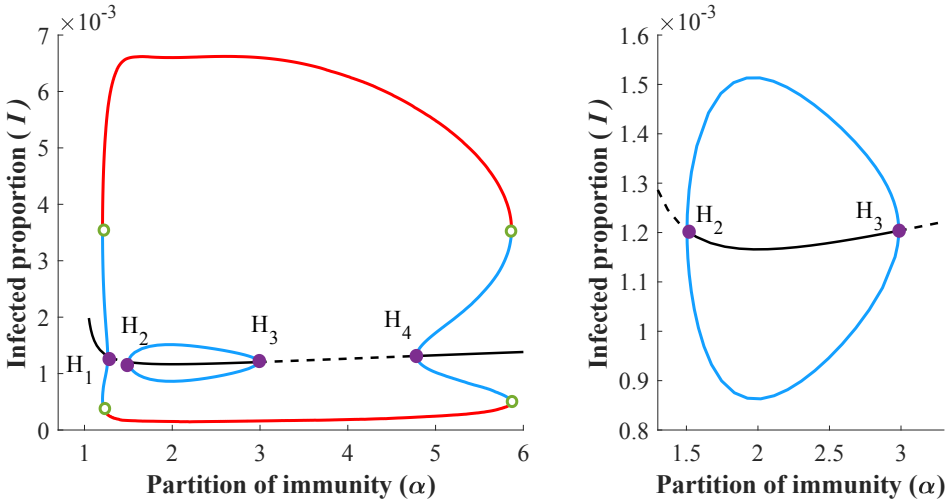

Figure 3.11: Bifurcation diagram w.r.t α, with $\nu = 13.7$ (left) and zoomed into the bubble (right).

When we increase the boosting in this region, i.e., still intersecting the subcritical Hopf curve, the Hopf points H_1 and H_2 as well as H_3 and H_4 move closer to each other, resulting in larger bistability regions, see also the heatmap Figure 3.5b.

Region: $\nu_4^* \equiv \nu_6^* < \nu$**.** As we enter this region we leave H_+ and do not intersect any Hopf branches, hence, the continuation method utilized so far leaves us with a single stable equilibrium, Figure 3.12.

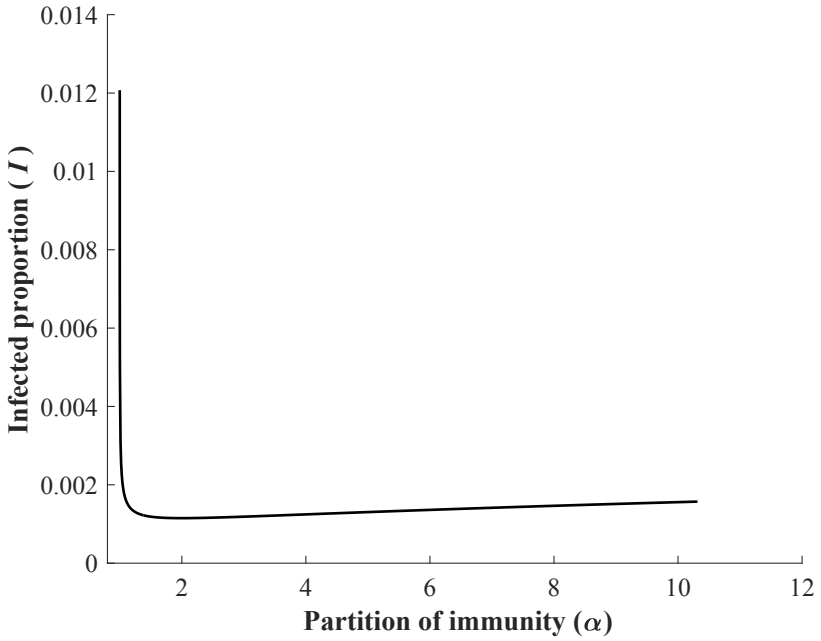

Figure 3.12: There are no bifurcations of equilibria when $\nu = 14.5$.

There is, however, a range of ν values in this region that belong to $\mathcal{B}$, as observed in Figure 3.6. For a better demonstration of the shape of the limit cycle branch, see Figure 3.13.

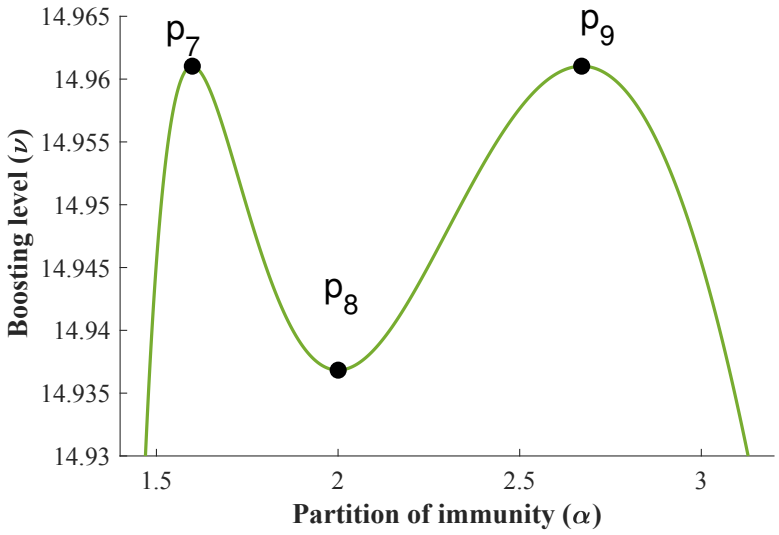

Figure 3.13: Branch of the limit points of periodic solutions.

The coordinates of the critical points are summarized in Table 3.4.

	α	ν
$p_7 = (\alpha_7^*, \nu_7^*)$	1.5987662507	14.9610290034
$p_8 = (\alpha_8^*, \nu_8^*)$	2	14.936830813
$p_9 = (\alpha_9^*, \nu_9^*)$	2.670631735	ν_7^*

Table 3.4: Critical points on the limit cycles branch as marked in Figure 3.13.

Considering the heatmaps in Figure 3.5, it was natural to investigate regions in the two-parameter plane (α, ν) where ν is constant and look at bifurcations with respect to α. To capture the extension of the bistability region in the ν direction we can investigate the dynamics for α fixed and consider the boosting rate ν as the bifurcation parameter. For a typical setting see Figure 3.14.

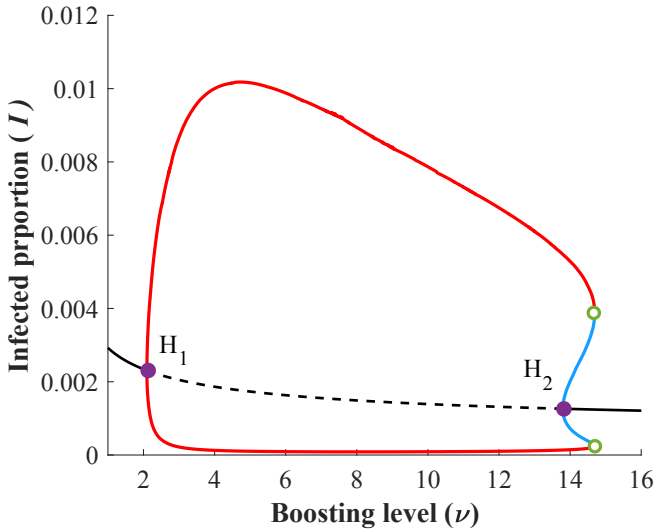

Figure 3.14: Bifurcation diagram w.r.t. ν, when $\alpha = 4$.

3.5 Summary

In this chapter, we generalized previous compartmental SIRWS models of waning and boosting of immunity by allowing different expected durations for individuals being in the fully immune compartment R and being in the waning immunity compartment W, from where their immunity can still be restored upon re-exposure. We proposed an asymmetric division of the immunity period in the SIRWS model to these two phases, characterized by a newly introduced bifurcation parameter. Other parameters were chosen to mimic pertussis. We observed and established a new symmetry in these divisions around the critical case of equal partitioning when analyzing the stability criterion of the endemic equilibrium. This, combined with numerical bifurcation methods, enabled us to characterize the model dynamics for a relevant range of parameter values. We composed global bifurcation diagrams and found complex and rich dynamics where stability switches, Hopf bifurcations, folds of periodic branches appeared, forming interesting structures in the parameter space. We found double endemic bubbles as well as regions of bistability. We note that in our model (similar to most previous waning-boosting models [19, 58]), the interesting dynamics occur in the case $\nu > 1$, which corresponds to the assumption that the probability of a partially immune person getting boosted is larger than that of a susceptible person contracting the infection.

In the next chapter, we will investigate the dynamics of the SIRWJS model where boosting of immunity occurs via secondary infections, again, with asymmetric partitioning of the total immune period.

Chapter 4

Bifurcation analysis of waning-boosting epidemiological models with repeat infections and varying immunity periods

Published in the Journal of Mathematics and Computers in Simulation
Authors: Richmond Opoku-Sarkodie, F. A. Bartha, Mónika Polner, Gergely Röst [64].

4.1 Introduction

Compartmental models based on the Susceptible-Infectious-Recovered (SIR) framework, have been used to study the transmission dynamics of infectious diseases in a population. The classical SIR model assumes lifelong and perfect immunity upon recovery from the infection. An extension of the SIR model, known as the Susceptible-Infectious-Recovered-Susceptible ($SIRS$) model, accounts for the loss of immunity and can capture the long term persistence of diseases in a population. However, it is unable to reproduce oscillatory dynamics, which has been frequently experienced in real life.

Through the addition of a W compartment, the Susceptible-Infectious-Recovered-Waned-Susceptible ($SIRWS$) model can incorporate both the waning and boosting of immunity. Individuals from the R compartment, after the some time, move to the W compartment where they have less immunity than the recovered class R, but still more immunity than the fully susceptible class S. Moreover, when an individual is in the W compartment, and exposed to the pathogen again, then their immunity can be boosted which can be modeled by moving back to the highly immune R compartment from W, without experiencing the infected state. The $SIRWS$ model already exhibits a surprisingly rich dynamics with three distinct features depending on the degree of boosting — fixed points, limit cycles, and bistability between the two. For a comprehensive study of this phenomenon in a very general setting, we refer to Barbarossa et al. [49].

Several authors have extended the SIRWS model to explore additional questions, such as the role of age structure, vaccination, seasonal forcing, and strain dynamics. Carlsson et al. [59] and Lavine et al. [16] examined the resurgence of pertussis by extending the SIRWS model to include age-structure and vaccination. The impact of waning and boosting of immunity on COVID-19 dynamics was studied using an age structured model in [60]. Leung et al. [52] showed that the relative duration of vaccine-induced immunity and infection-induced immunity plays a significant role in determining epidemiological dynamics. Dafilis et al. [19] considered seasonal forcing of disease transmission and found highly unpredictable behavior. Further work considered the interaction of similar pathogens and demonstrated the interesting behavior when two phenomena that can cause oscillations — strain dynamics with cross-immunity and waning/boosting of immunity — are coupled.

As earlier mentioned, a common feature of the previous SIRWS-models is the assumption of identical expected transition times from R to W and thereon from W to S. In Chapter 3, see also [61], we have investigated the effects of breaking this symmetry, *i.e.* we considered arbitrary partitioning of the total immune period (the overall expected transition time from

R to S) between the R and the W states. We found that the modified model exhibits rich dynamics and displays additional complexity with respect to the symmetric partitioning.

This chapter presents an extension of the SIRWS model where boosting of immunity occurs strictly via undergoing a secondary infection period, by inserting an additional compartment J from W to R. Such an extended system was already studied by Strube et al. [18] permitting, in addition, immune boosting directly from W to R for a fraction of the cases. We do not consider the latter possibility here, only the boosting via J. However, [18], similarly to [19, 52], assumed identical transition times from R to W and W to S, which is not biologically feasible. To address this gap in the literature, in contrast, here we investigate how the more *realistic* asymmetric partitioning of the total immune period affects the dynamics. We find that this natural extension of the model enables additional complexities in the long term disease dynamics.

We determine the stability of the endemic equilibria and analyze the parameter regimes in which fixed points, limit cycles, and bistability occur. We establish the possibility of a backward transcritical bifurcation at $\mathcal{R}_0 = 1$. Our analysis leads to very complicated dynamics and convoluted bifurcation diagrams.

4.2 Description of the SIRWJS model: a compartmental model with waning and boosting, where secondary exposure can make the host infective

In this section, we describe the SIRWJS model, which incorporates a secondary infectious state, labelled J, via which boosting of immunity occurs. Primarily, the SIRWJS model consists of the following compartments: those who are susceptible (S) to the infection may become infected (I) upon adequate contact with an infectious individual. The recovered population is further divided into two compartments based on their level of immunity. Upon

recovery from I, individuals move to R having full immunity. Later, their immunity may weaken and they progress to the W compartment representing waning immunity. Upon re-exposure to the pathogen, members of W move into the J compartment representing secondary infections. These individuals eventually recover from the secondary infection and transition back to R where hosts are fully immune. The path from W to R results in a boosting of the individual's immunity level. On the other hand, in the absence of re-exposure to the disease causing pathogen, hosts eventually lose their immunity modelled as a transition from W back to the S compartment where they are fully susceptible again to the infection.

Figure 4.1 shows the flow chart of the SIRWJS system, where boosting occurs via J. The primary force of infection is $\beta(I + \xi J)$, where ξ is the infectivity of secondary infection relative to primary infection and β is the transmission rate. Thus, both I and J are infectious compartments, and individuals in these compartments can infect susceptibles and also boost a waning immunity. The death rate, μ, is assumed to be the same as the birth rate, γ and ρ are the recovery rates from the primary and secondary infections respectively, while κ is the immune decay rate. Boosting of immunity occurs via the J compartment using the boosting coefficient ν.

Many previous waning-boosting models assumed that the average time spent in R and W compartments are the same. Here, following [61], we relax this restrictive assumption of symmetric partition of the immunity period, by introducing two additional parameters $\alpha > 1$ and $\omega > 1$, such that the time spent in R is $1/(\alpha\kappa)$ and the time spent in W is $1/(\omega\kappa)$. Then, the total period of immune protection is

$$\frac{1}{\alpha\kappa} + \frac{1}{\omega\kappa} = \frac{1}{\kappa}, \tag{4.1}$$

under the assumption of $\alpha + \omega = \alpha\omega$. Note that the formulation of similar models in earlier works such as [19] is equivalent with the restriction of parameters $\alpha = \omega = 2$.

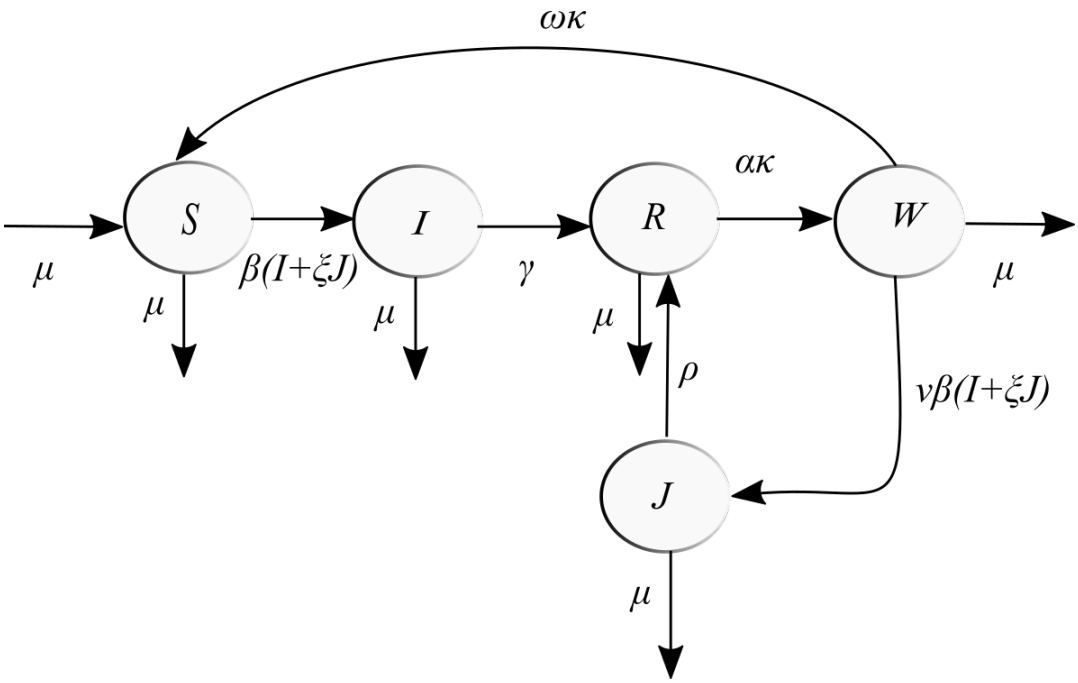

Figure 4.1: Flow diagram for the SIRWS system with secondary infections

The descriptions and assumptions on the system parameters are summarized in Table 4.1.

β	> 0	transmission rate
ξ	≥ 0	relative infectivity of secondary infections w.r.t. primary
μ	> 0	birth and death rate
γ	> 0	recovery rate from primary infection
ρ	> 0	recovery rate from secondary infection
κ	> 0	immune decay rate
α^{-1}	$\in (0,1)$	relative size of the first immune protection period from $R \longrightarrow W$
ω^{-1}	$(1-\alpha^{-1}) \in (0,1)$	relative size of the second immune protection period from $W \longrightarrow S$
ν	> 0	boosting coefficient

Table 4.1: Parameters of the SIRWJS system.

We consider all parameters to be positive, but ξ is allowed to take value zero as well. The case $\xi = 0$ represents the scenario when people in secondary infection are not infectious,

whilst $\xi = 1$ describes the scenario when the secondary infection is equally infectious to the primary infection. We may allow $\xi > 1$ modeling reinfections that are more severe than the primary.

We now formulate the governing system of ordinary differential equations describing the dynamics presented in Figure 4.1 as

$$\begin{aligned}
\frac{dS}{dt} &= -\beta(I + \xi J)S + \omega\kappa W + \mu(1 - S) && \text{(4.2a)}\\
\frac{dI}{dt} &= \beta(I + \xi J)S - \gamma I - \mu I && \text{(4.2b)}\\
\frac{dR}{dt} &= \gamma I - \alpha\kappa R + \rho J - \mu R && \text{(4.2c)}\\
\frac{dW}{dt} &= \alpha\kappa R - \omega\kappa W - \nu\beta(I + \xi J)W - \mu W && \text{(4.2d)}\\
\frac{dJ}{dt} &= \nu\beta(I + \xi J)W - \mu J - \rho J && \text{(4.2e)}
\end{aligned}$$

System (4.2) models a constant size population normalized to 1 as summing all equations yields

$$\frac{d(S + I + R + W + J)}{dt} = \mu(1 - S - I - R - W - J).$$

Also, non-negativity is preserved as assuming $S(t^*), I(t^*), R(t^*), W(t^*), J(t^*) \geq 0$ for some $t^* \geq 0$, we readily have that

$$\begin{aligned}
S'(t^*) &= \omega\kappa W(t^*) + \mu &&> 0, \quad \text{if } S(t^*) = 0,\\
I'(t^*) &= \beta\xi J(t^*)S(t^*) &&\geq 0, \quad \text{if } I(t^*) = 0,\\
R'(t^*) &= \gamma I(t^*) + \rho J(t^*) &&\geq 0, \quad \text{if } R(t^*) = 0,\\
W'(t^*) &= \alpha\kappa R(t^*) &&\geq 0, \quad \text{if } W(t^*) = 0, \text{ and}\\
J'(t^*) &= \nu\beta I(t^*)W(t^*) &&\geq 0, \quad \text{if } J(t^*) = 0.
\end{aligned}$$

Thus, our primary interest is in non-negative solutions satisfying $S+I+R+W+J=1$ for all t. These solutions we refer to as *epidemiologically feasible*.

Using the substitution

$$R = 1 - S - I - W - J \tag{4.3}$$

we get the reduced system

$$\begin{aligned}
\frac{dS}{dt} &= -\beta(I+\xi J)S + \omega\kappa W + \mu(1-S) && \text{(4.4a)}\\
\frac{dI}{dt} &= \beta(I+\xi J)S - \gamma I - \mu I && \text{(4.4b)}\\
\frac{dW}{dt} &= \alpha\kappa(1-S-I-W-J) - \omega\kappa W - \nu\beta(I+\xi J)W - \mu W && \text{(4.4c)}\\
\frac{dJ}{dt} &= \nu\beta(I+\xi J)W - \mu J - \rho J && \text{(4.4d)}
\end{aligned}$$

Note that the region relevant for our epidemiological setting

$$(S(t), I(t), W(t), J(t)) \in \mathcal{D} := \left\{(s,i,w,j) \in \mathbb{R}^4_{\geq 0} \mid 0 \leq s+i+w+j \leq 1\right\}$$

is forward invariant based on the above observations.

4.3 Equilibria and stability analysis

Now we turn our attention to finding equilibria $(S^*, I^*, R^*, W^*, J^*)$ of (4.2). The following lemma establishes that feasible ones arise from non-negative steady states of the reduced system (4.4).

Lemma 4.1. *Let (S^*, I^*, W^*, J^*) be a non-negative equilibrium of (4.4). Then*

$$(S^*, I^*, W^*, J^*) \in \mathcal{D}$$

and, hence, $(S^*, I^*, R^*, W^*, J^*)$ *with* $R^* := 1 - S^* - I^* - W^* - J^*$ *is epidemiologically feasible.*

Proof. Equilibria of (4.4) are obtained as solutions of

$$-\beta(I^* + \xi J^*)S^* + \omega\kappa W^* + \mu(1 - S^*) = 0, \tag{4.5a}$$

$$\beta(I^* + \xi J^*)S^* - \gamma I^* - \mu I^* = 0, \tag{4.5b}$$

$$\alpha\kappa(1 - S^* - I^* - W^* - J^*) - \omega\kappa W^* - \nu\beta(I^* + \xi J^*)W^* - \mu W^* = 0, \tag{4.5c}$$

$$\nu\beta(I^* + \xi J^*)W^* - \mu J^* - \rho J^* = 0. \tag{4.5d}$$

Summing all equations yields

$$(\mu + \alpha\kappa)(1 - S^* - I^* - W^* - J^*) - \gamma I^* - \rho J^* = 0,$$

thus, $S^* + I^* + W^* + J^* \leq 1$ as $0 < \gamma, \rho, (\alpha\kappa + \mu)$ and $0 \leq I^*, J^*$. □

The converse is readily satisfied, namely, given $(S^*, I^*, R^*, W^*, J^*)$ an epidemiologically feasible equilibrium of (4.2), we have $(S^*, I^*, W^*, J^*) \in \mathcal{D}$. Consequently, in the following we concentrate on finding non-negative equilibria of (4.4) and, then, we study their local stability.

Note that equation (4.5a) implies $S^* > 0$ for non-negative equilibrium.

4.3.1 Disease free equilibrium

Assume $I^* = 0$. Then, $J^* = 0$ follows from (4.5b) and the above observation on S^* being positive. The non-negativity implies $S^* = 1$ and, in turn, $W^* = 0$ from (4.5a). The resulting equilibrium $(S^*, I^*, W^*, J^*) = (1, 0, 0, 0)$ is referred to as the *disease free equilibrium* (DFE).

We note that even if we relax the non-negativity condition, no other equilibria exist with $I^* = 0$. We refer to our computer algebra codes for further details [63].

4.3.2 Existence of non-trivial equilibria

Let us now consider $I^* \neq 0$ and assume $\xi > 0$. We will return to the case $\xi = 0$ later. Equation (4.5d) implies $W^* = 0$ if and only if $J^* = 0$ and then

$$\begin{aligned} S^* &= \frac{\gamma+\mu}{\beta}, \\ I^* &= \mu\left(\frac{1}{\gamma+\mu} - \frac{1}{\beta}\right), \\ \alpha\kappa\gamma\left(\frac{1}{\gamma+\mu} - \frac{1}{\beta}\right) &= 0. \end{aligned}$$

Thus, in this case $\beta = \gamma + \mu$ and we, again, obtain the DFE. Hence, we may assume both $W^* \neq 0$ and $J^* \neq 0$. Also, $\rho + \mu - \nu\beta\xi W^* \neq 0$ as equality would imply $I^* = 0$ by (4.5d).

After these preliminary observations, we begin by expressing (S^*, I^*, J^*) in terms of W^*. From (4.5b) and (4.5d), we obtain

$$\frac{J^*}{I^*} = \frac{\gamma+\mu-\beta S^*}{\beta\xi S^*} = \frac{\nu\beta W^*}{\rho+\mu-\nu\beta\xi W^*}$$

yielding

$$S^* = \frac{\gamma+\mu}{\beta} - \frac{\nu\xi(\gamma+\mu)}{\rho+\mu}W^*. \tag{4.6}$$

Then, adding (4.5a) and (4.5b) results in

$$I^* = \frac{\omega\kappa W^* + \mu(1-S^*)}{\gamma+\mu}$$

that simplifies to

$$I^* = \mu\left(\frac{1}{\gamma+\mu} - \frac{1}{\beta}\right) + \left(\frac{\omega\kappa}{\gamma+\mu} + \frac{\mu\nu\xi}{\rho+\mu}\right)W^*. \tag{4.7}$$

Finally, (4.5d) and (4.6) gives

$$J^* = \frac{\nu\beta I^* W^*}{\rho+\mu-\nu\beta\xi W^*}. \tag{4.8}$$

We note that (4.8) could be expanded solely in terms of W^* using (4.7). Nevertheless, the

added complexity would serve no benefit and, thus, the expansion is omitted.

Using the above formulae and reducing (4.5), we obtain a quadratic equation for W^* from (4.5) as

$$f(W^*) := A(W^*)^2 + BW^* + C = 0, \tag{4.9}$$

with

$$\begin{aligned} A &= \nu\beta^2\Big[-\nu\xi^2(\gamma+\mu)Q_0 + \xi Q_1 + \big(\alpha\kappa(\rho+\mu) - \nu\xi\mu(\gamma+\mu) - \eta\kappa(\rho+\mu)\big)Q2\Big], \\ B &= \beta(\rho+\mu)\Big[\big(\nu\xi(\gamma+\mu) - \nu\xi(\beta-\gamma-\mu)\big)Q_0 - Q_1 - \nu\mu(\beta-\gamma-\mu)Q_2\Big], \\ C &= (\beta-\gamma-\mu)(\rho+\mu)^2Q_0, \end{aligned} \tag{4.10}$$

where

$$\begin{aligned} \eta &:= \alpha + \omega = \alpha\omega, \\ Q_0 &:= \alpha\kappa\gamma, \\ Q_1 &:= \Big[(\gamma+\mu)(\eta\kappa+\mu) + \eta\kappa^2\Big](\rho+\mu), \\ Q_2 &:= \alpha\kappa + \rho + \mu. \end{aligned} \tag{4.11}$$

Therefore, based on the sign of the discriminant $\Delta = B^2 - 4AC$, system (4.5) has 0, 1 or 2 additional real solutions besides the DFE. Note that equilibria originating from a real root of the quadratic equation coincides with the DFE iff the root is zero.

Let us now investigate the non-negativity of these new equilibria. Based on our initial considerations at the beginning of this section, we are looking for positive solutions and, thus, we assume that (4.9) has a solution $W^* > 0$. Then, the inequality

$$W^* < \frac{\rho+\mu}{\nu\beta\xi} =: \overline{W} \tag{4.12}$$

must hold in order to ensure $S^* > 0$ based on (4.6). Similarly,

$$W^* > \frac{\mu(-\beta+\gamma+\mu)(\rho+\mu)}{\beta(\mu\nu\xi(\gamma+\mu)+\omega\kappa(\rho+\mu))} =: \underline{W} \tag{4.13}$$

follows from (4.7).

Finally, one can see from (4.8) that $J^* > 0$ readily follows from (4.12), (4.13), and $W^* > 0$. Summarizing these findings and using Lemma 4.1 yield that a solution W^* of (4.9) leads to an epidemiologically feasible equilibrium other than the DFE by (4.3), (4.6), (4.7), and (4.8) if and only if

$$\max\{0, \underline{W}\} < W^* < \overline{W}. \tag{4.14}$$

Note that the above conditions guarantee the non-negativity of the equilibrium, hence, it follows from Lemma 4.1 that $(S^*, I^*, W^*, J^*) \in \mathcal{D}$. In particular, $W^* \leq 1$ must hold implying that no such W^* may exist if $\underline{W} \geq 1$.

For the upper bound, straightforward calculation shows that the quadratic formula (4.9) is negative at

$$f(\overline{W}) = -\frac{(\rho+\mu)^2(\mu\nu\beta\xi+(\eta-\alpha)\kappa(\rho+\mu))}{\nu\xi^2}Q_2 < 0 \tag{4.15}$$

given any parametrization conforming Table 4.1.

Let us now analyze the lower bound and the sign of f at that point. Clearly, $0 \geq \underline{W}$ if and only if $\beta \geq \gamma + \mu$. Note that the *basic reproduction number* $\mathcal{R}_0$ of the system (4.4) – and of

(4.2) – is obtained as the spectral radius of

$$-\mathbf{T}\mathbf{\Sigma}^{-1} = -\begin{bmatrix} \beta & 0 & \beta\xi \\ 0 & 0 & 0 \\ 0 & 0 & 0 \end{bmatrix} \times \begin{bmatrix} -(\gamma+\mu) & 0 & 0 \\ -\alpha\kappa & -(\alpha\kappa+\omega\kappa+\mu) & -\alpha\kappa \\ 0 & 0 & -(\rho+\mu) \end{bmatrix}^{-1}$$
$$= \begin{bmatrix} \frac{\beta}{\gamma+\mu} & 0 & \frac{\beta\xi}{\gamma+\mu} \\ 0 & 0 & 0 \\ 0 & 0 & 0 \end{bmatrix}$$

via the next generation matrix method [34], where $\mathbf{T}$ and $\mathbf{\Sigma}$ represent the transmission part describing the production of new infections, and the transition part describing changes in state, of the linearized infected subsytem composed of (I, W, J), respectively, where $\mathbf{T}+\mathbf{\Sigma}$ is the corresponding Jacobian. Therefore,

$$\mathcal{R}_0 = \frac{\beta}{\gamma+\mu},$$

and the condition $\beta \geq \gamma+\mu$ translates to $\mathcal{R}_0 \geq 1$.

Consider now $\mathcal{R}_0 > 1$. The y-intercept of the parabola in (4.9) is positive, i.e., $f(0) = C > 0$. Hence, f has exactly one root in the interval $(0, \overline{W})$ and, as a consequence, (4.4) has one other epidemiologically feasible equilibrium besides the DFE. This new equilibrium is referred to as the *endemic equilibrium* (EE). Note that, independent of the parametrization, the formula for EE is obtained by using the root

$$W^* \equiv W^*_- = \frac{-B - \sqrt{B^2 - 4AC}}{2A}. \tag{4.16}$$

The case $\mathcal{R}_0 < 1$ is more involved. The lower bound in (4.14) is now given by $\underline{W}$ and

elementary calculations yield

$$f(\underline{W}) = \frac{(\beta-\gamma-\mu)(\rho+\mu)^2(\omega\kappa(\rho+\mu)Q_0+\mu Q_1)(\mu\nu\beta\xi+\omega\kappa(\rho+\mu))}{\left(\mu\nu\xi(\gamma+\mu)+\omega\kappa(\rho+\mu)\right)^2} < 0. \tag{4.17}$$

Thus, by (4.15) and (4.17), if f has a root in $(\underline{W}, \overline{W})$, then f is a downward parabola with non-negative discriminant Δ. Moreover, if $\Delta > 0$, then it has two roots of the sought quality leading to two other epidemiologically feasible equilibria. A more thorough sign analysis of Δ reveals that if such equilibria exist then they do so for an interval of β values in the left neighbourhood of $\gamma+\mu$ distant from 0.

Theorem 4.1. *Let*

$$\Theta = \nu\xi(\gamma+\mu)Q_0 - Q_1, \tag{4.18}$$

with Q_0, Q_1 defined in (4.11). If $\Theta > 0$, then there is a $0 < \tilde{\beta} < \gamma+\mu$ such that, besides the DFE, there are two other epidemiologically relevant equilibria for $\beta \in (\tilde{\beta}, \gamma+\mu)$ and only the DFE for $\beta < \tilde{\beta}$. On the other hand, if $\Theta \leq 0$, then the only epidemiologically relevant equilibrium is the DFE for $\mathcal{R}_0 < 1$.

Remark We emphasize that the possibility of $\Theta > 0$ is not a consequence of the asymmetric partitioning we consider in this chapter as in the symmetric case it translates to

$$\nu\xi(\gamma+\mu)2\kappa\gamma - \left[(\gamma+\mu)(4\kappa+\mu)+4\kappa^2\right](\rho+\mu) > 0$$

that is clearly satisfiable with an appropriate choice of e.g. ν or ξ. Therefore, the associated results are applicable to [18] as well.

Proof. We consider $\beta \in (0, \gamma+\mu]$ that is $\mathcal{R}_0 \leq 1$. By the formulae (4.9), (4.10), (4.12), and (4.13) we have that A, B, C, Δ, f, $\underline{W}$, and $\overline{W}$ are continuous in β. Recall that f is guaranteed to take negative values at the endpoints of the interval $[\underline{W}, \overline{W}]$ as seen in (4.15) and (4.17). Hence, if for a $\beta_0 \in (0, \gamma+\mu]$ the parabola f has two roots in $(\underline{W}, \overline{W})$

(and consequently the discriminant $\Delta(\beta_0) > 0$), then, due to the continuity of all relevant expressions, there exists a corresponding maximal sub-interval $(\underline{\beta}, \overline{\beta})$ with

$$(0, \gamma + \mu) \supseteq (\underline{\beta}, \overline{\beta}) \ni \beta_0$$

such that the two roots persist (and $\Delta(\beta) > 0$) for $\beta \in (\underline{\beta}, \overline{\beta})$. Clearly, if $0 < \underline{\beta}$, then $\Delta(\underline{\beta}) = 0$ and, analogously, $\overline{\beta} < \gamma + \mu$ implies $\Delta(\overline{\beta}) = 0$.

From (4.10), we see that the discriminant Δ, as a function of β, takes the form

$$\Delta(\beta) = (\rho + \mu)^2 \cdot \beta^2 \cdot g(\beta),$$

where g is an upward parabola with lead coefficient $\nu^2(\xi Q_0 + \mu Q_2)^2 > 0$. Hence, $\Delta(\beta)$ can have at most two zeros in $\beta \in (0, \gamma + \mu]$.

These observations imply that the subset of $(0, \gamma+\mu)$ where f has two roots in $(\underline{W}, \overline{W})$ must have one of the forms;

- Δ has no zeros in $(0, \gamma + \mu)$: $\quad \emptyset$ or $(0, \gamma + \mu)$,
- Δ has one single zero $\tilde{\beta}$ in $(0, \gamma + \mu)$: $\quad (0, \tilde{\beta})$ or $(\tilde{\beta}, \gamma + \mu)$,
- Δ has two single zeros $\tilde{\beta}_1, \tilde{\beta}_2$ in $(0, \gamma + \mu)$: $\quad (0, \tilde{\beta}_1) \cup (\tilde{\beta}_2, \gamma + \mu)$.
  (or a double zero at $\tilde{\beta}_1 = \tilde{\beta}_2$)

We can rule out the options having 0 as a left endpoint by noting that

$$\lim_{\beta \to 0} \underline{W} = \lim_{\beta \to 0} \overline{W} = \infty,$$

thus, in a neighbourhood of 0, the inequality $\underline{W} > 1$ holds guaranteeing that no suitable root exists. Therefore, we are left with two possible forms $\emptyset$ and $(\beta^*, \gamma + \mu)$ with $\beta^* > 0$ in the latter.

In order to finish our proof, we now show that the sign of Θ determines if f has a root in the left neighbourhood of $\beta = \gamma + \mu$. First, note that the sign of the y-intercept of f is given as $C(\beta) = 0$ when $\beta = \gamma + \mu$ and $C(\beta) < 0$ for $\beta < \gamma + \mu$ and that $\underline{W}(\beta) = 0$ when $\beta = \gamma + \mu$. Next, the discriminant at the critical point is

$$\Delta(\beta)\Big|_{\beta=\gamma+\mu} = \Theta^2(\gamma+\mu)^2(\rho+\mu)^2.$$

Finally, the slope of the parabola f in (4.9) at $W^* = 0$ is given by

$$B(\beta) = \beta(\rho+\mu)\Big[\Theta - (\beta-\gamma-\mu)\nu(\xi Q_0 + \mu Q_2)\Big]$$

Clearly, for $\beta = \gamma + \mu$, the inequality $\Theta > 0$ implies that the above slope is positive securing the existence of another root of the parabola f in $(0, \overline{W})$ as $f(\overline{W}) < 0$ holds. Then, by continuity and by $\Delta(\beta)|_{\beta=\gamma+\mu} > 0$, we have that this root persists in an open neighbourhood of $\beta = \gamma + \mu$. On the other hand, when $\Theta \leq 0$, the slope is non-positive in an open left neighbourhood of $\beta = \gamma + \mu$, thus, no other root may exist there as the y-intercept is negative. □

It is apparent that $\mathcal{R}_0 = 1$ marks a significant change in the dynamics. We analyze the corresponding bifurcation in the following section. Not surprisingly, the key expression Θ of Theorem 4.1 will appear there as well, broadening our understanding of its origin.

4.3.3 Transcritical bifurcation at $\mathcal{R}_0 = 1$

In this section, we analyze the local stability of the DFE and its connection with $\mathcal{R}_0$. First, let us consider the Jacobian matrix of our SIRWJS system (4.4)

$$\mathbf{J} = \begin{bmatrix} -\beta(I+\xi J)-\mu & -\beta S & \omega\kappa & -\beta\xi S \\ \beta(I+\xi J) & \beta S-(\gamma+\mu) & 0 & \beta\xi S \\ -\alpha\kappa & -\nu\beta W-\alpha\kappa & -\nu\beta(I+\xi J)-(\alpha\kappa+\omega\kappa+\mu) & -\nu\beta\xi W-\alpha\kappa \\ 0 & \nu\beta W & \nu\beta(I+\xi J) & \nu\beta\xi W-(\rho+\mu) \end{bmatrix}.$$

and evaluate at the DFE

$$\mathbf{J}|_{(1,0,0,0)} = \begin{bmatrix} -\mu & -\beta & \omega\kappa & -\beta\xi \\ 0 & \beta-(\gamma+\mu) & 0 & \beta\xi \\ -\alpha\kappa & -\alpha\kappa & -(\alpha\kappa+\omega\kappa+\mu) & -\alpha\kappa \\ 0 & 0 & 0 & -(\rho+\mu) \end{bmatrix}.$$

The corresponding eigenvalues are

$$\lambda_1 = \beta-(\gamma+\mu), \quad \lambda_2 = -(\alpha\kappa+\mu), \quad \lambda_3 = -(\omega\kappa+\mu), \quad \lambda_4 = -(\rho+\mu). \tag{4.19}$$

Then, as the eigenvalues λ_2, λ_3, and λ_4 are negative and $\lambda_1 < 0$ if and only if $\beta < \gamma+\mu$, we can conclude that the DFE is locally asymptotically stable when $\mathcal{R}_0 < 1$ and unstable if $\mathcal{R}_0 > 1$.

The following theorem establishes that a transcritical bifurcation happens at $\mathcal{R}_0 = 1$. We show that the sign of Θ, defined in (4.18), gives the direction of this bifurcation. The proof relies on Theorem 4.1 of [45].

Theorem 4.2. *If $\Theta > 0$, then a transcritical bifurcation of backward type occurs at $\mathcal{R}_0 = 1$, and when $\Theta < 0$, then a transcritical bifurcation of forward type occurs at $\mathcal{R}_0 = 1$.*

Proof. We apply Theorem 4.1 of [45] to the system $\dot{\mathbf{x}} = g(\mathbf{x}, b)$, where the vector field

$$g = (g_S, g_I, g_W, g_J)$$

is obtained by applying the substitutions for our bifurcation parameter $\beta \to b+\beta^*$ with $\beta^* = \gamma + \mu$, corresponding to the critical case $\mathcal{R}_0 = 1$, and for the state variables $(S, I, W, J) \to (x_S, x_I, x_W, x_J) + (1, 0, 0, 0)$ which are then written as

$$\mathbf{x} = (x_S, x_I, x_W, x_J).$$

Then, $M := D_{\mathbf{x}} g(\mathbf{0}, 0)$ equals to the Jacobian matrix of (4.4) at the DFE, namely to $\mathbf{J}|_{(1,0,0,0)}$ with $\beta = \beta^*$. Hence, M has one simple zero eigenvalue and three eigenvalues with negative real part as in (4.19). Now, we calculate the right and left eigenvectors w, v of M corresponding to the zero eigenvalue. The system $Mw = 0$ is underdetermined, so we may fix $w_I = 1$. Then,

$$w_S = -\frac{Q_1}{(\alpha\kappa + \mu)(\kappa\omega + \mu)(\rho + \mu)}, \quad w_I = 1, \quad w_W = \frac{Q_0}{(\alpha\kappa + \mu)(\kappa\omega + \mu)}, \quad w_J = 0.$$

Similarly, setting $v_I = 1$ yields

$$v_S = 0, \quad v_I = 1, \quad v_W = 0, \quad v_J = \frac{\xi(\gamma + \mu)}{\rho + \mu}.$$

Now, we need to calculate the following quantities

$$Z_1 = \sum_{k,i,j \in \{S,I,W,J\}} v_k w_i w_j \frac{\partial^2 g_k}{\partial x_i \partial x_j}(\mathbf{0}, 0) \qquad \text{and}$$
$$Z_2 = \sum_{k,i \in \{S,I,W,J\}} v_k w_i \frac{\partial^2 g_k}{\partial x_i \partial b}(\mathbf{0}, 0).$$

Since $v_S = v_W = 0$, the partial derivatives of g_S and g_W have no influence on the above

expressions. Also, as $w_J = 0$, partial derivatives with respect to x_J can be omitted. Thus, we are left with the following relevant nonzero second order partial derivatives

$$\frac{\partial^2 g_I}{\partial x_S \partial x_I}(\mathbf{0}, 0) = \beta^*, \quad \frac{\partial^2 g_J}{\partial x_I \partial x_W}(\mathbf{0}, 0) = \nu\beta^*, \quad \frac{\partial^2 g_I}{\partial x_I \partial \beta}(\mathbf{0}, 0) = 1$$

leading to the simplified expressions

$$\begin{aligned} Z_1 &= 2v_I w_S w_I \frac{\partial^2 g_I}{\partial x_S \partial x_I}(\mathbf{0}, 0) + 2v_J w_I w_W \frac{\partial^2 g_J}{\partial x_I \partial x_W}(\mathbf{0}, 0) \\ &= \frac{2\beta^*}{(\alpha\kappa + \mu)(\kappa\omega + \mu)(\rho + \mu)} \Big[\nu\xi(\gamma + \mu)Q_0 - Q_1\Big] \\ &= \frac{2\beta^*}{(\alpha\kappa + \mu)(\kappa\omega + \mu)(\rho + \mu)} \cdot \Theta \qquad \text{and} \\ Z_2 &= v_I w_I \frac{\partial^2 g_I}{\partial x_I \partial \beta}(\mathbf{0}, 0) = v_I w_I = 1. \end{aligned}$$

As $Z_2 > 0$ for all model parameters, only the sign of Z_1 decides upon the direction of the bifurcation. Therefore, if $\Theta > 0$ (< 0), then a transcritical bifurcation of backward (forward) type occurs at $\mathcal{R}_0 = 1$. □

Let us summarize our epidemiological feasible findings. Depending on the parameters in the system, there can be two types of bifurcations at $\mathcal{R}_0 = 1$, forward (supercritical) or backward (subcritical), Figure 4.2. In a forward bifurcation, a small positive asymptotically stable equilibrium appears and the disease free equilibrium losses its stability at $\mathcal{R}_0 = 1$. On the other hand, in a backward bifurcation, a branch of unstable endemic equilibria emerges from the DFE.

This phenomenon was also observed for example in [20, 62], where the qualitative properties of a simple two-stage contagion model was investigated. The backward bifurcation case is of particular importance as it leads to a bistable situation and the potential persistence of the disease in the population even for $\mathcal{R}_0 < 1$.

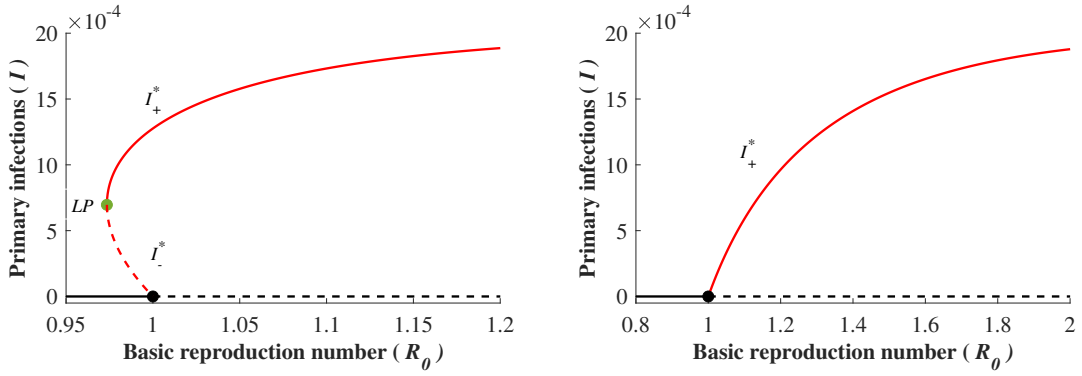

Figure 4.2: Backward bifurcation (left) and forward bifurcation (right) at $\mathcal{R}_0 = 1$. Stable branches are marked with continuous and unstable branches with dashed lines. Note that the depicted stability may be lost for $\mathcal{R}_0 \gg 1$ as it will be discussed in later sections. The parameters used for both cases are $\rho = 17, \kappa = 0.1, \gamma = 17, \mu = 0.0125, \nu = 150, \alpha = 200$. The relative infectivity in the backward case is $\xi = 0.9$ and in the forward case $\xi = 0.001$.

Moreover, when $\Theta > 0$, i.e., the backward bifurcation case, the system undergoes a saddle-node bifurcation at a certain $\tilde{\beta} \in (0, \gamma + \mu)$, the existence of which is established in Theorem 4.1. The saddle-node bifurcation point is marked with LP on the equilibria branch. The upper branch of LAS positive equilibria extends beyond $\mathcal{R}_0 > 1$ which corresponds to the unique EE branch. In Section 4.3.5, we will analyze the local stability of the EE for $\mathcal{R}_0 \gg 1$ and observe the possibility of both losing and regaining local stability depending on the boosting coefficient, the partitioning of the period of immune protection, and the relative infectivity.

4.3.4 Case $\xi = 0$

In the analysis so far, we assumed $\xi > 0$. By considering a non-infectious J compartment, i.e. $\xi = 0$, the derivation of the formulae is slightly different. We omit details of the entire calculation here and only share the results.

The expressions (4.6), (4.7), (4.8), (4.9), and (4.10) for the equilibria (other than the DFE) stay valid. The bound $\overline{W}$ becomes infinity indicating that any root of the quadratic equation

that is conforming the lower bound in (4.14) leads to an epidemiologically feasible equilibrium. Moreover $\Theta < 0$, so it is guaranteed that a transcritical bifurcation of forward-type occurs at $\mathcal{R}_0 = 1$ and that no other equilibrium of interest exists for $\mathcal{R}_0 \leq 1$. For $\mathcal{R}_0 > 1$, it is easy to see that the lead coefficient of (4.9) is negative

$$A|_{\xi=0} = \nu\beta^2\Big[\big(\alpha\kappa(\rho+\mu) - \eta\kappa(\rho+\mu)\big)Q2\Big] = -\nu\beta^2\omega\kappa(\rho+\mu)Q_2 < 0,$$

hence, the parabola f is downward with the positive y-intercept C. These ensure the existence and uniqueness of the endemic equilibrium.

For an in-depth analysis, the reader is referred to our computer algebra codes [63].

4.3.5 Stability of the endemic equilibrium for $\mathcal{R}_0 > 1$

The Jacobian evaluated at the endemic equilibrium is

$$\mathbf{J} = \begin{bmatrix} -\mu - \beta(I^* + \xi J^*) & -\beta S^* & \omega\kappa & -\xi\beta S^* \\ \beta(I^* + \xi J^*) & \beta S^* - \gamma - \mu & 0 & \xi\beta S^* \\ -\alpha\kappa & -\alpha\kappa - \nu\beta W^* & -\alpha\kappa - \mu - \omega\kappa & -\alpha\kappa - \beta\nu\xi W^* \\ & & -\nu\beta(I^* + \xi J^*) & \\ 0 & \nu\beta W^* & \nu\beta(I^* + \xi J^*) & \beta\nu\xi W^* - \rho - \mu \end{bmatrix} \tag{4.20}$$

yielding the characteristic equation

$$\det(\mathbf{J} - \lambda I) = \lambda^4 + a_1\lambda^3 + a_2\lambda^2 + a_3\lambda + a_4 = 0 \tag{4.21}$$

with $a_4 = \det(\mathbf{J})$.

In order to analyze the stability of the EE, we shall use the Routh-Hurwitz criterion [41, 53] that gives information on the sign of the real parts of the roots of (4.21) through inequalities formulated in terms of a_i.

Theorem 4.3 (Routh-Hurwitz). *Let $\mathcal{R}_0 > 1$, EE as given by (4.6), (4.7), (4.8), (4.16) and* $\mathbf{J}$ *the Jacobian evaluated there as in (4.20).*

Then, EE is locally asymptotically stable if and only if the coefficients of the characteristic polynomial (4.21) satisfy

(i) $a_i > 0$ *for* $i = 1, 2, 3, 4$,

(ii) $a_1 a_2 > a_3$, *and*

(iii) $a_1 a_2 a_3 > a_1^2 a_4 + a_3^2$.

First, note that *(ii)* can be derived from the other two conditions. Then, let's turn our attention to the positivity of the coefficients that is to condition *(i)*.

Using that

$$I^* + \xi J^* = \frac{I^*(\rho+\mu)}{\rho+\mu-\beta\nu\xi W^*}$$

by (4.8) and the formula (4.6), we obtain

$$\mathbf{J} = \begin{bmatrix} -\mu - \frac{I^*\beta(\rho+\mu)}{\rho+\mu-\beta\nu\xi W^*} & -\frac{(\gamma+\mu)(\rho+\mu-\beta\nu\xi W^*)}{\rho+\mu} & \omega\kappa & -\frac{\xi(\gamma+\mu)(\rho+\mu-\beta\nu\xi W^*)}{\rho+\mu} \\ \frac{I^*\beta(\rho+\mu)}{\rho+\mu-\beta\nu\xi W^*} & \frac{\beta\nu\xi W^*(\gamma+\mu)}{\rho+\mu} & 0 & \frac{\xi(\gamma+\mu)(\rho+\mu-\beta\nu\xi W^*)}{\rho+\mu} \\ -\alpha\kappa & -\alpha\kappa - \nu\beta W^* & -\alpha\kappa - \mu - \omega\kappa & -\alpha\kappa - \beta\nu\xi W^* \\ & & -\frac{I^*\nu\beta(\rho+\mu)}{\rho+\mu-\beta\nu\xi W^*} & \\ 0 & \nu\beta W^* & \frac{I^*\nu\beta(\rho+\mu)}{\rho+\mu-\beta\nu\xi W^*} & -\rho - \mu + \beta\nu\xi W^* \end{bmatrix}.$$

When expanding $\det(\mathbf{J} - \lambda I)$, terms appear with positive and negative signs in each expression. We employed a series of operations grouping *all* negative ones with *some* of the positive terms leading to simplified residual expressions. For the technical details, we refer to the supplementary computer algebra codes [63]. As not all positive terms were used, these

residuals may serve as lower bounds on a_i and are listed below

$$a_1 = \eta\kappa + 2\mu + \frac{\gamma+\mu}{\rho+\mu}\beta\nu\xi W^* + \Big(\rho+\mu-\beta\nu\xi W^*\Big) + \frac{\beta I^*(\nu+1)(\rho+\mu)}{\rho+\mu-\beta\nu\xi W^*}, \tag{4.22a}$$

$$a_2 > \beta I^*(\rho+\mu) + \rho\frac{\eta\kappa+2\mu}{\rho+\mu}\Big(\rho+\mu-\beta\nu\xi W^*\Big), \tag{4.22b}$$

$$a_3 > \beta I^*(\rho+\mu)\Big(\eta\kappa+\gamma+2\mu\Big) + \Big(\rho+\mu-\beta\nu\xi W^*\Big)\rho\frac{\eta\kappa(\kappa+\mu)+\mu^2}{\rho+\mu}, \tag{4.22c}$$

$$a_4 > -\beta I^*\Theta. \tag{4.22d}$$

Clearly, the positivity of a_i for $i = 1, 2, 3$ is established by (4.22a), (4.22b), (4.22c) as $\rho+\mu-\beta\nu\xi W^* > 0$ must hold by (4.8) and by the positivity of the components of the EE. In addition, we see that assuming $\Theta \leq 0$ (*i.e.* the case of forward transcritical bifurcation) readily implies the positivity of a_4 in (4.22d).

To fully analyze this final coefficient, let us recall that $a_4 = \det(\mathbf{J})$. In order to obtain an alternative bound, we carry out a series of transformations on $\mathbf{J}$ in (4.20), all of which are preserving the sign of the determinant with the intermediate goal of obtaining a tractable row-echelon form. These transformations fall into four categories:

1. multiplication from left or right by a matrix with positive determinant:
   - scaling of a row/column by a positive number,
   - multiple row and column changes given by permutation matrices with det = 1,
   - carrying out row/column elimination towards the echelon form,
2. adding the zero matrix:
   - use (4.5) to hop back-and-forth between transmissional and transitional terms,
3. substitution of (4.6), (4.7), and (4.8),
4. algebraic manipulation of expressions.

Again, the exact steps of this procedure are documented in the supplementary computer algebra codes [63]. Here, we just present the final form obtained from the reduction that is the matrix $\tilde{\mathbf{J}}$ such that $\text{sign}(a_4) = \text{sign}(\det(\mathbf{J})) = \text{sign}(\det(\tilde{\mathbf{J}}))$:

$$\tilde{\mathbf{J}} = \begin{bmatrix} 1 & 0 & 0 & \beta\nu\xi\left(\frac{\mu}{\rho+\mu}Q_1 + \eta\kappa^2\gamma\right) \\ 0 & 1 & -\frac{1}{F_1} & -\left(F_1 - \frac{\mu(\beta-\gamma-\mu)}{\beta W^*}\right)Q_0 \\ 0 & 0 & 1 & F_2\left(\frac{\mu}{\rho+\mu}Q_1 + \eta\kappa^2\gamma\right) \\ 0 & 0 & 0 & F_1^2 Q_0 - F_2\left(\frac{\mu}{\rho+\mu}Q_1 + \eta\kappa^2\gamma\right) \end{bmatrix},$$

where

$$F_1 = \left((\gamma+\mu) + (\beta-\gamma-\mu)\frac{\rho+\mu}{\beta\nu\xi W^*}\right)\frac{\mu\nu\xi}{\mu+\rho} + \omega\kappa \qquad \text{and} \qquad F_2 = \beta\frac{\mu\nu\xi}{\mu+\rho} + \omega\kappa.$$

Clearly $F_1 > F_2 > 0$ by $\mathcal{R}_0 > 1$, (4.8) and $I^*, J^*, W^* > 0$, hence, it suffices to show that

$$F_2 Q_0 - \left(\frac{\mu}{\rho+\mu}Q_1 + \eta\kappa^2\gamma\right)$$

is positive. Note that

$$F_2 Q_0 = \frac{\mu}{\rho+\mu}\beta\nu\xi Q_0 + \eta\kappa^2\gamma$$

leads to analyzing the sign of

$$\beta\nu\xi Q_0 - Q_1.$$

Then, as $\beta\nu\xi Q_0 - Q_1 > \Theta$ when $\mathcal{R}_0 > 1$, we obtain the positivity of a_4 for $\Theta > 0$. Hence, using the implications of (4.22d) when $\Theta \leq 0$, we established that $a_4 > 0$ is satisfied that is condition *(i)* of Theorem 4.3 holds.

Therefore, by defining

$$y_\nu(\alpha, \xi) = a_1 a_2 a_3 - (a_1^2 a_4 + a_3^2), \tag{4.23}$$

all conditions of Theorem 4.3 are satisfied if and only if $y_\nu(\alpha, \xi) > 0$. When ξ is fixed, we

use the notation $y_\nu(\alpha)$. In the following, condition (4.23) is referred to as the RH criterion. The sign of (4.23) will be studied using numerical techniques in the next section.

4.4 Exploring bifurcations using numerics

In this section, we investigate numerically how the asymmetric partition of the immunity period, the boosting rate, and the relative infectivity influence the stability changes of the EE. Of particular interest are the formation of bistability regions influenced by the relative infectivity ξ.

For our numerical investigations, we set the parameters as

$$\begin{aligned} \gamma &= 17, \\ \kappa &= 1/10, \\ \mu &= 1/80, \\ \beta &= 260, \\ \rho &= 17, \end{aligned} \tag{4.24}$$

and $\xi \in (0, 1)$, taken from [16, 18], where authors studied natural immune boosting in pertussis dynamics.

In Chapter 3, a similar epidemic model (SIRWS) was investigated where the J compartment was absent and boosting resulted in immediate immunity, namely, a return to R from W. The current system reconstructs the same dynamics in the limit that is for $\xi = 0$ and $\rho \to \infty$. As a starting point, we briefly review the structure of the aforementioned scenario via Figure 4.3.

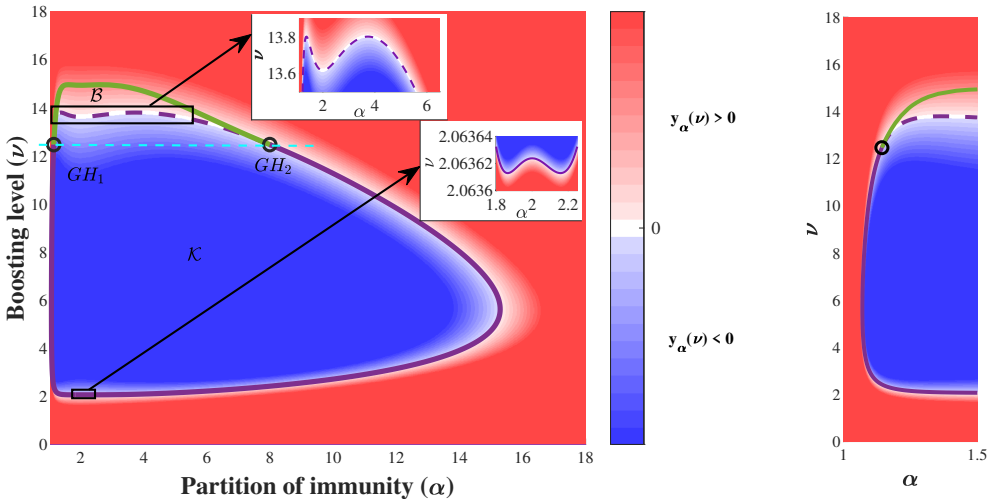

(a) (b)

Figure 4.3: Baseline dynamics: $\xi = 0$, $\rho \to \infty$. Heatmap of the RH stability criterion and bistability region. Purple curve represents $y_\nu(\alpha) = 0$.

First, we recall that at $\mathcal{R}_0 = 1$ the transcritical bifurcation was shown to be solely of forward type. At the baseline parametrization $\mathcal{R}_0 \approx 15.28$ and the endemic equilibrium is LAS but for the compact set $\mathcal{K}$ marked by blue. Note the symmetric presence of endemic double bubbles around the baseline partitioning $\alpha = \omega = 2$ at boosting $\nu \approx 2.06362$ and the stability switches at $\nu \approx 2.06362$, as highlighted in the insets of Figure 4.3a. The corresponding bifurcation diagrams are given in Figure 4.4. By an endemic bubble, we mean the structure in the bifurcation diagram which is formed when an endemic equilibrium is losing its stability via a Hopf bifurcation, but increasing further this parameter the stability of the endemic equilibrium is regained and the limit cycle disappears. The figure shows that such stability switches can occur twice with respect to the same parameter, hence the name endemic double bubble.

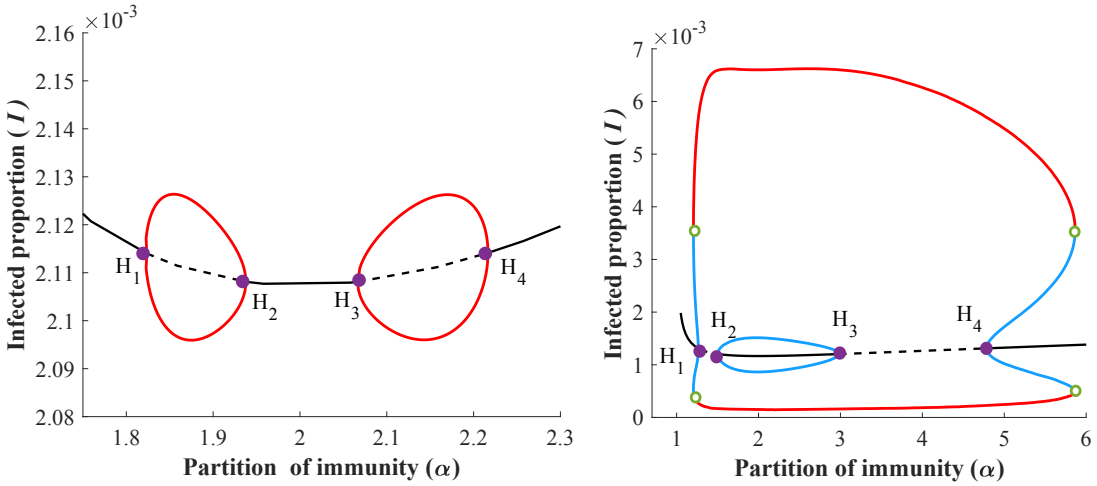

Figure 4.4: Baseline dynamics: $\xi = 0$, $\rho \to \infty$. Bifurcation diagram w.r.t α, with $\nu = 2.06362$ (left) and $\nu = 13.7$ (right). The depicted two bubbles of instability appear and disappear simultaneously. The latter phenomenon is referred to as *symmetric presence of bubbles*.

For slightly larger boosting $\nu \approx 14$, a bistable region $\mathcal{B}$ was observed where the EE is LAS together with a stable periodic orbit. The appearance of this bistable region is characterized by two *generalized Hopf points* GH_1 and GH_2 with identical ν coordinates.

Now, focusing on the current model and parametrization, first, we briefly study the direction of the transcritical bifurcation that is determined by the sign of Θ in Section 4.4.1, second, we analyze the stability of the EE through sign analysis of the RH criterion in Section 4.4.2. Then, we carry out numerical analysis of the bifurcations of the equilibrium branch and study how the bistable region is affected by the relative infectivity ξ in Section 4.4.3.

4.4.1 Direction of the transcritical bifurcation

Substituting the baseline parametrization (3.14) into (4.18), we have that $\Theta > 0$ is equivalent to

$$\nu\xi > \frac{1.00662\alpha}{\alpha - 1} + \frac{0.125092}{\alpha} =: \mathbf{b}(\alpha)$$

with the corresponding zero contour displayed in Figure 4.5.

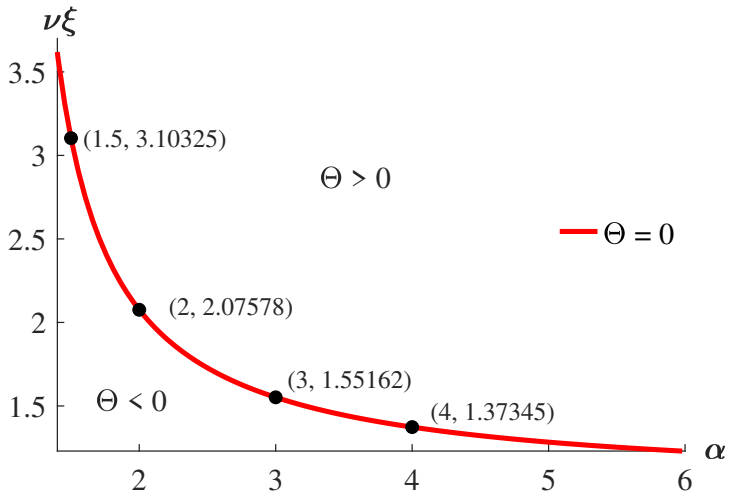

Figure 4.5: $\Theta = 0$ contour on the $(\alpha, \nu\xi)$ plain using the parametrization (3.14).

Clearly $\lim_{\alpha\to 1^+} \mathbf{b}(\alpha) = \infty$ and $\lim_{\alpha\to\infty} \mathbf{b}(\alpha) = 1.0062$, moreover, $\mathbf{b}(\alpha)$ is decreasing function of α. Consequently, the faster the transition from W to R, the smaller boosting coefficient ν is sufficient to activate backward transcritical bifurcation at $\mathcal{R}_0 = 1$ that is at $\beta = \gamma + \mu = 17 + 1/80$ while keeping the relative infectivity ξ fixed, or vice versa, smaller ξ is required with keeping ν fixed. For example, assuming a moderate boosting coefficient, *i.e.* $\nu < 3$, and a relative infectivity $\xi \sim O(1)$ may very well result in a backward bifurcation for $\alpha \geq 1.5$.

4.4.2 Stability switches of the EE

We constructed similar heatmaps to study the sign of $y_\alpha(\nu, \xi)$, given by (3.12), for various values of relative infectivity $\xi \geq 0$. Recall that $\rho = \gamma = 17$ in our setting, thus, for $\xi = 0$ we readily experience changes in the dynamics with respect to Figure 4.3. The instability set, marked as $\mathcal{K}_\xi$ to emphasize its dependence of ξ, is somewhat similar but the regular shape resulting in simultaneous appearance of double-bubbles of instability is lost, see Figure 4.6.

Note that in all figures that follow, $\mathcal{K}_\xi = \mathcal{K}$ for fixed ξ. Now, the region around $\nu \approx 2.06$ displays much simpler behaviour. Additionally, for $\nu \approx 13.5$, we still see bubbles, though

without the symmetry they possess in the limit $\rho \to \infty$.

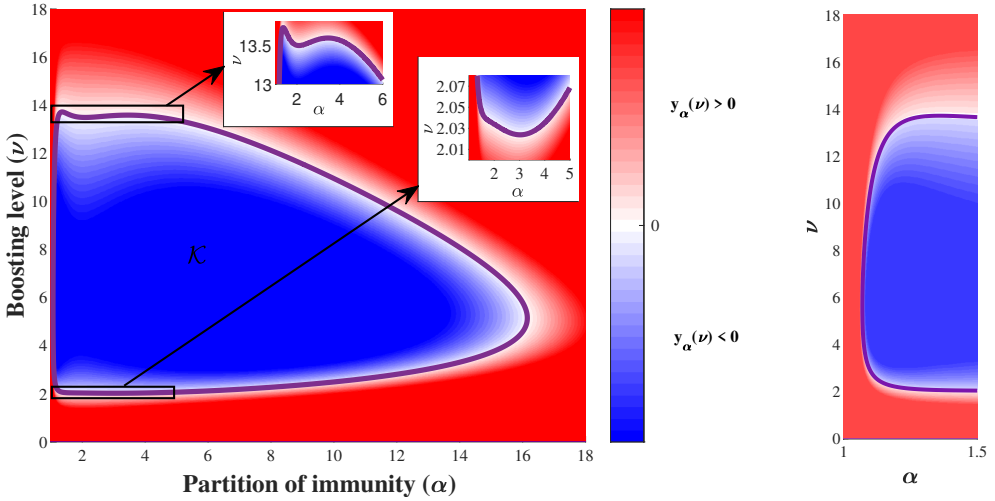

(a) (b)

Figure 4.6: Heatmap of the RH criterion (4.23) for $\xi = 0$. Purple curve represents $y_\nu(\alpha) = 0$.

By increasing $\xi \in (0, 1)$, we observe the following two phenomena. First, the shape of the $y_\alpha(\nu, \xi) = 0$ curve that bounds the set $\mathcal{K}_\xi$ changes, therefore it influences the number of stability switches of the EE in the (α, ν) plane. Second, the region $\mathcal{K}_\xi$ is shrinking and then disappearing, hence it results in the increase of local asymptotic stability region of the EE.

Dynamics of stability switches For small ξ, the RH criterion changes sign multiple times for boosting rates around 13.5 as α is varied, suggesting the continued presence of multiple stability switches that is the aforementioned bubbles, see again Figures 4.6. As ξ grows, the curve $y_\nu(\alpha, \xi) = 0$ is deforming so that these double-bubbles disappear, as in Figure 4.7.

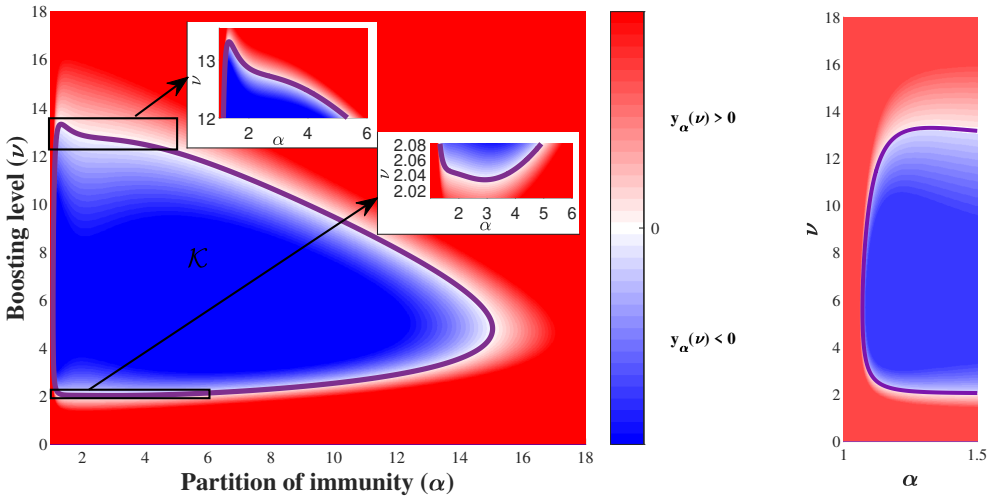

(a) (b)

Figure 4.7: Heatmap of the RH criterion (3.12) for $\xi = 10^{-4}$. Purple curve represents $y_\nu(\alpha) = 0$.

We localize the threshold value ξ_1^*, at which the relevant change in the qualitative behavior of the curve $y_\nu(\alpha, \xi) = 0$ occurs, as follows. In the region of interest ($1 < \alpha < 6$ and $13 < \nu$), the level curve $\alpha \mapsto \nu : y_\nu(\alpha) = 0$, originally (when $\xi = 0$), has two local maxima and one local minimum. As ξ gets larger, the right maximum and the minimum collide, then disappear. Thus, the threshold scenario may be found by looking for (ν, α, ξ) such that

$$\begin{bmatrix} y_\nu(\alpha, \xi) \\ \frac{\partial}{\partial \alpha} y_\nu(\alpha, \xi) \\ \frac{\partial^2}{\partial \alpha^2} y_\nu(\alpha, \xi) \end{bmatrix} = \begin{bmatrix} 0 \\ 0 \\ 0 \end{bmatrix},$$

yielding $\xi_1^* \approx 4.0098 \times 10^{-5}$. Figure 4.8 visualizes the transition in the qualitative behavior of the curve $y_\nu(\alpha, \xi) = 0$ highlighting the one corresponding to the threshold value in black.

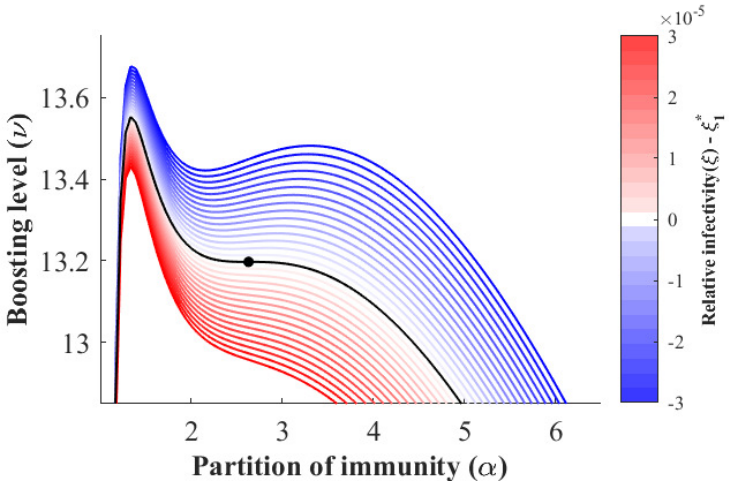

Figure 4.8: Level curves $y_\nu(\alpha, \xi) = 0$ for $\xi \in [\xi_1^* - 3 \times 10^{-5}, \xi_1^* + 3 \times 10^{-5}]$. The black curve corresponds to the threshold value ξ_1^*.

Shrinking of K_ξ The second phenomenon we analyze is how the compact region of instability K_ξ shrinks and disappears as we increase ξ, see Figure 4.9.

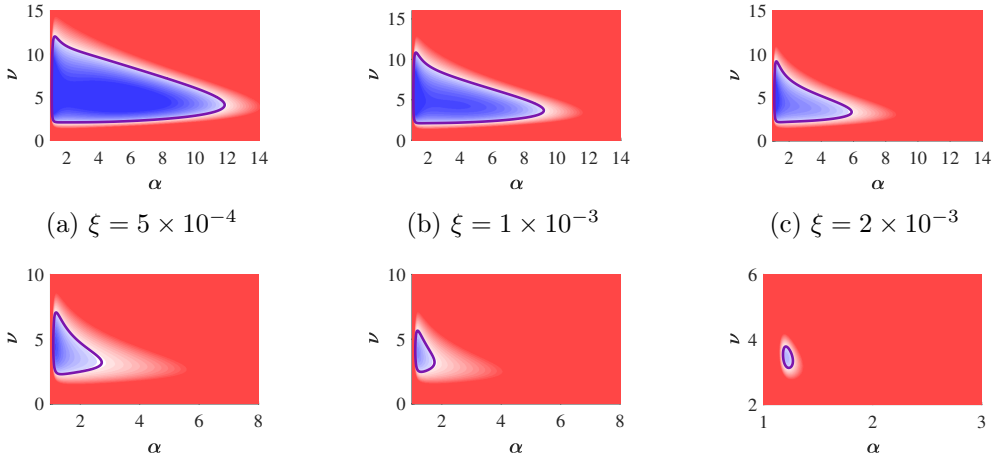

(a) $\xi = 5 \times 10^{-4}$ (b) $\xi = 1 \times 10^{-3}$ (c) $\xi = 2 \times 10^{-3}$

(d) $\xi = 4 \times 10^{-3}$ (e) $\xi = 6 \times 10^{-3}$ (f) $\xi = 9 \times 10^{-3}$

Figure 4.9: Heatmap of the RH criterion (4.23)

At the critical value ξ_2^*, the region K_ξ has shrunk to a single point. Clearly, this is a zero of the RH criterion, moreover, it is a local minimum both w.r.t. α and ν. Hence, we look for

(ν, α, ξ) solving

$$\begin{bmatrix} y_\nu(\alpha,\xi) \\ \frac{\partial}{\partial\alpha} y_\nu(\alpha,\xi) \\ \frac{\partial}{\partial\nu} y_\nu(\alpha,\xi) \end{bmatrix} = \begin{bmatrix} 0 \\ 0 \\ 0 \end{bmatrix}$$

leading to $\xi_2^* \approx 9.19845 \times 10^{-3}$. For larger relative infectivity *i.e.* $\xi > \xi_2^*$, there is no region of instability, $K_\xi = \emptyset$, that is, the EE is LAS for all (α, ν). The localized transition is visualized in Figure 4.10.

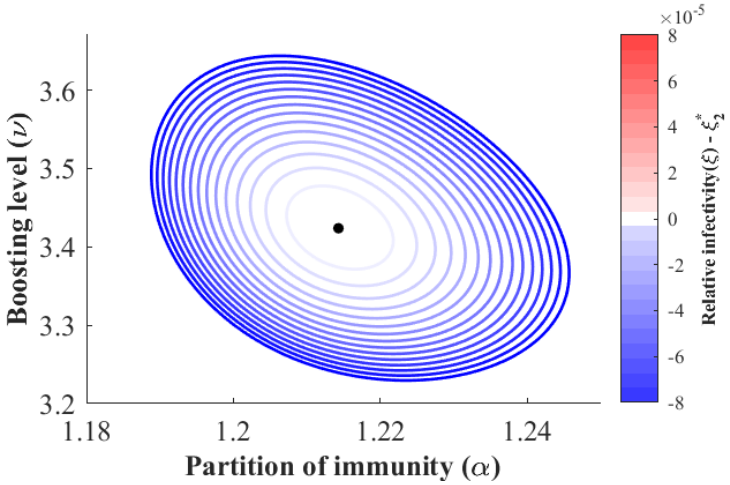

Figure 4.10: Level curves $y_\nu(\alpha, \xi) = 0$ for $\xi \in [\xi_2^* - 8 \times 10^{-5}, \xi_2^* + 8 \times 10^{-5}]$. The curves cease to exist for $\xi > \xi_2^*$, hence, no red is drawn. The black dot corresponds to the shrinking of K_ξ to a single point at the threshold value ξ_2^*.

Note that we did not investigate the dependence of these phenomena, and of the corresponding threshold values, on the other parameters fixed in (3.14).

4.4.3 Numerical bifurcation examples

In this section, we present numerical examples of one parameter (α) and two parameter (α, ν) bifurcations of the endemic equilibria branch using `MatCont` [21]. An identical analysis we carried out in [61] for an SIRWS system, therefore here we show some interesting examples

to highlight the dynamics in the presence of the J compartment.

We briefly summarize the dynamics on the two parameter (α, ν) bifurcation diagram when $\xi = 10^{-5} < \xi_1^*$, see Figure 4.11. The instability region $\mathcal{K}(= \mathcal{K}_\xi$ for fixed $\xi)$ is enclosed by the purple-colored Hopf curve, which is continuous when supercritical (called H_-) and dashed when subcritical (called H_+).

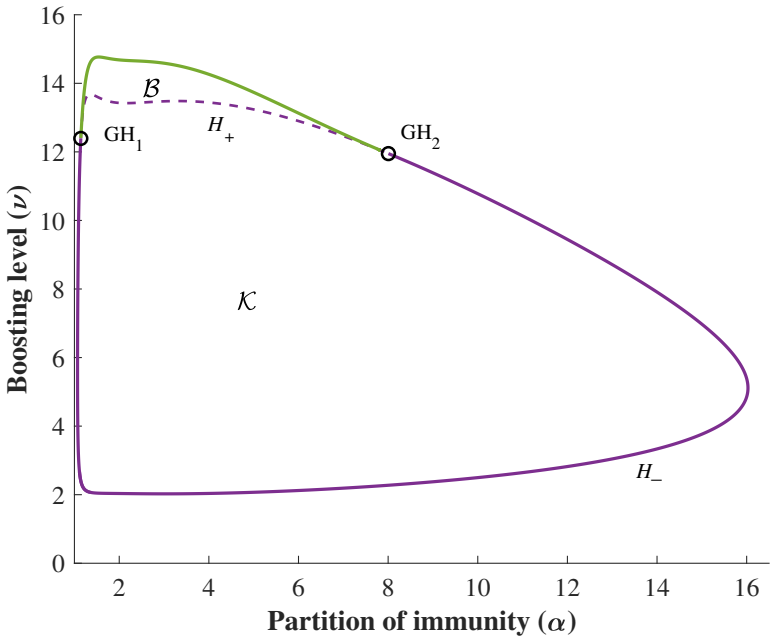

Figure 4.11: Two-parameter bifurcation diagram in the (α, ν)-plane, with $\xi = 10^{-5}$.

The two generalized Hopf points GH_1 and GH_2, mark the parameter values where the Hopf bifurcation changes from supercritical to subcritical. Note that these points now possess different ν coordinates as opposed to the limiting case in Figure 4.3. The branch of the limit points of periodic cycles appears in green, which together with the dashed purple curve H_+ enclose a bistability region $\mathcal{B}$, where there exists a stable periodic solution alongside the LAS endemic equilibrium.

Let us now examine the bifurcation diagram in more detail over regions, characterized by

various levels of boosting rate ν, where the dynamics is similar, see Figure 4.12 for such partition and Table 4.2 for the critical boosting values.

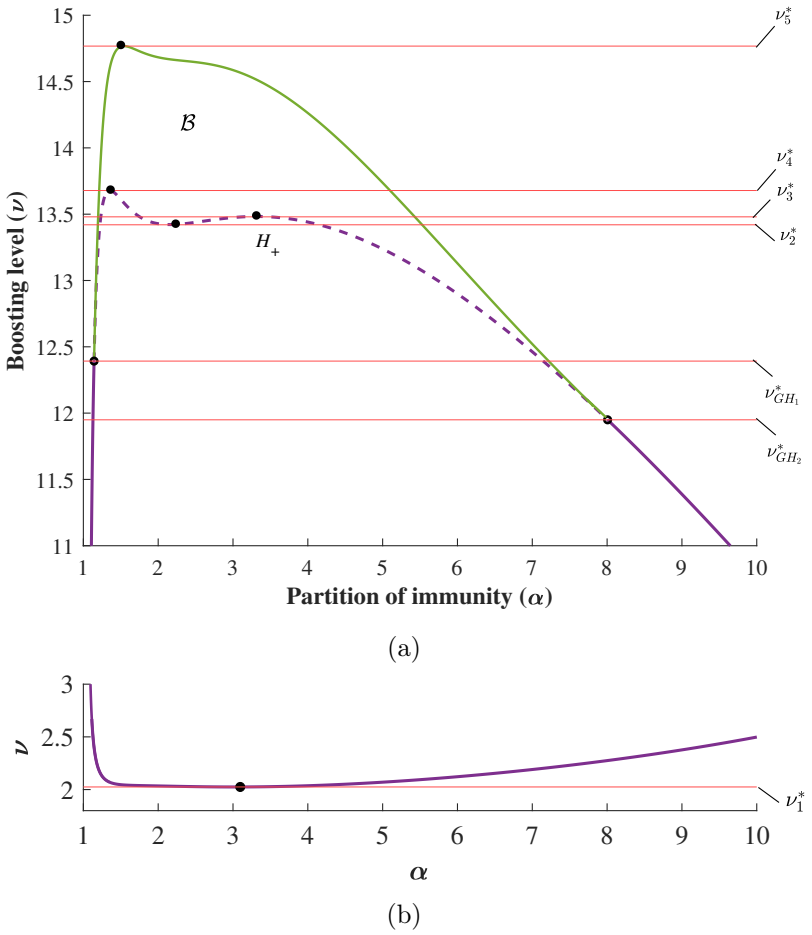

(a)

(b)

Figure 4.12: Two-parameter bifurcation diagram in the (α, ν)-plane, with $\xi = 10^{-5}$ and critical ν values.

ν_1^*	$\nu_{GH_2}^*$	$\nu_{GH_1}^*$	ν_2^*	ν_3^*	ν_4^*	ν_5^*
2.0248	11.9494	12.3922	13.42	13.48	13.6785	14.7675

Table 4.2: Approximate critical boosting values (ν_k^*) using the parametrization (3.14) and fixing $\xi = 10^{-5}$ as in Figure 4.12.

In all bifurcation plots that follow, the endemic equilibria branch (particularly the I and J

components) is marked with black curve, solid when LAS and dashed when unstable. Red and blue curves represent branches of stable and unstable limit cycles, respectively, and Hopf bifurcation points are marked with purple dots.

Boosting: $\nu < \nu_1^*$ The system has a stable point attractor for all $\alpha > 1$.

Boosting: $\nu_1^* < \nu < \nu_{GH_2}^*$ There are two supercritical Hopf bifurcation points on the endemic equilibria branch, see the lower inset in Figure 4.7a. Continuation of limit cycles with respect to α starting from two Hopf bifurcation points, H_1 and H_2, forms an endemic bubble, where the two branches of stable limit cycles coincide, see Figure 4.13.

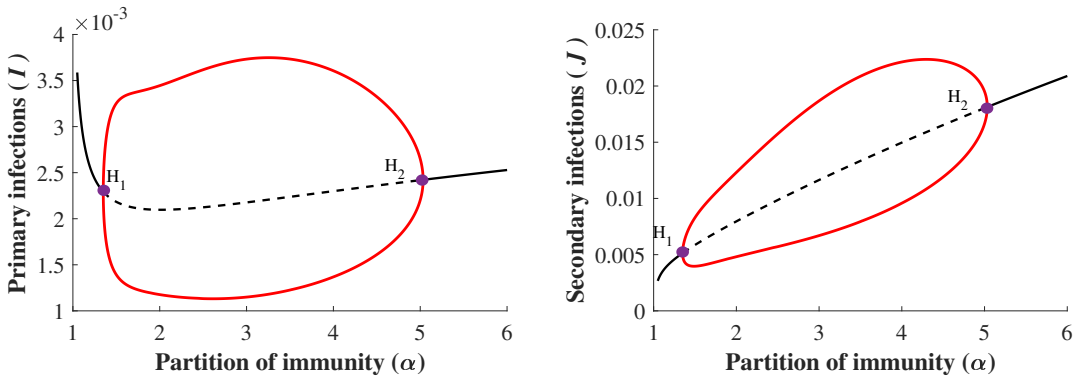

(a) (b)

Figure 4.13: One-parameter bifurcation diagram with $\xi = 10^{-5}$ and $\nu = 2.07$, (a) primary and (b) secondary infections.

Boosting: $\nu_{GH_2}^* < \nu < \nu_{GH_1}^*$ As ν continues to grow in the two-parameter plane in Figure 4.12 the generalized Hopf point GH_2 appears, which separates branches of sub- and supercritical Hopf bifurcations. The stable limit cycles survive when we enter the region $\mathcal{B}$. Crossing the subcritical Hopf boundary H_+ leads to an additional unstable cycle inside the first one, while the equilibrium regains its stability. Two cycles of opposite stability exist inside the bistable region $\mathcal{B}$ and disappear at the green curve.

Let us fix ν in this boosting region. Then Figure 4.14 shows a typical bifurcation w.r.t.

α. Observe here the small α-parameter range of bistability where the EE and the larger amplitude periodic solution are both stable. The points marked with green circle are limit points of periodic orbits. The stable and unstable cycles collide and disappear on the green curve in Figure 4.12, corresponding to a fold bifurcation of cycles.

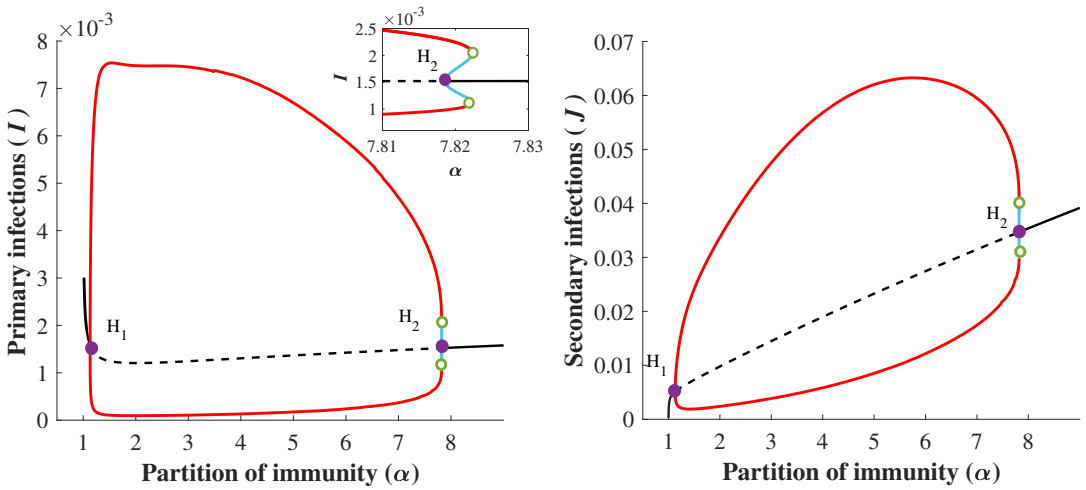

(a) (b)

Figure 4.14: One-parameter bifurcation diagram with $\xi = 10^{-5}$ and $\nu = 12.05$, (a) primary and (b) secondary infections.

Boosting: $\nu^*_{GH_1} < \nu < \nu^*_2$ In this boosting range, as we passed GH_1, the Hopf curve changed to subcritical. Figure 4.15 confirms the appearance of two subcritical Hopf bifurcations on the equilibria branch, then again a fold bifurcation of cycles occurs (marked with green circles), resulting in two small α-parameter intervals of bistability.

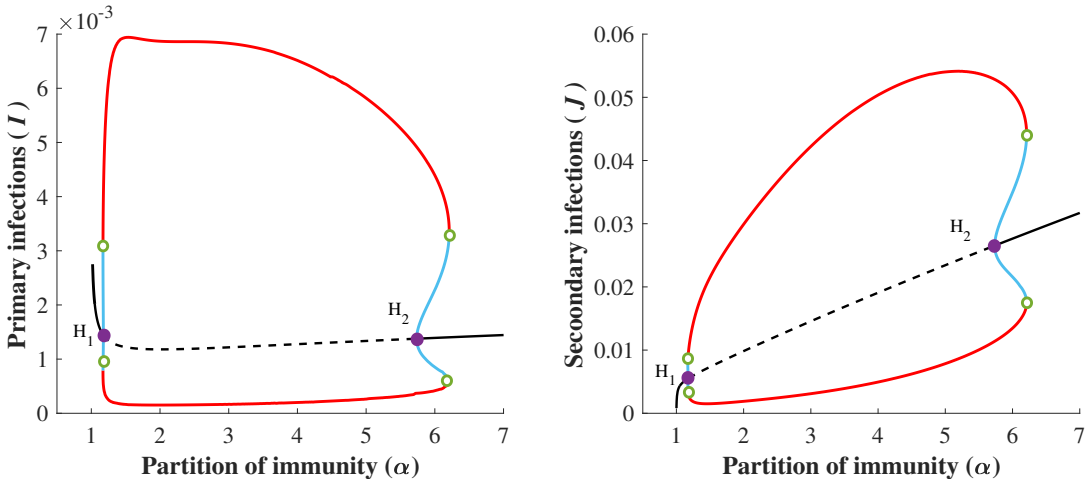

(a) (b)

Figure 4.15: One-parameter bifurcation diagram with $\xi = 10^{-5}$ and $\nu = 13$, (a) primary and (b) secondary infections.

Boosting: $\nu_2^* < \nu < \nu_3^*$ In this region, we can observe how the shape of the Hopf curve H_+ that bounds the set K_ξ influences the number of stability switches of the EE. In Figure 4.16, the bifurcation diagram shows the existence of four subcritical Hopf bifurcation points. Here, a small bubble appears inside the region of stable oscillations, which leads to an additional bistable region compared to the previous case. When we increase the boosting but still in this region, then the Hopf points H_1 and H_2 as well as H_3 and H_4 move closer to each other, resulting in larger bistability regions, see also Figure 4.12.

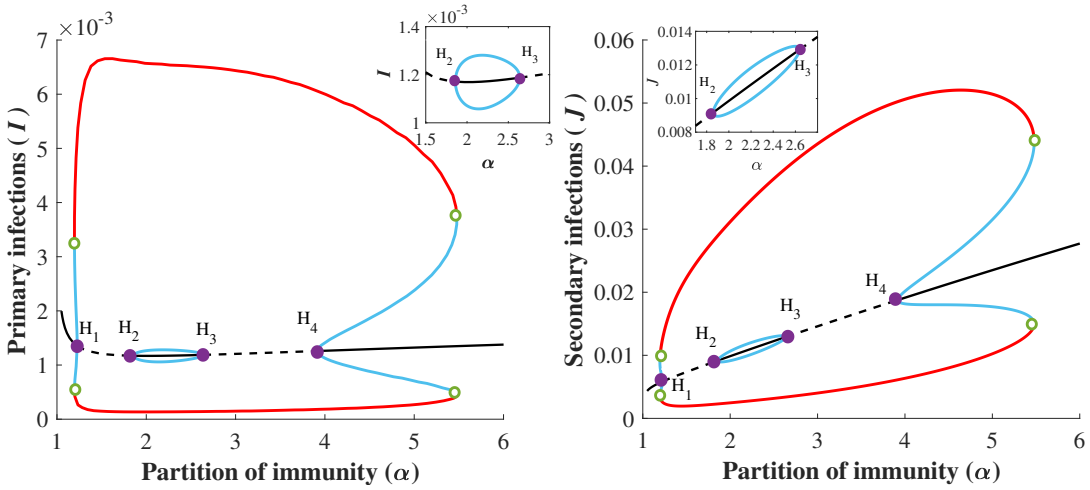

Figure 4.16: One-parameter bifurcation diagram with $\xi = 10^{-5}$ and $\nu = 13.45$, (a) primary and (b) secondary infections.

Boosting: $\nu_3^* < \nu < \nu_4^*$ Here, the two Hopf points H_3 and H_4 seen in the region before collided and disappeared, see Figure 4.17. The dynamics is similar to Figure 4.15 but the boosting values in this range lead to much larger bistability regions.

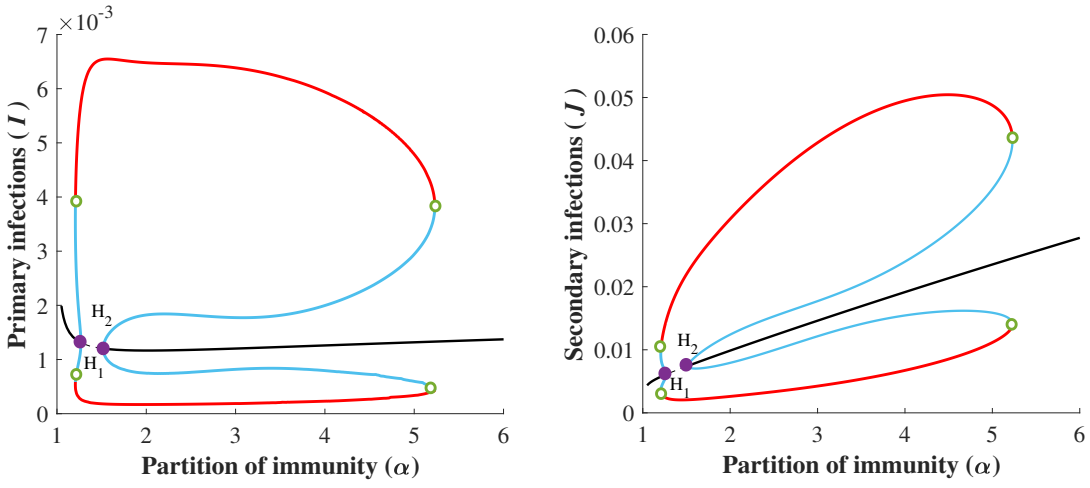

Figure 4.17: One-parameter bifurcation diagram with $\xi = 10^{-5}$ and $\nu = 13.6$, (a) primary and (b) secondary infections.

Boosting: $\nu_4^* < \nu < \nu_5^*$ Although, we are in the bistability region in the two-parameter bifurcation plot, we do not cross any Hopf curve, hence the numerical continuation method finds a stable equilibrium branch, see Fig 4.18.

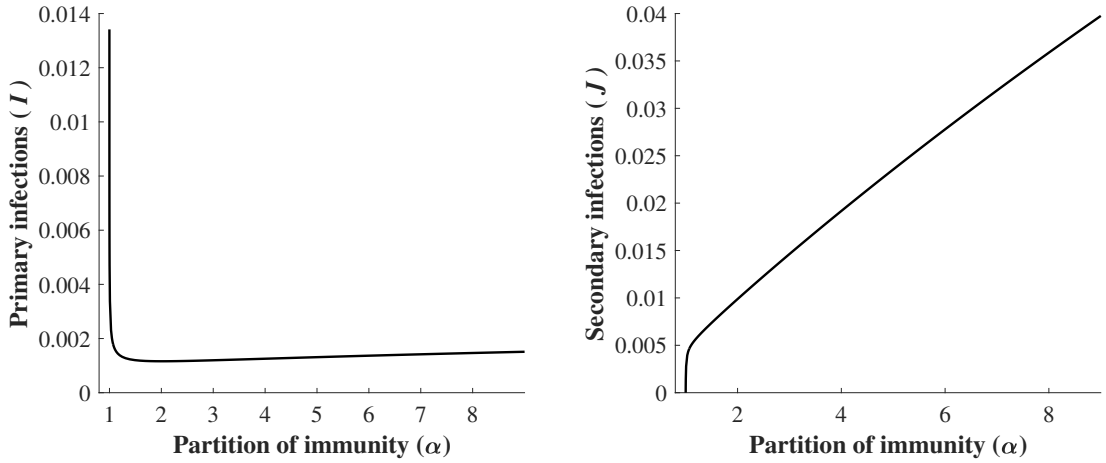

(a) (b)

Figure 4.18: One-parameter bifurcation diagram with $\xi = 10^{-5}$ and $\nu = 13.8$, (a) primary and (b) secondary infections.

Boosting: $\nu_5^* < \nu$ The system has a stable point attractor for all $\alpha > 1$.

Shrinking of the bistability region In Section 4.4.2 we analyzed the shrinking of the instability region $\mathcal{K}_\xi$ as ξ increases. As a consequence, the bistability region $\mathcal{B}$ becomes smaller, the generalized Hopf points move towards each other, then collide and disappear as illustrated in Figure 4.19. We did not localize further the threshold value $\xi_{\mathcal{B}}^* \in (8.3, 8.4) \times 10^{-3}$ at which this region disappears.

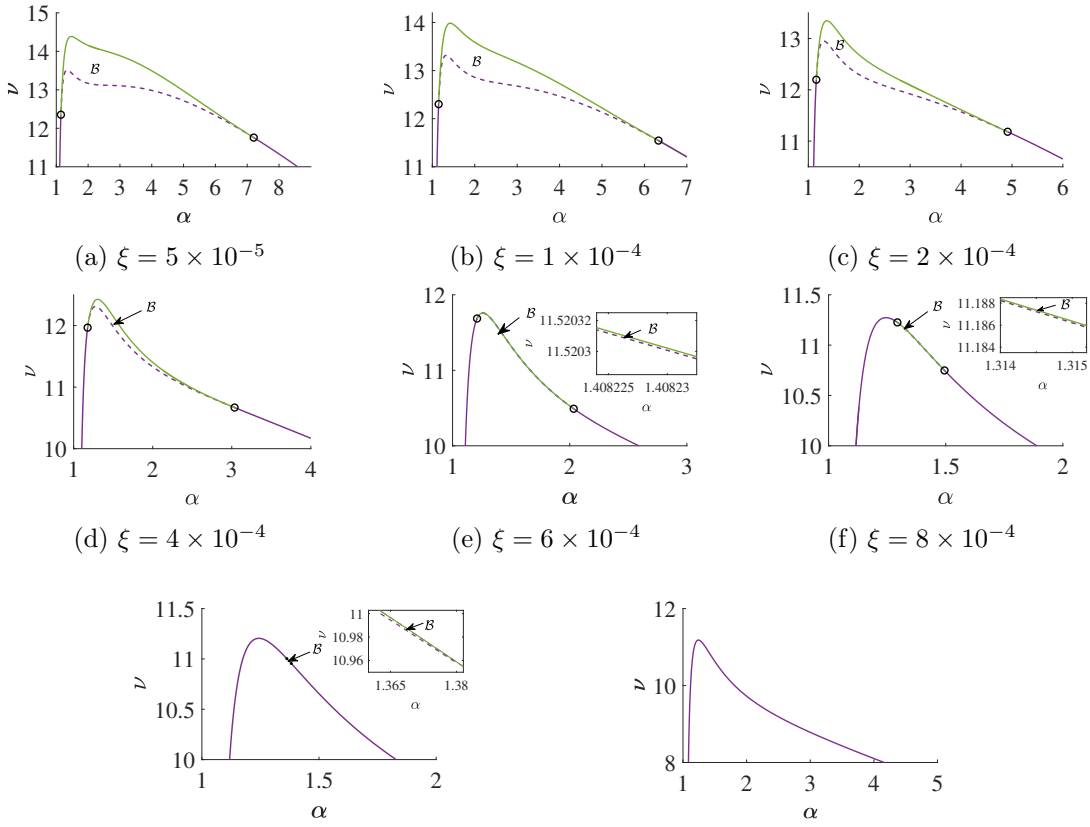

Figure 4.19: Bistabilty region ($\mathcal{B}$) on the two-parameter bifurcation diagram. The region is shrinking as demonstrated by figures a) - g) and has completely disappeared in figure h).

4.5 Summary

In this chapter, we carried out combined analytical and numerical investigations of the SIRWJS system with the presence of secondary infections and potentially asymmetric partitioning of the immune boosting period. As the model population is assumed to be constant, the system is inherently four dimensional resulting in rather complicated formulae describing the equilibria and their stability. The analysis presented in this chapter is giving us novel insights into this complexity and a better understanding of the dynamics. We concluded an exact condition in the form of Θ determining the direction of the bifurcation at $\mathcal{R}_0 = 1$, and

showed that backward bifurcation is possible. This means that the disease can still persist despite the reproduction number being below one. This scenario makes the control of an established disease more difficult.

For $\mathcal{R}_0 > 1$, we derived a numerically tractable Routh-Hurwitz stability criterion and carried out its sign analysis together with numerical continuation techniques. We observed rich and interesting dynamics in the (ν, α, ξ)-space that is varying the immune boosting rate, the partitioning of the boosting period, and the relative infectivity of secondary infections, where other disease parameters were set according to pertussis parameter values taken from the literature. Our numerical investigations show that, in these boosting regions, bifurcations w.r.t. α lead to the emergence of (double) bubbles. This means that as α is varied, the EE can lose its stability at a critical point through a Hopf bifurcation. Then, we observe periodic oscillations only in an intermediate α-interval, and finally, the endemic equilibrium always regains its stability through a second Hopf bifurcation. Naturally, converging to a stable periodic oscillation or a stable endemic equilibrium poses different challenges and burden in disease management. For example, one has to be very careful when evaluating the impact of a mitigation measure when the epidemiological dynamics is inherently oscillatory. Nevertheless, we note that most of the mathematically appealing phenomena occur for a rather large boosting rate (ν) and very small relative infectivity (ξ). But in this case, our results show, that the parameter α, which was ignored in previous studies, in fact has a crucial role in determining the dynamics of the disease in the population.

Our results highlight the challenges in the prediction of the long term dynamics of diseases whenever waning and boosting of immunity is relevant, such as COVID-19 or pertussis, due to the potential complexities generated by the combination of these factors, in particular the asymmetry in partitioning the immune period into high level of immunity and waning immunity that can be boosted. That, in contrast with the simplified modelling approach of symmetric partitioning commonly used in the literature [18, 19, 52], is more realistic. As the

disease dynamics can vastly differ in the asymmetric setup, devising mitigation efforts may benefit from estimates of the relative lengths of these immune periods.

Concluding remarks

Compartmental ODE models are a key tool in epidemics to better understand disease dynamics. The focus of this thesis is on a plausible model for waning of immunity where recovered, *i.e.* fully immune, individuals demonstrate weakened resistance to the disease pathogen after a certain time period whilst maintaining the potential for boosting of immunity upon re-exposure, in the absence of which, they eventually lose their immunity as a whole. Our main goal was to investigate the effect on the disease dynamics of the relative length of these two transitional periods.

In Chapter 2, we introduced the basics of compartmental ODE modeling of infectious diseases. Then, we discussed the equilibria of these dynamical systems, in particular, we demonstrated the calculation of the disease-free and the endemic equilibrium on elementary models. We briefly reviewed the concept of the basic reproduction number $\mathcal{R}_0$ and the next-generation matrix method that may be utilized for its computation. That was followed by a standard analysis of the local asymptotic stability of the equilibria. We also introduced a computationally more practical method for assessing such stability via the so-called Routh-Hurwitz criteria. Then, we discussed the transcritical, saddle-node, and Hopf bifurcations that all appear later in our analysis of mathematical models of waning immunity. Finally, we briefly presented `MatCont` a numerical Matlab package based on continuation techniques that we used to study the aforementioned bifurcations.

The main results of this thesis are coming from our analysis of SIRWS-type systems readily used for studying pertussis dynamics where the boosting is governed by the boosting coefficient ν and the loss of immunity is modeled by two consecutive transitions between the compartments $R \to W \to S$ assuming identical expected duration for the two transitions [18–20]. We have relaxed the later assumption and considered the possibility of asymmetric partitioning of the total immune period that is we allowed varying rates for each of the relevant transitions, modeled by introducing the parameters α and ω, whilst keeping the total expected time of losing immunity, *i.e.* the duration of $R \to \ldots \to S$, constant. In particular, we studied the SIRWS and SIRWJS systems that primarily differ in the modeling of the boosting of immunity that is the mechanics of the transition W to R.

Chapter 3 presents our work on the SIRWS model, where re-exposure results in a direct transition from the waned status to the recovered compartment. We have established a concise formula for the endemic equilibrium $\mathbf{EE}_+$ and proved that at $\mathcal{R}_0 = 1$ the system undergoes a transcritical bifurcation of forward type. Then, we analyzed the Routh-Hurwitz criterion RH for the stability of $\mathbf{EE}_+$ and discovered a certain symmetry of it that later led to a better understanding of the intriguing dynamics that we observed by carefully constructing heatmaps of the criterion on the (α, ν)-plane and by utilizing the capabilities of `MatCont`. Namely, we found a compact region of instability $\mathcal{K}$ of the $\mathbf{EE}_+$ and established the symmetric appearance and disappearance of endemic double bubbles. We used `MatCont` to study the associated Hopf bifurcations and found a region of bistability $\mathcal{B}$ adjacent to $\mathcal{K}$.

In Chapter 4, we considered the SIRWJS model where during the process of immune boosting the individual experiences a secondary infection before regaining full immunity. This intermediate stage is represented by the J compartment and is allowed to exhibit a different level of infectivity, described by the relative infectivity parameter ξ, compared to that of I. An in-depth analysis similar to that described in the previous chapter was carried out. We have shown that, upon large enough boosting and relative infectivity of secondary infections,

the transcritical bifurcation at $\mathcal{R}_0 = 1$ might be of backward type. We emphasize that this phenomenon is present also when one considers the conventional partitioning of the total immune period that is equal expected duration for the transitions $R \to W$ and $W \to S$. The previously observed symmetry in the RH criterion is now gone and the associated computation is much more involved, in particular, it is far from trivial to establish the positivity of the coefficients of the characteristic polynomial. The (α, ν) heatmap analysis for various ξ values reveals how $\mathcal{K}$ and $\mathcal{B}$, *i.e.* the regions of instability and bistability, are becoming first distorted, then shrink until disappearing completely.

The thesis has investigated the impact of the asymmetric partitioning of the total immune period on the SIRWS and SIRWJS models. We found rich and interesting dynamics that highlight the importance of considering this aspect in studies of waning immunity. In the future, we plan to extend our results to a variant of the SIRWJS model allowing immune boosting to happen both directly and via secondary infection.

Publications

The dissertation is based on the following two scientific papers:

- Richmond Opoku-Sarkodie, Ferenc A. Bartha, Mónika Polner, Gergely Röst, Dynamics of an SIRWS model with waning of immunity and varying immune boosting period, Journal of Biological Dynamics, 16 (1) (2022) 596-618, [61].
- Richmond Opoku-Sarkodie, Ferenc A. Bartha, Mónika Polner, Gergely Röst, Bifurcation analysis of waning-boosting epidemiological models with repeat infections and varying immunity periods, Journal of Mathematics and Computers in Simulation, 218 (2024) 624-643, [64].

Összefoglalás

A kompartmentális ODE-modellek a járványok esetében kulcsfontosságú eszköznek számítanak a betegség dinamikájának jobb megértéséhez. E dolgozat középpontjában az immunitás csökkenésének egy plauzibilis modellje áll, ahol a felépült, azaz teljes immunitású egyének, egy bizonyos idő után, gyengébb ellenállást mutatnak a betegség kórokozójával szemben. Eközben, ismételt expozíció esetén fenntartják az immunitás erőssödésének lehetőségét (boosting), melynek hiányában viszont végül teljes egészében elveszítik az immunitásukat. Fő célunk annak vizsgálata volt, hogy e két átmeneti időszak relatív hossza milyen hatással van a járvány dinamikájára.

A 2. fejezetben bemutattuk a fertőző betegségek kompartmentális ODE modellezésének alapjait. Ezután e dinamikus rendszerek egyensúlyi helyzeteit tárgyaltuk, speciálisan a fertőzésmentes és az endemikus egyensúly számítását mutattuk be elemi modelleken. Röviden áttekintettük az $\mathcal{R}_0$ reprodukciós szám fogalmát és annak számítására az úgynevezett "next-generation matrix" módszert. Ezt követően az egyensúlyi helyzetek lokális aszimptotikus stabilitását taglaltuk. Bemutattunk egy gyakorlati eljárást, amely az úgynevezett Routh-Hurwitz-kritériumok alkalmazásával vizsgálja a stabilitást. Ezután tárgyaltuk a transzkritikus, a nyereg-csomó és a Hopf-bifurkációkat, amelyek mind-mind megjelennek később a gyengülő immunitás matematikai modelljeinek dinamikájában. Végül röviden bemutattuk a `MatCont` numerikus technikákon alapuló Matlab-csomagot, amelyet a fent említett bifurkációk tanulmányozásához használtunk.

A dolgozat fő eredményei a szamárköhögés (pertussis) dinamikájának tanulmányozására is használható SIRWS típusú rendszerek elemzéséből származnak, ahol a boostingot a ν együttható szabályozza és az immunitás elvesztését két egymást követő átmenettel $R \to W \to S$ modellezzük, azonos várható időtartamot feltételezve ezen két átmenetre [18–20]. Az utóbbi megkötést elengedve kaptuk a teljes immunitási időszak aszimmetrikus felosztásának lehetőségét, azaz lehetővé tettük, hogy az egyes releváns átmenetek különböző sebességgel történjenek, amit az α és ω paraméterek bevezetésével modelleztünk, miközben a teljes immunitásvesztés várható időtartamát, azaz az $R \to \ldots \to S$-ig tartó időtartamot változatlanul hagytuk. Elsősorban az SIRWS és az SIRWJS rendszereket vizsgáltuk, amelyek főként a védettség erősödésének azaz a $W \to \ldots \to R$ (esetlegesen többlépcsős) átmenetnek modellezésében különböznek.

A 3. fejezet az SIRWS modellel kapcsolatos munkánkat mutatja be, ahol az ismételt expozíció közvetlen átmenetet eredményez az átmeneti immunitás állapotából a teljesen immunis kompartmentbe. Tömör formulát adtunk az endemikus egyensúlyra $\mathbf{EE}_+$, és bebizonyítottuk, hogy $\mathcal{R}_0 = 1$ esetén a rendszer egy forward típusú transzkritikus bifurkáción megy keresztül. Ezután elemeztük a $\mathbf{EE}_+$ stabilitását leíró Routh-Hurwitz-kritériumot és igazoltuk annak egy bizonyos szimmetriáját. Ez a szimmetria később a kritériumnak az (α, ν)-síkon képezett hőtérképével és a `MatCont` eredményeivel a megfigyelt dinamika nagyobb fokú megértéséhez vezetett. Nevezetesen, megtaláltuk az $\mathbf{EE}_+$ kompakt instabilitási régióját ($\mathcal{K}$) és észleltük dupla endemikus buborékok szimmetrikus megjelenését és eltűnését. A `MatCont` segítségével megvizsgáltuk a kapcsolódó Hopf-bifurkációkat, és a $\mathcal{K}$ szomszédságában bistabilitási régiót ($\mathcal{B}$) találtunk.

A 4. fejezetben az SIRWJS modellt vizsgáltuk, ahol az immunitás visszanyerésének folyamata során az egyén másodlagos fertőzésen megy keresztül. Ezt a köztes szakaszt a J kompartment modellezi megengedve az I kompartmenthez képest más szintű fertőzőképességet, amelyet a ξ relatív fertőzőképességi paraméter ír le. Az előző fejezetben leírtakhoz hasonló mélyreható

elemzést végeztünk a rendszeren. Megmutattuk, hogy elég nagy boosting és relatív fertőzőképesség esetén az $\mathcal{R}_0 = 1$-nél bekövetkező transzkritikus bifurkáció backward típusú is lehet. Hangsúlyozzuk, hogy ez a jelenség akkor is megtapasztalható, ha a teljes immunperiódus hagyományos felosztását tekintjük, azaz, ahol az $R \to W$ és $W \to S$ átmenetek várható időtartama egyenlő. A korábban megfigyelt szimmetria az RH-kritériumban már nincs jelen, a kapcsolódó számítások sokkal bonyolultabbak, különösképpen a karakterisztikus polinom együtthatóinak pozitivitásának megállapítása korántsem triviális. Az (α, ν) hőtérképelemzés különböző ξ értékekre megmutatja, hogy a $\mathcal{K}$ és $\mathcal{B}$, azaz az instabilitás és a bistabilitás területei először torzulnak, majd zsugorodnak, míg végül teljesen eltűnnek.

A dolgozat a teljes immunitási időszak aszimmetrikus felosztásának hatását vizsgálta az SIRWS és SIRWJS modellekre. Gazdag és érdekes dinamikát találtunk, amely rávilágít annak fontosságára, hogy az aszimmetrikus felosztást figyelembe vegyük az immunitási vizsgálatában. A jövőben tervezzük, hogy eredményeinket kiterjesztjük az SIRWJS modell egy olyan változatára is, amely lehetővé teszi, hogy az immunerősödés közvetlenül és másodlagos fertőzésen keresztül is megtörténjen.

A disszertáció a következő két, megjelent tudományos dolgozaton alapul:

- Richmond Opoku-Sarkodie, Ferenc A. Bartha, Mónika Polner, Gergely Röst, Dynamics of an SIRWS model with waning of immunity and varying immune boosting period, Journal of Biological Dynamics, 16 (1) (2022) 596-618, [61].
- Richmond Opoku-Sarkodie, Ferenc A. Bartha, Mónika Polner, Gergely Röst, Bifurcation analysis of waning-boosting epidemiological models with repeat infections and varying immunity periods, Journal of Mathematics and Computers in Simulation, 218 (2024) 624-643, [64].

Bibliography

[1] K.H.T. Yeung, P. Duclos, E.A.S. Nelson, R.C.W. Hutubessy, An update of the global burden of pertussis in children younger than 5 years: a modelling study, Lancet Infect. Dis. 17 (9) (2017) 974–980.

[2] C. B. McGuiness, J. Hill, E. Fonseca, G. Hess, W. Hitchcock, G. Krishnarajah, The disease burden of pertussis in adults 50 years old and older in the United States: a retrospective study, BMC Infect. Dis. 13 (1) (2013) 1–14.

[3] National Center for Immunization and Respiratory Diseases, Division of Bacterial Diseases, Whooping cough is deadly for bodies, 2022.
https://www.cdc.gov/pertussis/pregnant/mom/deadly-disease-for-baby.html

[4] D. L. Miller, E. M. Ross, R. Alderslade, M. H. Bellman, N. S. Rawson, Pertussis immunization and serious acute neurological illness in children, Br. Med. J. (Clin. Res. Ed.) 282 (6276) (1981) 1595–1599.

[5] M.J. Bart et al., Global population structure and evolution of Bordetella pertussis and their relationship with vaccination, MBio. 5 (2) (2014) 10–1128.

[6] R.E. Black et al., Global, regional, and national causes of child mortality in 2008: a systematic analysis, Lancet 375 (9730) (2010) 1969–1987.

[7] European Centre for Disease Prevention and Control, Pertussis annual epidemiological report 2018.

https://www.ecdc.europa.eu/sites/default/files/documents/AER_for_2018_pertussis.pdf

[8] A. Burton, et al., WHO and UNICEF estimates of national infant immunization coverage: methods and processes, Bull. World Health Organ. 87 (2009) 535–541.

[9] D. Breda, O. Diekmann, W.F. De Graaf, A. Pugliese, R. Vermiglio, On the formulation of epidemic models (an appraisal of Kermack and McKendrick), J. Biol. Dyn. 6 (sup2) (2012) 103–117.

[10] O. N. Bjørnstad, B.F. Finkenstädt, B.T. Grenfell, Dynamics of measles epidemics: estimating scaling of transmission rates using a time series SIR model, Ecol. Monogr. 72 (2) (2002) 169–184.

[11] S. Side, A.M. Utami, M.I. Pratama, Numerical solution of SIR model for transmission of tuberculosis by Runge-Kutta method, J. Phys: Conf. Ser. 1040 (1) (2018) 012021.

[12] O. Zakary, M. Rachik, I. Elmouki, On the impact of awareness programs in HIV/AIDS prevention: an SIR model with optimal control, Int. J. Comput. Appl. 133 (9) (2016) 1–6.

[13] T. Berge, J.S. Lubuma, G.M. Moremedi, N. Morris, R. Kondera-Shava, A simple mathematical model for Ebola in Africa, J. Biol. Dyn. 11 (1) (2017) 42–74.

[14] D. Osthus, K.S. Hickmann, P.C. Caragea, D. Higdon, S.Y. Del Valle, Forecasting seasonal influenza with a state-space SIR model, Ann. Appl. Stat. 11 (1) (2017) 202.

[15] I. Cooper, A. Mondal, C.G. Antonopoulos, A SIR model assumption for the spread of COVID-19 in different communities, Chaos Solitons Fractals 139 (2020) 110057.

[16] J.S. Lavine, A.A. King, O.N. Bjørnstad, Natural immune boosting in pertussis dynamics and the potential for long-term vaccine failure, Pro. Natl. Acad. Sci. 108 (17) (2011) 7259–7264.

[17] J.S. Lavine, A. A. King, V. Andreasen, O. N. Bjørnstad, Immune boosting explains regime-shifts in prevaccine-era pertussis dynamics, PLoS One 8 (8) (2013) e72086.

[18] L.F. Strube, M. Walton, L.M. Childs, Role of repeat infection in the dynamics of a simple model of waning and boosting immunity, J. Biol. Syst. 29 (2) (2021) 1–22.

[19] M.P. Dafilis, F. Frascoli, J.G. Wood, J.M. McCaw, The influence of increasing life expectancy on the dynamics of SIRS systems with immune boosting, ANZIAM J. 54(1–2) (2012) 50–63.

[20] J. Heidecke, M.V. Barbarossa, When Ideas Go Viral—Complex Bifurcations in a Two-Stage Transmission Model, In: Mondaini, R.P. (eds) Trends in Biomathematics: Chaos and Control in Epidemics, Ecosystems, and Cells. BIOMAT 2020. Springer, Cham.

[21] A. Dhooge, W. Govaerts, Y.A. Kuznetsov, B. Sautois, Limit cycles and their bifurcations in `MatCont`, 2004.

[22] A. Dhooge, W. Govaerts, Y.A. Kuznetsov, `MatCont`: a Matlab package for numerical bifurcation analysis of ODEs, SIGSAM Bull. 38 (1) (2004) 21–22.

[23] W. Govaerts, Y. A. Kuznetsov, H. Meijer et al., `MatCont`: Continuation toolbox for ODEs in Matlab, 2018.

[24] I. Cooper, A. Mondal, C.G. Antonopoulos, A SIR model assumption for the spread of COVID-19 in different communities, Chaos Solitons Fractals 139 (2020) 110057.

[25] Y.C. Chen, P.E, Lu, C.S. Chang, T.H. Liu, A time-dependent SIR model for COVID-19 with undetectable infected persons, IEEE Trans. Netw. Sci. Eng. 7 (4) (2020) 3279–3294.

[26] Y. Ucakan, S. Gulen, K. Koklu, Analysing of tuberculosis in turkey through SIR, SEIR and BSEIR mathematical models, Math. Comput. Model Dyn. Sys. 27 (1) (2021) 179–2021.

[27] S. Side, A susceptible-infected-recovered model and simulation for transmission of tuberculosis, Adv. Sci. Lett. 21 (2), (2015) 137–139.

[28] P. Boldog, T. Tekeli, Z. Vizi, A. Dénes, F.A. Bartha, G. Röst, Risk assessment of novel coronavirus COVID-19 outbreaks outside China, J. Clin. Med. 9 (2) (2020) 517.

[29] S. He, Y. Peng, K. Sun, SEIR modeling of the COVID-19 and its dynamics, Nonlinear Dyn. 101 (2020) 1667–1680.

[30] S. Mwalili, M. Kimathi, V. Ojiambo, D. Gathungu, R. Mbogo, SEIR model for COVID-19 dynamics incorporating the environment and social distancing, BMC Res. Notes 13 (1) (2020) 1–5.

[31] N. Wang, Y. Fu, H. Zhang, H. Shi, An evaluation of mathematical models for the outbreak of COVID-19, Precis. Clin. Med. 3 (2), (2020) 85–93.

[32] S. Annas, M.I. Pratama, M. Rifandi, W. Sanusi, S. Side, Stability analysis and numerical simulation of SEIR model for pandemic COVID-19 spread in Indonesia, Chaos Solitons Fractals 139 (2020) 110072.

[33] P.E. Fine, The interval between successive cases of an infectious disease, Am. J. Epidemiol. 158 (11) (2003) 1039–1047.

[34] O. Diekmann, J. Heesterbeek, M.G. Roberts, The construction of next-generation matrices for compartmental epidemic models, J. R. Soc. Interface 7 (47) (2010) 873–885.

[35] K. Dietz, The estimation of the basic reproduction number for infectious diseases, Stat. Methods Med. Res. 2 (1) (1993) 23–41.

[36] I. Locatelli, T. A. Bastien, V. Rousson, Estimating the basic reproduction number for covid-19 in Western Europe, PLoS One 16 (3) (2021) e0248731.

[37] P. Holmes, J. Guckenheimer, Nonlinear oscillations, dynamical systems, and bifurcations of vector fields, Springer Science & Business Media 44 (2013).

[38] T.C. Sideris, Ordinary differential equations and dynamical systems, Atlantis Press, Paris, 2013.

[39] J.C. Maxwell, I. On governors, Proc. R. Soc. Lond. 16 (1868) 270–283.

[40] S. Bennett, A history of control engineering, IET 47 (1993) 1930–1955.

[41] E.J. Routh, A treatise on the stability of a given state of motion: particularly steady motion, Macmillan and Co., London, 1877.

[42] A. Hurwitz et al., On the conditions under which an equation has only roots with negative real parts, Selected papers on mathematical trends in control theory, 1964.

[43] Y.A. Kuznetsov, Elements of Applied Bifurcation Theory, Springer, New York, New York, 2004.

[44] S. Wiggins, Introduction to Applied Nonlinear Dynamical Systems and Chaos, Springer, New York, New York, 2003.

[45] C. Castillo-Chavez, B. Song, Dynamical models of tuberculosis and their applications, Math. Biosci. Eng. 1 (2) (2004) 361–404.

[46] J. Carr, Center manifold, Scholarpedia 12 (1) (2006) 1826.

[47] S. Wiggins, Global Bifurcations and Chaos: Analytical Methods, Springer, New York, New York, 2013.

[48] N. Neirynck, Advances in numerical bifurcation software: `MatCont`, Doctoral dissertation, Ghent University, 2019.

[49] M.V. Barbarossa, G. Röst, Immuno-epidemiology of a population structured by immune status: a mathematical study of waning immunity and immune system boosting, J. Math. Biol. 71 (6) (2015) 1737–1770.

[50] H. Jardón-Kojakhmetov, C. Kuehn, A. Pugliese, M. Sensi, A geometric analysis of the SIR, SIRS, and SIRWS epidemiological models, Nonlinear Anal.: Real World Appl. 58 (2021) 103220.

[51] T. Leung, B.D. Hughes, F. Frascoli, J.M. McCaw, Periodic solutions in an SIRWS model with immune boosting and cross-immunity, J. Theor. Biol. 410 (2016) 55–64.

[52] T. Leung, P.T. Campbell, B.D. Hughes, F. Frascoli, J.M. McCaw, Infection-acquired versus vaccine-acquired immunity in an SIRWS model, Infect. Dis. Model. 3 (2018) 118–135.

[53] J.D. Murray, Mathematical Biology: I. An Introduction. Interdisciplinary Applied Mathematics, 17, Springer-Verlag, New York, New York, 2002.

[54] M. Liu, E. Liz, G. Röst, Endemic bubbles generated by delayed behavioral response – global stability and bifurcation switches in an SIS model, SIAM J. Appl. Math. 75 (1) (2015) 75–91.

[55] M.V. Barbarossa, M. Polner,G. Röst, Stability switches induced by immune system boosting in an SIRS model with discrete and distributed delays, SIAM J. Appl. Math. 77 (3) (2017) 905–923.

[56] V.G. LeBlanc, A Degenerate Hopf Bifurcation in Retarded Functional Differential Equations, and Applications to Endemic Bubbles, J. Nonlinear Sci. 26 (2016) 1–25.

[57] N. Sherborne, K.B. Blyuss, I.Z. Kiss, Bursting endemic bubbles in an adaptive network, Phys. Rev. E. 97 (4) (2018) 042306.

[58] T. Krisztin, E. Liz, Bubbles for a Class of Delay Differential Equations, Qual. Theory Dyn. Syst. 10 (2011) 169–196.

[59] R.M. Carlsson, L.M. Childs, Z. Feng, J.W. Glasser, J.M. Heffernan, J. Li, G. Röst, Modeling the waning and boosting of immunity from infection or vaccination, J. Theor. Biol. 497 (2020) 110265.

[60] L. Childs, D.W. Dick, Z. Feng, J.M. Heffernan, J. Li, G. Röst, Modeling waning and boosting of COVID-19 in Canada with vaccination, Epidemics, 39 (2002) 100583.

[61] R. Opoku-Sarkodie, F.A. Bartha, M. Polner, G. Röst, Dynamics of an SIRWS model with waning of immunity and varying immune boosting, J. Biol. Dyn. 16 (1) (2022) 596–618.

[62] G. Katriel, The dynamics of two-stage contagion, Chaos Solitons Fractals 2 (2019).

[63] Computer Algebra Codes, Github, 2023. https://github.com/epidelay/waning-boosting-epidemiological-models.

[64] R. Opoku-Sarkodie, F.A. Bartha, M. Polner, G. Röst, Bifurcation analysis of waning-boosting epidemiological models with repeat infections and varying immunity periods, Math. Comput. Simul. 218 (2024) 624–643.